INSULATIVE (DIRECT CURRENT) DIELECTROPHORETIC FOUL-LESS FILTRATION IN MICROFUIDIC SYSTEMS

A Thesis

presented to

the Faculty of California Polytechnic State University,

San Luis Obispo

In Partial Fulfillment

of the Requirements for the Degree

Master of Science in Biomedical Engineering

by

Matthew A. A. Whitman

January 2020

COMMITTEE MEMBERSHIP

TITLE: Direct Current Dielectrophoretic Foul-less Filtration in Microfluidic Systems

AUTHOR: Matthew A. A. Whitman

DATE SUBMITTED: January 2020

COMMITTEE CHAIR: David Clague, Ph.D.
Professor of Biomedical Engineering

COMMITTEE MEMBER: Benjamin Hawkins, Ph.D.
Assistant Professor of Biomedical Engineering

COMMITTEE MEMBER: Hans Mayer, Ph.D.
Assistant Professor of Mechanical Engineering

ABSTRACT

Insulative (Direct Current) Dielectrophoretic Foul-Less Filtration in Microfluidic Systems

Matthew A. A. Whitman

Filtration is a technology that is used almost ubiquitously in society from uses raging from filtration of macroparticles from water to pharmaceutical grade filtration products to remove anything larger than a protein. However, with such a wide range of uses, most filtration products have the same issue; membrane clogging (fouling) that prevents continuous use and requires frequent maintenance. This thesis hypothesizes that by applying a direct current (DC) to an insulating array of posts, they will create a foul-less insulative dielectrophoretic filter (iDEP) that does not clog since particles will levitate above the insulating array.

Past work has shown that viable cells and bacteria can be trapped owing to Dielectrophoretic (DEP) forces between insulative obstacles.[8] This work led to the hypothesis that there exists an obstacle geometries and arrangements that would predictably project the DEP field preferentially repelling target particles from entering the array of insulative obstacles thus creating a foul-less filter. Within the Biofluidics group an initial analysis was performed and a device fabricated to test this hypothesis. In the work presented here, the device (legacy device) was tested and did not perform as desired. This led to a new investigation that included model-based design via COMSOL Multiphysics®, design and fabrication of new devices and validating experiments.

Using COMSOL Multiphysics®, the insulative obstacle geometries, obstacle arrangements and operating conditions were found and optimized to yield the desired in

silico device functionality. The resultant device designs were fabricated, experimentally tested to assess DEP force effects on yeast. Designs were found that successfully levitate the yeast above the insulative obstacles providing promising evidence toward the creation of microfluidic instantiation foul-less filtration array using a direct current insulative dielectrophoretic (iDEP). Although a microfluidic instantiation of a fully functional foul-less filter was not demonstrated over the course of this thesis, insulative obstacle designs, microdevice dimensions and operating conditions were found that could enable the development of a foul-less DC iDEP microfilteration system.

Keywords: Insulative Dielectrophoresis, Microfluidics, Filtration, Direct Current Dielectrophoresis

ACKNOWLEDGMENTS

I would like to thank Dr. Clague for his support, guidance, and patience throughout this process. His insight and seemingly endless energy and passion for this project, instilled in me a deep interest in the theory and science surrounding this project. Without his commitment to this project and dozens of hours of his time given, this project would not have been possible.

I would like to thank my other committee members, Dr. Hawkins and Dr. Mayer for their support through giving their time to answer my questions and helping to propel this thesis.

I would like to thank my family and friends for their unwavering support throughout my life and throughout my career.

I would also like to thank Tarra Sanders and Wyatt Warfield for their help and time in the clean room.

TABLE OF CONTENTS

Page

LIST OF TABLES

LIST OF FIGURES

CHAPTER 1 INTRODUCTION

1.1 Hypothesis

Direct Current Dielectrophoresis/Insulative Dielectrophoresis (iDEP) can be applied to microfluidic systems to create a continuous flow foul-less filtration system for filtering microparticles from media and particulates of different properties.

In this thesis, FEA analysis and experiments were performed on a legacy iDEP device aimed at creating a microfluidic, foul-less filter; however, as designed, the device did not perform as expected and needed design modifications and optimization of the electrical, chemical, and mechanical conditions . Therefore this thesis sets out to answer the questions: i) why does the legacy device not perform as desired? ii) Can a microfluidic, iDEP device be created that effectively filters particles in a foul-less nature? iii) What possible design changes could be made to enable this concept and improve its effectiveness? iv) What are the optimal operating conditions?

1.2 Goals

The overall goal of this thesis is to take steps to create a novel DC iDEP filter where particles are continuously filtered and do not foul the device. Continuous flow DEP filtration devices have been created using AC fields but use of DC has yet to be performed due to the added electrokinetic factors; therefore, simulations, designs, and experimentation will be the focuses to perform foul-less DC iDEP filtration for the first time. In this work the aims were to determine the following:

i): How does the legacy design performs under simulated and experimental conditions.

ii): If there are optimal experimental conditions for successful performance for the legacy device.

iii): If an insulative dielectrophoretic microfluidic device can be created that enables a foul-less filter like separation.

iv): If necessary, design changes that can be made to the legacy device to design a new device with improves and allows function.

1.3 Motivation

This thesis was driven by the significant cost to industry, e.g., in medicine, agriculture, waste management, and clinical diagnostics, due to filter fouling. Given this wide range of application and frequency of, many industries would benefit from a prolonged quality filtration while maintaining selectivity and high flowrates, i.e., a foul-less filters [1][3][4]. However, throughout all applications, currently filters and filtration systems require a frequent maintenance at significant costs due to membrane fouling by particles and debris accumulation and build-up on the retentate side of the membranes. Consequently, physical filtration is ripe for innovative improvements that can either significantly increase the time it takes for a filter to foul or eliminating fouling all together. Given the proper design and conditions, it is postulated that a form of DEP can be employed to create a repulsive force at the membrane surface that acts on particles, independent of the surrounding fluid making it a natural, ideal candidate to enable the desired goal of creating a foul-less filter.

In the medical space alone, dielectrophoretic technology has been used in a lab to isolate breast cancer cells from red blood cells and T-lymphocytes [2]. In the future

where dielectrophoretic separations are brought to a clinical setting, removal of cancerous cells from diluted blood could be done to a high degree of specificity [2].

In waste management, heavy metal contamination of ground water from mining and agriculture has become a widespread issue, causing tap and well water in some parts of the country to become unsafe for consumption. Heavy metal contamination poses a severe risk to human health and studies are starting to find heavy metal contamination across the world in drinking water and agriculture [3][4]. Dielectrophoresis could become a technology that could help remove heavy metals from our drinking water and water used in agriculture [5]. These applications for dielectrophoresis are numerous and as the technology continues to develop, more applications and improved efficacy will arise.

Due to all the possible applications, research in DEP separations using alternating current, standing and traveling wave DEP [2], and direct current, iDEP, [6][7][8] to separate particles has increasingly become more common in recent decades. Each application of this form of DEP takes a slightly different physical/geometric design and experimental conditions to effect the desired separations. When considering these previous successful applications of iDEP, it is clearly plausible that a filter can be designed that makes use of a DC electric field induced iDEP forces to preferentially levitate particulates from filter surfaces preventing fouling.

Such a filtration device would have a wide range of applications from removal of macroscopic particles down to molecules, DNA and proteins, and in principle, various methods of DEP filtration can be applied at every scale to accomplish the desired level of filtration.

1.4 Overview and Background

When looking at the need for a continuous flow foul-less filter, the main application would be towards the advancement of pharmaceutical development and production. Current methods of protein production in the pharma industry involve "Pharming," that is to say transfecting protein DNA sequences into bacterial gDNA to exploit the normal protein production mechanisms for mass production of a desired protein, e.g., insulin. To harvest the desired proteins, the host organism, e.g., bacteria, is sacrificed and the therapeutic proteins must be separated from the debris/lysate [9]. A membrane is the gold standard to separate the desired product from non-viable product and other production media. To be considered "sterile" filtrate, these physical barriers require pore sizes to be no larger than 0.2 microns in diameter [10]. This small size restricts flowrate of the medium, leading to long filtration times and fouling of the filter, requiring frequent replacement. The application of a dielectrophoretic filter to a system like this could have the ability to increase throughput of product since flowrate through a dielectric filter allows filtrate to be concentrated in fractions of the time. Additionally, when compared to physical membranes, the dielectric filter has the added benefit of a foul-less nature, therefore eliminating the need for frequent replacement of the filter.

The concept of using insulating dielectrophoretic filtration has been a subject of research in recent years and several methods of particle filtration have been developed. In 2011 Hector and Blanca employed the use of an array of insulating posts in a DC field device to trap E. coli and S. cerevisiae using dielectrophoretic trapping. Both species of bacteria were placed in the device and allowed to move through the device under the influence of an applied electric field. Due to the differing properties of each bacteria, they

would become trapped in separate bands between posts and at certain voltages, S. cerevisiae would become trapped while E. coli would pass through the array as other electrokinetic phenomena overwhelmed the DEP force and pulled particles towards the exit of the device [8].

In another paper by Cummings in 2003, insulating dielectrophoresis was used to focus particles through an array of angled posts by applying a DC field. The device used DEP force to focus particles into streamlines through the post array. This paper looked at how particles would act under differing ratios of the DEP mobility to the electrokinetic mobility. By increasing the ratio, Cummings found that particles with focus into tighter streamlines and eventually retarding the motion of particles to the point where particle trapping begins [6].

In another approach, Gascoyne [2] used a microelectrode array to dielectrically separate human breast cancer cells from erythrocytes and lymphocytes. Gascoyne [2] applied an AC field between alternating rows of electrodes and was able to successfully separate breast cancer cells from other constituents of blood. Human breast cancer cells would become trapped on the electrodes while erythrocytes and lymphocytes would be swept downstream leaving only the breast cancer cells. This showed that using DEP, a single species of particles could be selectively separated from a medium of several particle types with the specific application for testing for cancer cells in blood [2].

The structure of this thesis will begin with an explanation of the various theoretical components that play roles in performing dielectrophoresis in chapter 2. Then the outline of how the simulations and experiments for testing the legacy device are outlined in chapter 3. The results and data from the simulations and experiments on the

legacy device are discussed and shown in chapter 4. The design process of the new device using insight gained from testing, simulations, and lessons learned from the Legacy device are detailed in chapter 5. Everything learned over the course of this thesis is discussed in chapter 6 and chapter 7 wraps everything up with conclusions and future directions for the continuation of this project.

CHAPTER 2 THEORY

The purpose of this project is to design a dielectrophoretic filter that prevents clogging or fowling. To accomplish this task, it is important to understand such factors as fluid properties, pressure driven flow in a microfluidic system, electrical impedance, electroosmotic flow, electrophoretic flow, electric double layer, zeta potential, drag force, dielectrophoretic force, cell electrical properties, and some micro-electro-mechanical (MEMs) manufacturing techniques.

2.1 Fluid Properties and Dynamics

While designing, simulating, and testing any microfluidic system it is essential to understand the properties of the fluid that are applicable and how alterations to the fluid or conditions will alter its properties. This section will discuss various fluid properties that are integral in a dielectrophoretic microfluidic system. Important fluid properties to this project include electrical conductivity, permittivity, viscosity, and density. These fluid properties determine how the fluid itself will act within the system.

2.1.1 Fluid Dynamics

Understanding the fluid dynamics of the device in question is essential to allow for fine tuning the flow accordingly. Hagen-Poiseuille flow allows for simplified calculation of fluid flow at steady state in creep flow systems. Traditionally the Hagen-Poiseuille equation is used to describe the volumetric flow rate, Q through a circular cross section vessel and is expressed as:

$$Q = \frac{1}{R}\Delta P \tag{1}$$

$$R = \frac{8\eta L}{\pi r^4} \quad (2)$$

Where R is the hydrodynamic resistance, r is the radius of the vessel being observed, η is the viscosity of the fluid, L is the length of the vessel, and ΔP is the pressure drop across the vessel [11]. However, in the case of many microfluidic devices, the cross section is not circular, and instead are made up of rectangular cross sections due to soft lithography methods employed to create microfluidic devices. Therefore, Equation (2) cannot be applied to describe volumetric flow in the legacy device so it can be modified to apply to rectangular cross sections. To estimate volumetric flow rate in a rectangular cross section, the hydrodynamic resistance term is changed to:

$$\frac{\Delta P}{Q} = R = \frac{12\eta L}{h^3 w(1 - 0.630\frac{h}{w})} \quad (3)$$

Where h and w are the height and width of the channel respectively, Q is the volumetric flowrate, and ΔP is the pressure drop across a channel. This rectangular channel approximation requires that calculations be done the frame of reference that the width is greater than the height [11].

Understanding how the hydrodynamic resistance affects the legacy device and any future iterations is important to controlling flow in the device. Hydrodynamic resistance plays a role in the legacy device in the inlet and outlet channels where the fluid dynamics are purely pressure driven.

2.1.2 Reynold's Number

Since the fluid mechanics of the system being observed are on the scale of millimeters down to micrometers, some phenomena of fluid mechanics do not occur as

this section explains. Microscopic fluid mechanics is dominated by the laminar flow regime. Laminar or turbulent flow is determined by the Reynold's number, which can be characterized by [12]:

$$Re = \frac{\rho \bar{V} D}{\eta} \tag{4}$$

Where ρ is the fluid density, $\bar{V}$ is the average fluid velocity, and D is the hydraulic diameter. When considering a microfluidic system involving liquids, the Reynold numbers tend to be <<1 due to the small channel sizes and low flowrates (<1mm/s) [11]. This type of flow is called Stokes or Creep flow where the inertial terms in the Navier-Stokes equations are neglected [12].

2.1.3 Stoke's Drag

The intended use of a dielectrophoretic microfluidic device is to separate particles from each other and the surrounding medium, so understanding particle movement in a moving fluid is essential. Just as a fluid will not deform without agitation, a particle within the fluid will not accelerate unless acted upon by a force. Stokes Drag is used to describe the force the fluid exerts on the particle due to fluid and sphere motion and is as seen in Equation (5).

$$\vec{F}_{drag} = 6\pi\eta a \Delta\vec{v} \tag{5}$$

Where a is the radius of the particle in question and Δv is the fluid velocity relative to the particle velocity in each principal direction. When looking at biologics, it is infrequent that the particles being observed will be perfectly spherical and will often take

on more complex shapes [13]. For the sake of simplicity, all particles observed in this thesis are considered to be spherical in nature.

2.2 Surface Chemistry and Chemistry of Solutions

When looking at a system that works on a scale of microns, macroscopic forces begin playing less and less of a role in the motion of fluids and particles. On the microscopic level, surface forces begin to play a larger role in the effects on the system. In particular for microfluidic systems that includes electric fluids; zeta potential and its effect on electroosmotic flow and electrophoresis, play large roles in how the fluid dynamics of the system act. For a DC iDEP filter, this is important to understanding and predicting the effects on the fluid dynamics within the device.

2.2.1 Electric Double Layer

When looking at surfaces in a microfluidic system the forces occurring at the surface become increasingly important [11]. Water is a fluid that is often used in microfluidics and has a highly dielectric nature that allows ions to easily dissolve into solution. This physical property of water allows for easy diffusion of ions into solution [13]. Charged surfaces create electrical fields, attracting counterions towards them and repelling coions away [14]. When combined with random thermal motion, these phenomena form the Electric Double Layer (EDL) [14]. At equilibrium, the concentration of counterions will from a cloud of ions that has an equal and opposite charge to the surface, establishing electro-neutrality. Within the EDL there is an increased concentration of counterions due to attractive electrostatic forces and decreased concentration of coions from repulsive electrostatic forces [13].

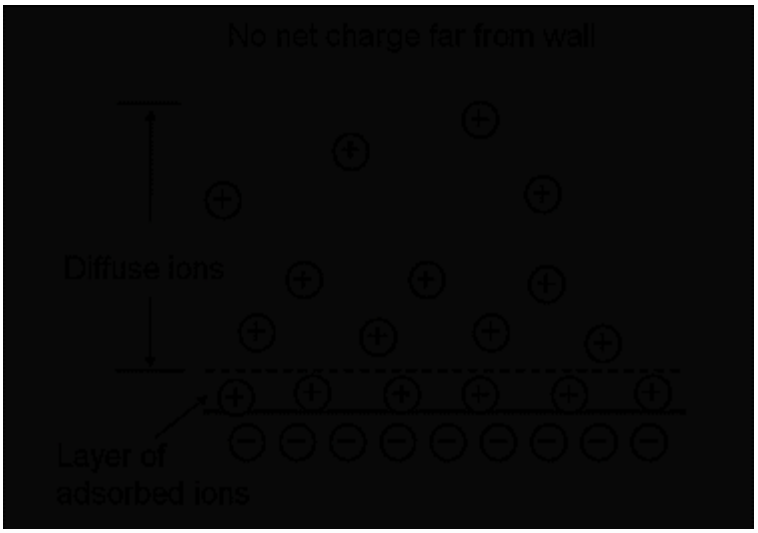

Figure 01: Image of the EDL with cations adsorbed to the negatively charged surface and diffuse layer of cations and anions in aqueous solution. [15]

When looking at an aqueous solution with a charged surface, the electric potential and charge density can be determined using the Poisson equation [14]:

$$\nabla^2\phi = \frac{\partial^2\phi}{\partial x^2} + \frac{\partial^2\phi}{\partial y^2} + \frac{\partial^2\phi}{\partial z^2} = -\frac{\rho_e}{\varepsilon\varepsilon_o} \tag{6}$$

Where ρ_e is the local charge density in C/m^3. The local charge density can also be described as shown in Equation (7):

$$\rho_e = F\sum z_i c_i \tag{7}$$

Where F is the Faraday constant, z is the charge on the ion in question, and c is the average molar counterion concentration [13]. Then the electrical potential energy per mol of counterions can be described as:

$$W = -Fz\phi \tag{8}$$

The change in W from one plane to the next with width x can then be obtained by integrating Equation (8) to get [13]:

$$\Delta W = -\frac{F^2 z^2 x^2}{2\varepsilon\varepsilon_o} \tag{9}$$

By setting the absolute value of ΔW equal to RT, the point at which the potential energy is approximately equal to the thermal energy of the system, also known as the Debye Length [13]. The Debye length is the thickness of the diffuse layer that balances the system in electro-neutrality [14].

$$x \equiv \lambda_D = \left(\frac{\varepsilon\varepsilon_o RT}{2F^2 z^2 c}\right)^{1/2} \tag{10}$$

Or for symmetrical electrolytes at 25°C:

$$\lambda_D = \frac{9.61x10^{-9}}{(z^2 c)^{\frac{1}{2}}} \text{ [=] meters} \tag{11}$$

Within the Debye length there are two layers, hence the name the double layer. The layer closest to the surface is called the Stern layer and the layer further from the surface is the diffuse layer. The Stern layer is composed of counterions that are adsorbed to the surface while the diffuse layer is composed of diffuse counter and coions in solution (Figure 02).

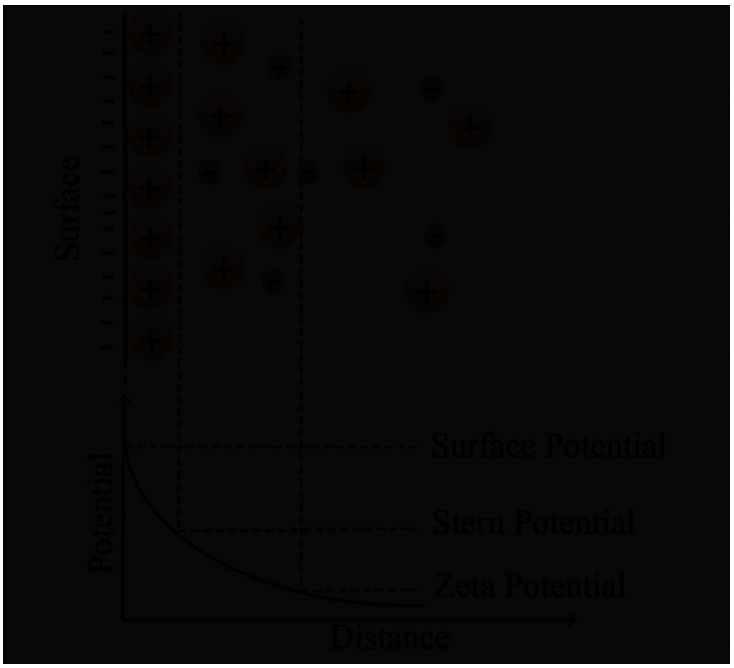

Figure 02: Sketch of a surface-solution interface showing surface potential, Stern potential, and zeta potential. Pluses represent cations and negatives represent anions [16]

2.2.2 Zeta Potential

The property that is taken from the theory of the electric double layer is that when a surface is in contact with a fluid, a surface potential is formed, attracting counterions to the surface in turn leads to the formation of the electric double layer. At the edge of the Stern layer where counterions become diffuse and not adsorbed, electric potential from the surface is not fully equalized by the counterion. The reduced bare surface potential from adsorbed ions at the barrier between the Stern and diffuse layer is called the zeta potential (ζ) [14] as seen in Figure 02.

One of the most common substrates to use for microfluidics is Poly (dimethyl) siloxane (PDMS; silicon) due to is ease of use, favorable cost, and rapid device fabrication. Much like other surfaces, PDMS has a surface potential and that surface potential will change depending on the chemical properties of the fluid in which it is contact with. Kirby and Hasselbrink [17] detailed how concentration of counterions and pH can both affect the zeta potential of various substrates used commonly in microfluidics, including PDMS. The paper details the use of pC which is defined as the negative logarithm (base 10) of the counterion concentration to normalize the zeta potential [18].

$$\text{pC} = (-\log(\text{c}z^2)) \tag{12}$$

By making this assumption and assuming a univalent electrolyte, Equation 13 can be used [18].

$$\zeta = a_0 + a_1 * pC \tag{13}$$

Where a_0 and a_1 are constants determined for each substrate.

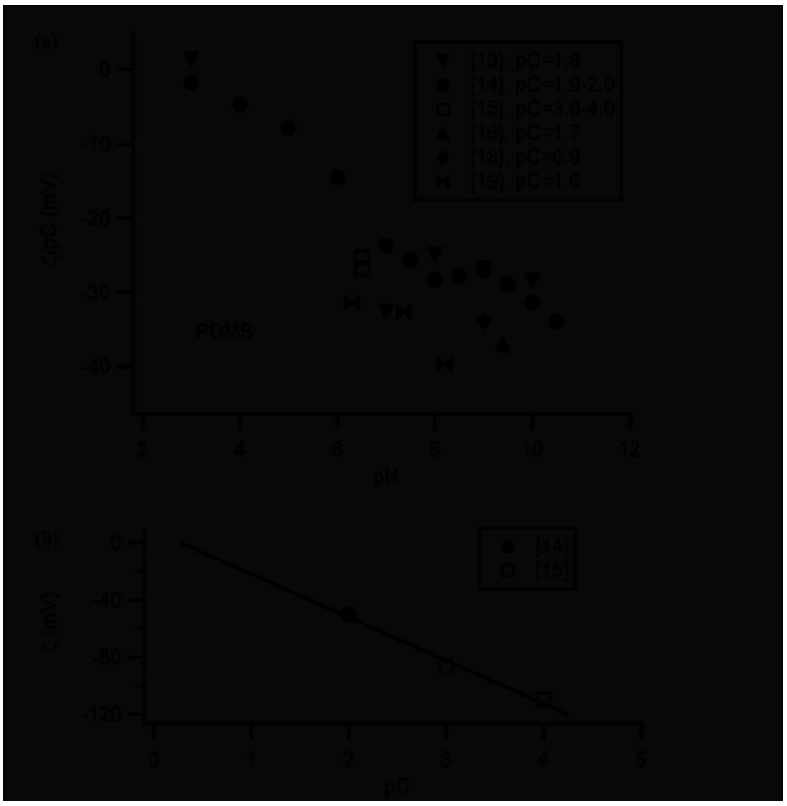

Figure 03: Shows plots of (A) $\frac{\zeta}{pC}(mV)$ vs. pH at different pC for PDMS and (B) ζ vs. pC of PDMS (6.5<pH<7). For this figure, closed symbols denote electroosmotic or electrophoretic measurements, open symbols denote streaming current or steaming potential measurements [18].

It was assumed that the PDMS was in its native state and did not have its surface modified to reduce the surface potential. The best fit line shown in Figure 03B was determined to have an a_0 value of 6.75 mV and a_1 value of -29.75 mV. If the data from Figure 03B is normalized, a_0 becomes 0 mV and a_1 becomes -27.65 mV.

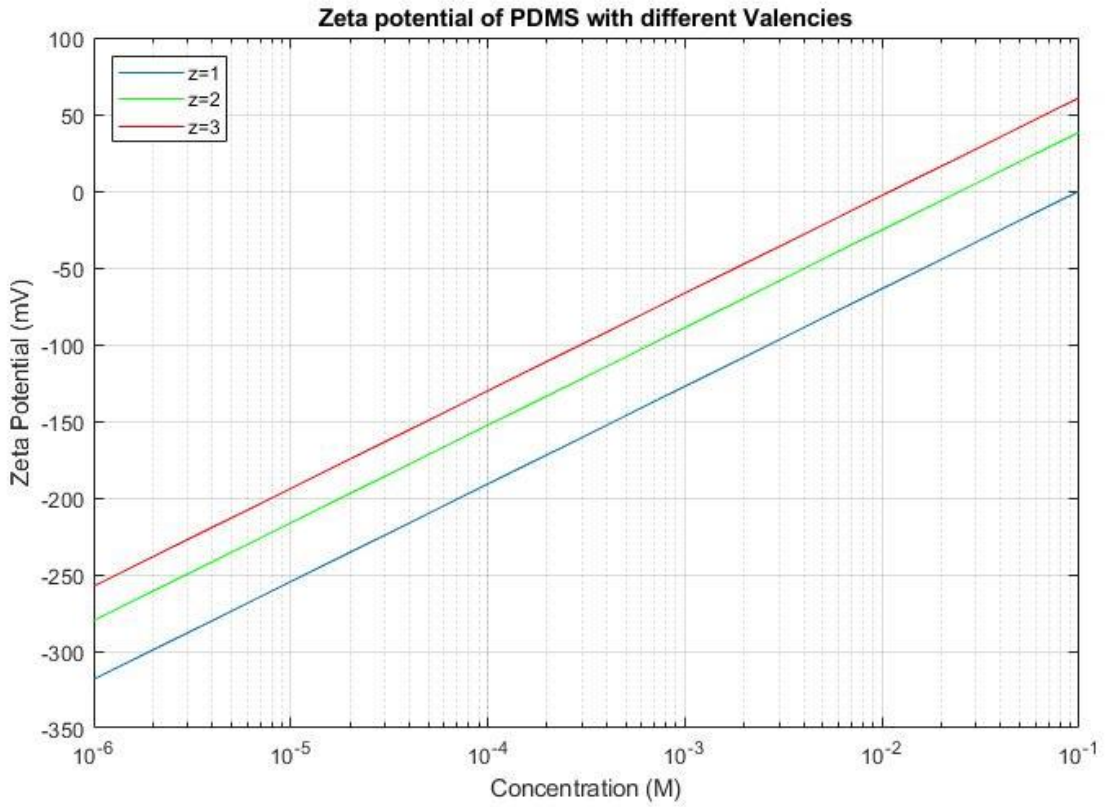

Figure 04: Plot of the normalized zeta potential equation against concentration with varying valency of ions in solution. As ion concentration increases the zeta potential of the surface decreases.

From the data shown by Kirby and Hasselbrink [17], the zeta potential for PDMS will decrease as the concentration of electrolytes in solution increases. Having the ability to control the zeta potential allows for increased control over the magnitude of the EO flow in the DC system.

As seen from Figure 04 and stated by Kirby and Hasselbrink [17][18], when ions are added to solution, the zeta potential of interfaces will change. As stated above, counterions in solution adhere to solid/liquid interfaces, forming the Stern and diffuse

layers that both contain higher concentrations of counterions than bulk solution. This is expressed in Equation (14) [19].

$$\rho_{oi} = \rho_{\infty i} * e^{-\frac{z_i e \psi_o}{kT}} \tag{14}$$

Where ρ_{oi} and $\rho_{\infty i}$ are the electrolyte concentration at the wall and electrolyte concentration in the bulk solution and ψ_o is the surface potential. Electrolyte concentrations can then be expressed as:

$$[Counterion]_x = [Counterion]_\infty * e^{-\frac{z_i e \psi_x}{kT}} \tag{15}$$

$$[Counterion]_o = [Counterion]_\infty * e^{-\frac{z_i e \psi_o}{kT}} \tag{16}$$

$$[Coion]_x = [Coion]_\infty * e^{+\frac{z_i e \psi_x}{kT}} \tag{17}$$

$$[Coion]_o = [Coion]_\infty * e^{+\frac{z_i e \psi_o}{kT}} \tag{18}$$

If there is a lack of counterions in solution to adhere to surfaces, the potential difference across the Stern layer (zeta potential) will more closely resemble values of the surface potential [19]. The Grahame equation relates surface charge density to the surface potential which can then be related to the zeta potential by assuming equivalency to the surface potential.

$$\sigma = \sqrt{8\varepsilon_o \varepsilon_m kT} \sinh\left(\frac{e\psi_o}{2kT}\right)\left\{\sum [Counterion]_0 + \sum [Coions]_o - \sum [Counterion]_\infty - \sum [Coions]_\infty\right\} \tag{19}$$

Where temperature (T) is equal to 25C, concentrations are expressed in mol/L, surface potential is in mV, and charge density is expressed in C/m^2. By applying this equation to the data in [20] the surface charge density of PDMS can be determined.

2.2.3 Chemistry of Solutions

By adding electrolytes to solution to change the zeta potential, conductivity of the solution will also change. The conductivity of a solution is determined by the types of ions in solution and their respective concentrations which is expressed as [13]:

$$\sigma_i = \Lambda_i c_i \tag{20}$$

Where Λ_i is the molar conductivity of the ion and c_i is the concentration of that ion. For diffused symmetrical ions in solution the fluid conductivity can be expressed as [13]:

$$\sigma_i = c(\Lambda_{anion} + \Lambda_{cation}) \tag{21}$$

Every ion and polar molecule diffusible into solution will have a different molar conductivity. Values for ion and polar molecule molar conductivities of organic and inorganic ions can be found in Appendix A.

2.3 Theory of Electrokinetics

Electrokinetics is defined as the study of the motion of bulk fluids or selected particles embedded in fluids when they are subjected to electric fields [13]. Electrokinetics can be applied to micro and nano systems to effectively manipulate particles, fluids, and how the two interact with each other. Electrokinetic theory covers electroosmotic flow (EOF) and electrophoresis (EP) and this section will cover electrokinetics and the relevant theory.

2.3.1 Electroosmotic Flow

Electroosmotic flow is a physiochemical hydrodynamic phenomenon that is defined as liquid flow relative to a stationary surface plus material attached relative to a stationary charged surface by an applied electric field [13]. As stated previously, all

surfaces in contact with a solution will form an EDL. From the EDL, the most important parameter dictating electroosmotic flow is the zeta potential at the surface. When an electric field is applied to a surface, the ions in the diffuse layer will begin to move parallel to the surface, with direction being determined by the surface potential. The velocity induced by the applied electric field tangential to a charged surface is the Helmholtz-Smoluchowski Equation [13].

$$U_{eo} = -\left(\varepsilon \frac{\zeta}{\eta}\right) \vec{E} \cdot \vec{t} \tag{22}$$

Where η is the dynamic viscosity of the fluid,ε is the permittivity of free space multiplied by the relative permittivity of the fluid, (ε_r *= 78.5 for water*), $\vec{E}$is the applied electric field , $\vec{t}$ is the unit tangent to the surface, and U_{eo} is the bulk fluid velocity. Another way to represent EOF velocity is through EOF mobility (μ_{eo}) which is shown in Equation (23).

$$\mu_{eo} = -\left(\varepsilon \frac{\zeta}{\eta}\right) \tag{23}$$

In an isolated case where only EO flow acts on a system, it will pull particles along with it, accelerating them due to Stokes' Drag. At steady state where the only force acting on the system is EO flow, particles in the suspending medium will travel at v_{eo}. EO flow will produce an almost uniform fluid velocity profile, unlike the parabolic flow profile produced by pressure driven flow. If particles experience an alteration in the velocity of the surrounding medium, they will experience a Stokes' drag force proportional to the difference in velocity of the particle relative to surrounding medium (Equation (23)).

2.3.2 Electrophoresis

Electrophoresis (EP) is defined as the movement of a charged surface plus material attached relative to a stationary liquid by an applied electric field [13]. Electrophoresis affects all particles with an induced charge suspended in an aqueous solution, where the particle is generally considered to be non-conducting. Under the application of an electrical field, a charged or uncharged particle will begin to accelerate in the direction of the opposite charge. If the particle has a net negative charge, it will accelerate towards the high potential (+) of the field and positively charged particles will accelerate to the low potential (-) of the electric field. When observing a particle in a diffuse medium, the particle will form a diffuse double layer around its' surface much like other surfaces in contact with an aqueous solution. The diffuse double layer of particles, much like other surfaces in contact with a fluid, will be primarily composed of oppositely charged ions. Depending on the strength of the surface charge on the particle, temperature of the medium, and the concentration of ions in solution will change the Debye length as shown in Equations (10) and (11).

When the Debye length of the particle is large compared to the radius of the particle ($\lambda_D \gg a$), the particle can be considered as a point charge. When the Debye length is small when compared to the radius of the particle the fluid velocity at the surface of the particle will exhibit characteristics of a "slip" surface ($\lambda_D \ll a$). With all these factors under consideration, the electrophoretic velocity of particles with large and small Debye lengths are [13][14]:

$$U_{ep} \approx \frac{2}{3}\frac{\varepsilon\zeta E_x}{\eta} \quad \lambda_D \gg a \tag{24}$$

$$U_{ep} \approx \frac{\varepsilon\zeta E_x}{\eta} \quad \lambda_D \ll a \tag{25}$$

The electrophoretic velocity of particles with large Debye lengths is called the Hückel equation and small Debye length, as indicated above, is the Hemlholtz-Smoluchowski equation. When observing a particle moving in relation to a stationary fluid, the equations above describe the velocity of a particle. When observing from the point of view of a stationary charged particle in an electric field the negative of the above equations will describe the velocity of the fluid flowing past the particle. Then by removing the electric field (E_x) from the equations, the above become the EP mobilities of large and small Debye lengths.

$$\mu_{ep} \approx \frac{2}{3}\frac{\varepsilon\zeta}{\eta} \tag{26}$$

$$\mu_{ep} \approx \frac{\varepsilon\zeta}{\eta} \tag{27}$$

Typically, biological particles will carry a negative surface charge and therefore carry a negative zeta potential. This causes biologics to be drawn towards the high potential of an applied electric field. If the electrical force on a particle is set equal to Stokes Drag on the particle the result is:

$$qE_x = 6\pi\eta U a \tag{28}$$

Where q is the net charge between the charged particle sphere and concentric spherical double layer. Equation (28) will give the equilibrium velocity through a fluid that a charged particle will achieve. By moving E_x to the right side, the U/E_x can be replaced

by μ_{ep} and the q can be determined charged particles of large and small Debye lengths in solution.

$$q = 4\pi\varepsilon\zeta a \tag{29}$$

$$q = 6\pi\varepsilon\zeta a \tag{30}$$

2.4 Dielectrophoresis

Dielectrophoresis (DEP) can be described as the second term in the multipole expansion of the electric force on a particle in a fluid. [2] This secondary force particles experience can be induce using an applied direct current (DC) or alternating current (AC). The DEP force is a consequence of a particle's polarizability, which accounts for differing electrical and physical properties of particles and the suspending fluid medium and non-uniform electric fields to cause particle movement. By altering applied electrical fields and properties of the suspending medium, DEP forces can be tuned to change direction and strength. This section will cover DEP and the theory behind it.

2.4.1 Dielectrophoretic Force

The DEP force on a given particle is dependent on the conductivity of the particle in relation to the conductivity of the surrounding medium for the direct current (DC) case and alternating current (AC) is dependent on the complex permittivity of the particle in relation to the surrounding medium and the frequency of the applied electrical field. Both DC and AC require the formation of a non-uniform electric field to have any effect on particles in the system.

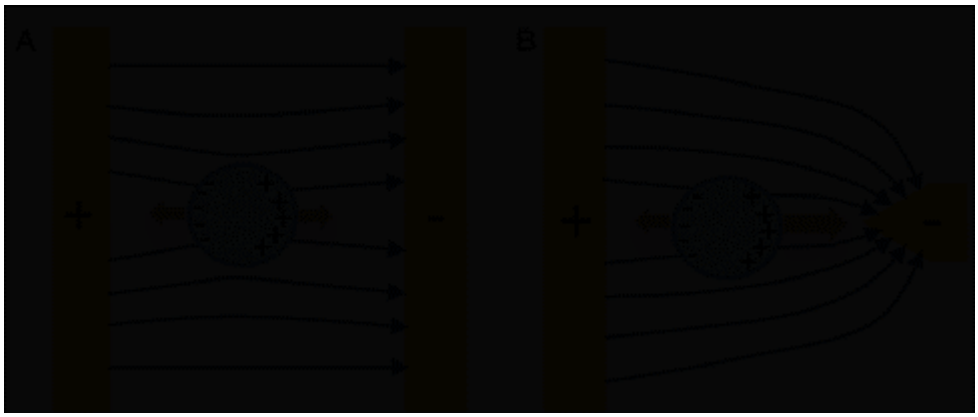

Figure 5: (A) a polarized particle in a uniform electric field experiencing equal and opposite forces at the poles, and (B) a polarized particle in a non-uniform electric field experiencing a force imbalance at the poles, i.e., a DEP force.

As shown above in Figure 6 A and B, a particle with differing electrical properties than the suspending fluid in the presence of an electric field will experience charge polarization. The continuum approximation of this polarization is described by the Clausius-Mossotti factor, or,

$$f_{cm} = \frac{\varepsilon_p^* - \varepsilon_m^*}{\varepsilon_p^* + 2\varepsilon_m^*}$$

Here ε_p^* and ε_m^* are the complex permittivities of the particle and medium respectively. The complex permittivity being a function of the electric field frequency, ω, and the constituents electric permittivity, ε and conductivity, σ.

$$\varepsilon^* = \varepsilon - j\frac{\sigma}{\omega}$$

where $j = \sqrt{-1}$.

Once polarized in an electric field, the particle experiences a Lorentz force at the newly induced poles, $\vec{F} = q_{\pm}\vec{E}$. If the electric field is that same or uniform, the Lorentz force is equal and opposite; however, if the electric field is non-uniform, there is an imbalance in the Lorentz force causing particle motion. As a consequence, much of DEP research revolves around creating conditions to achieve the desired Clausius-Mossotti factor, f_{cm}, and how to precisely create non-uniform electric fields to induce the desired force strength and direction.

For more complicated species in solution, e.g., cells, spores, the different "layers" of the organism are accounted for using what is known as the Shell Model.

2.4.2 Shell Theory

All theories detailed above are based on a single-shell spherical model. When looking at biologics, a single conductivity cannot be easily determined due to the heterogeneity of the particles [21]. Biologics contain multiple layers of different materials with varying electrical properties and therefore no one material can be used to represent the properties of the whole. When looking at complex structures each layer must be accounted for to reduce a multilayered system to a single conductivity and permittivity. The two-shell model is employed to combine the differing conductivities into a single value to be used in the CM factor [8]. Figure 05 shows an example of a case where the shell model would be employed.

Figure 06: Shows a particle with varying numbers of layers as it gets simplified to a single element [21].

When calculating an equivalent conductivity or permittivity of the particle using the two-shell model, each layer is accounted for from the innermost layer going outward to the outermost layer going two layers at a time. As an example of the two-shell model, the center particle in Figure 05 is assumed to have differing properties in the shell (R1, ε_1) and in the central region (R2, ε_2) [8][22]:

$$\varepsilon_{equ} = \varepsilon_2 \frac{\left(\frac{a_1}{a_2}\right)^3 + 2\left(\frac{\varepsilon_2 - \varepsilon_1}{\varepsilon_2 + 2\varepsilon_1}\right)}{\left(\frac{a_1}{a_2}\right)^3 - \left(\frac{\varepsilon_2 - \varepsilon_1}{\varepsilon_2 + 2\varepsilon_1}\right)} \tag{31}$$

$$\sigma_{equ} = \sigma_2 \frac{\left(\frac{a_1}{a_2}\right)^3 + 2\left(\frac{\sigma_2 - \sigma_1}{\sigma_2 + 2\sigma_1}\right)}{\left(\frac{a_1}{a_2}\right)^3 - \left(\frac{\sigma_2 - \sigma_1}{\sigma_2 + 2\sigma_1}\right)} \tag{32}$$

These equations should match the image

By using the two-shell model, the multilayered complex structure can be represented by a single permittivity and conductivity. This allows multilayered biologics like yeast, with

differing electrical properties in the outer wall, inner wall, membrane, and cytoplasm to be simplified to a single conductivity value and single permittivity value [28].

With the continuum approximation of the particle electrical polarization defined, i.e., the Clausius-Mossotti factor, the dielectrophoretic force exerted on a spherical particle can be expressed as:

$$\vec{F}_{DEP} = 2\pi a^3 \varepsilon_m \, Re[f_{cm}] \vec{\nabla}(\vec{E}_{rms} \cdot \vec{E}_{rms}) \tag{33}$$

where a is the radius of the particle in question, ε_m is the absolute permittivity of the medium, $\vec{E}_{rms}$ is the root mean square value of the electric field, and $Re[f_{cm}]$ is the real part of the Clausius-Mossotti (CM) factor.

$$fcm = \frac{\varepsilon_p^* - \varepsilon_m^*}{\varepsilon_p^* + 2\varepsilon_m^*} \tag{34}$$

$$Re[f_{cm}] = \frac{(\sigma_p - \sigma_m)(\sigma_p + 2\sigma_m) + \omega^2(\varepsilon_p - \varepsilon_m)(\varepsilon_p + 2\varepsilon_m)}{(\sigma_p + 2\sigma_m)^2 + \omega^2(\varepsilon_p + 2\varepsilon_m)^2} \tag{35}$$

where ε_p^* is the complex permittivity of the particle, ε_m^* is the complex permittivity of the medium, σ_p is the absolute conductivity of the particle, σ_m is the absolute conductivity of the medium, and ω is the angular frequency of the AC field. The complex permittivity can be expressed as [21]:

$$\varepsilon^* = \varepsilon - i\frac{\sigma}{\omega} \tag{36}$$

When looking at a case that only uses a DC field where $\omega = 0$, Equation (35) reduces to [8]:

$$Re[f_{cm}] = \frac{\sigma_p - \sigma_m}{\sigma_p + 2\sigma_m} \quad (37)$$

The CM factor determines how the DEP force will act upon each individual particle based on the polarizability of the particle relative to the fluid. When conductivity of the particle in question is greater than that of the suspending medium, the DEP force imparted on the particle will be positive DEP. Positive DEP will attract particles to stronger electric field region, as seen in Figure 7A. Conversely, when the conductivity of the suspending medium is greater than that of the particle, the DEP force is negative, and particles will be repelled from regions of strong electric fields as seen in Figure 7B [23]. When looking at the equation, it should be noted that the maximum CM factor for positive DEP is 1 and the maximum CM factor for negative DEP is -0.5 as shown in Figure 7.

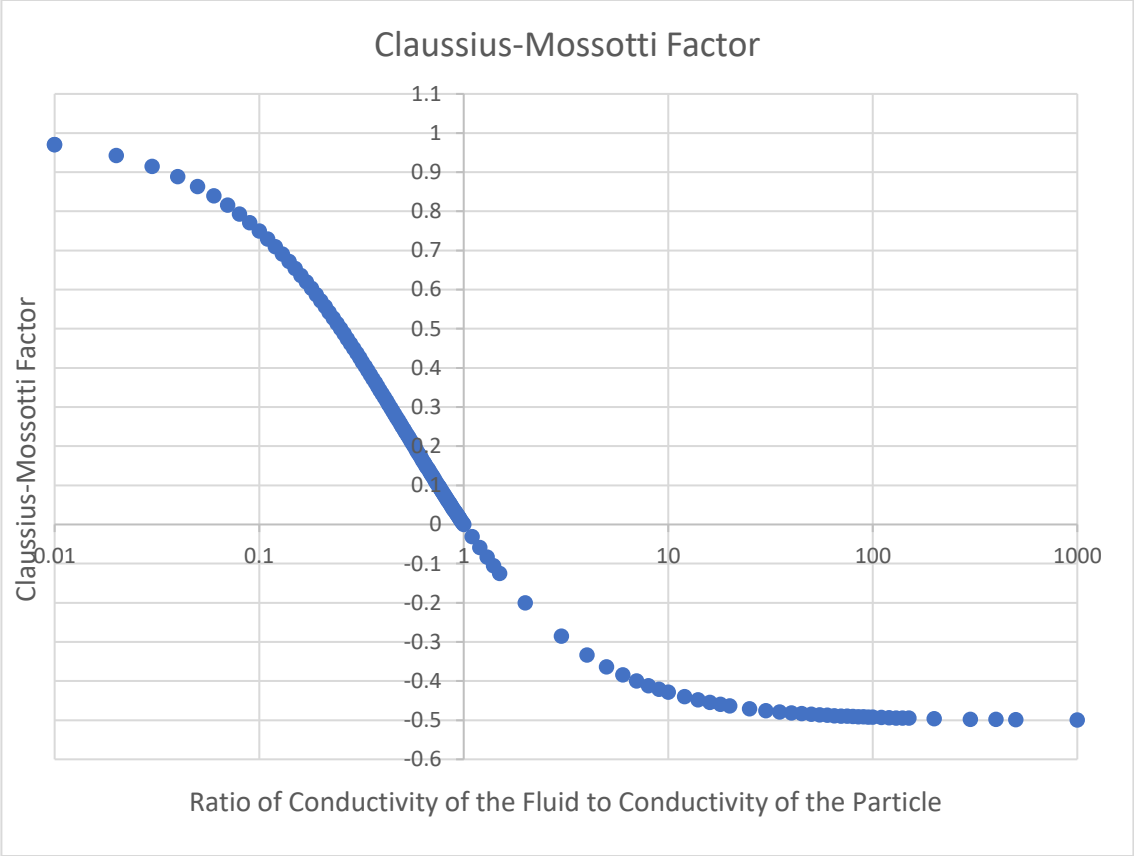

Figure 07: Shows the CM factor in relation to the ratio of the conductivity of the fluid to the conductivity of the particle in question.

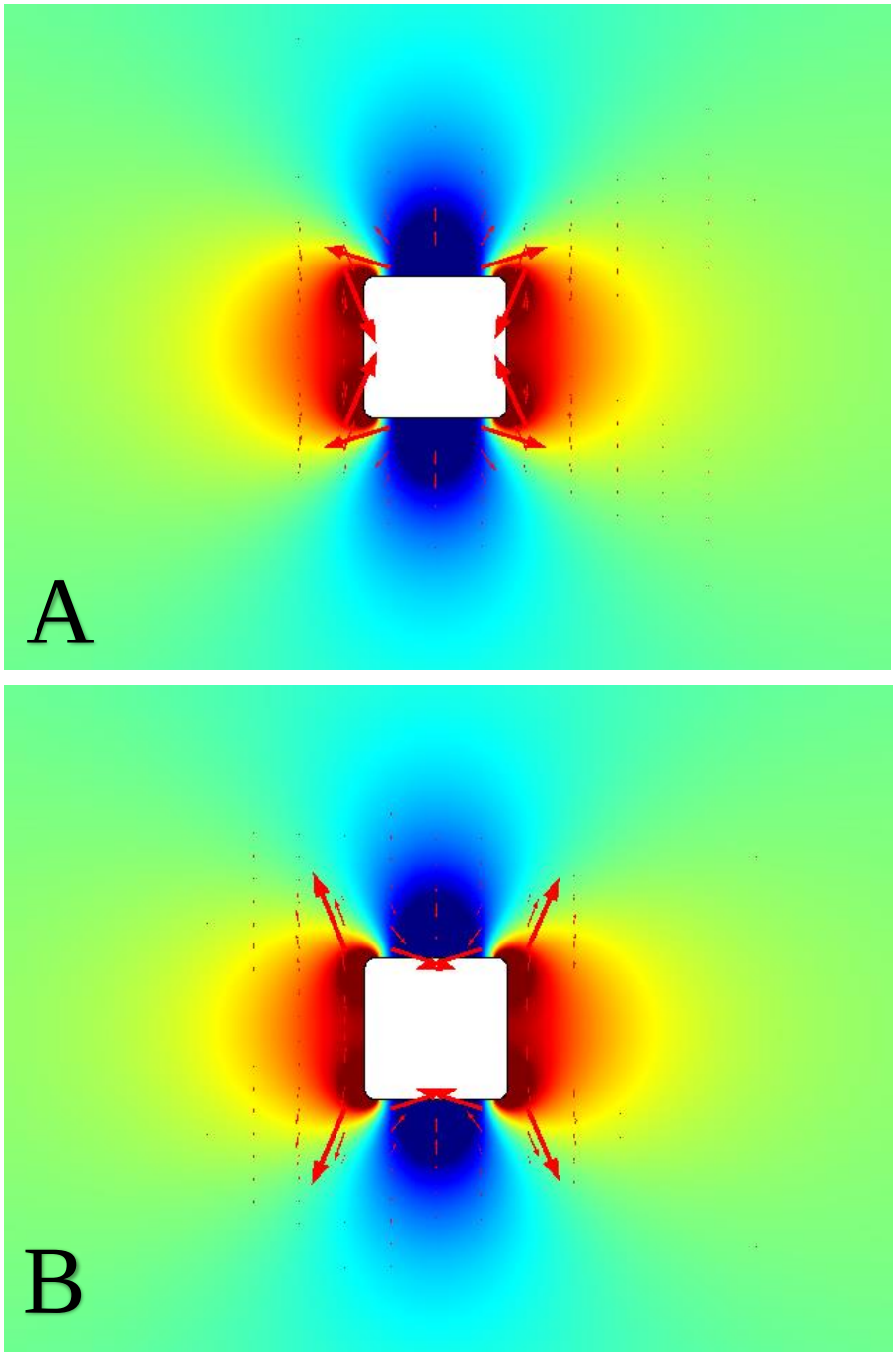

Figure 08: Shows the direction of the DEP force for an applied DC electric field with a square insulative obstacle with the electric field running North to South (A) vectors positive DEP, $\varepsilon_P^* > \varepsilon_m^*$, force, (B) vectors positive DEP, $\varepsilon_P^* < \varepsilon_m^*$, force.

As shown above in Figure 8, a positive DEP force will attract particles to the regions of strong electric fields (red), and negative DEP force will attract particles from the regions of weak electric fields (blue) as indicated by the arrows.

From the DEP force the DEP mobility can be determined and is found to be [8]:

$$\mu_{DEP} = \frac{a^2 \varepsilon_m Re[f_{cm}]}{3\eta} \tag{40}$$

2.4.3 Particle Properties

When using iDEP it is essential to understand the physical and electrical properties of desired and undesired particles being observed. iDEP can be applied to both organic and inorganic particles of a wide array of shapes, sizes, and electrical properties. By understanding relationships between these properties and how they affect the DEP force, different microscopic particles can be filtered.

Electrical properties that are essential to understand are the permittivity and conductivity. All materials have an electrical conductivity and a permittivity. DEP requires that both the electrical conductivity and permittivity of the particle and fluid are known, so that a device using DEP may be optimized to perform its function. This project focuses on DC electrical fields so the $Re[fcm]$ is dictated solely by the conductivity of the particles and medium, so Equation (40) will be used to calculate DEP force and Equation (41) will be used to find DEP mobility. For applications of DEP in particle separation from a medium, the conductivity of various solid and liquid materials can be found throughout literature.

Physical properties of particles determine how they will interact with the fluid and be affected under both dielectrophoretic and electrokinetic phenomena. The primary

property that affects both is the volume and shape of particles. As shown in Equation (40) for dielectrophoretic force, the radius is raised to the third power indicating a large reliance on particle size. In Equation (5) for drag force on a particle, the radius is included and plays a role in how much the flow of surrounding medium will affect the movement of the particle in space. Properties such as density do not play a significant role in how particles act due to the scale at which these forces are acting on and the similarity in densities of biological particles to water.

2.5 MEMS Manufacturing Techniques

In this thesis there were two manufacturing techniques used to create devices. Both techniques were performed on silicon wafers and soft lithography was implemented to create devices. All in house manufacturing and casting was done in the Cal Poly Microfabrication lab and off-site manufacturing was done in the UC Santa Barbara microfabrication lab.

2.5.1 Reactive Ion Etching

RIE is an anisotropic etching technique that has high selectivity. Plasmas that are used in RIE are chlorine (Cl), chlorine precursors, fluorine, iodine, and bromine. When silicon is undoped and in the presence of Cl or Cl_2, it will etch at a slow rate. However, when the silicon substrate is negatively doped (n-type), the wafer will etch at high rates when in contact with Cl, but not Cl_2 [24].

On an undoped Si wafer Cl atoms tend to chemisorb to the surface of the Si wafer, but not break Si-Si bonds and attachment of additional Cl atoms is hindered by

repulsion by the Cl monolayer. Cl penetration drastically increases upon plasma activation and bombardment commencement. Surfaces exposed to ion bombardment will etch at a much higher rate than those not exposed. Since sidewalls of the etching area do not receive much exposure to the ion bombardment, they will etch at a much slower rate which is what allows RIE to have its high aspect ratio [24].

On an n-type wafer, Cl atoms will chemisorb to the surface and ionically bond with Si, producing silicon chlorides that will etch the n-type Si wafer. With bombardment similar aspect ratios will be produced, but there is the additional consideration of the chemical reaction between the Cl and Si which could etch away at the sidewalls of the channel. Chemical reactions with sidewalls can be reduced by reducing the partial concentration of Cl and increasing concentration of an inhibitor forming gas ($BCl_3, CCl_4,\ SiCl_4$, or fluorinated precursors) to reduce undercut [24].

2.5.2 Photolithography

Photolithography is a microfabrication process in which photoresist is patterned onto an Si wafer and soft lithography is used to lift the pattern from patterned photoresist. Photolithography is performed independent of doping of the Si substrate and is instead dependent on the photoresist used. There are two polarities of photoresist; positive and negative, and each have their benefits and drawbacks [24].

When choosing the type of photoresist to use, two properties must be considered: sensitivity and resolution. Sensitivity refers to the light energy required to induce the chemical change in the photoresist. If a photoresist is more sensitive, it will take less light energy to cause the change and less sensitive resists will do the opposite. Resolution refers to the smallest feature reproducible in photoresist. Positive photoresists will be

removed in areas exposed to UV light and will have a higher resolution than negative resists. This is because developer does not permeate the positive resist that isn't exposed to light while developer does permeate negative resist in both exposed and unexposed regions leading to pattern distortion. However, negative photoresists have a higher sensitivity, better substrate adhesion to certain materials, and significantly lower operating costs of replicating devices after an SU-8 negative has been fabricated.

To perform photolithography, a wafer is used as the substrate and is coated in photoresist. A mask with the necessary polarity is then used to cover the wafer during exposure. Upon UV exposure, the chemicals in the resist will react depending on the photoresist used. Next the wafer is placed in developer where the undesired resist is removed and ready for soft lithography.

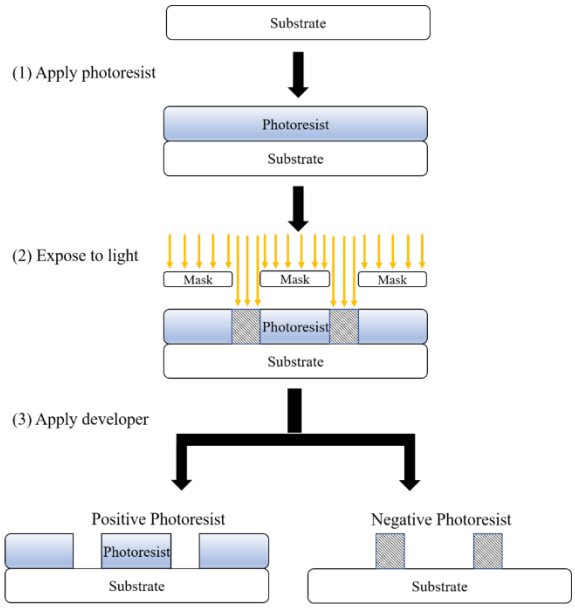

Figure 09: Example of resulting patterns from positive and negative photoresists [25].

2.6 Fluid Heating

2.6.1 Joule Heating

When running an electrical current through a conducting material or medium, a phenomenon called Joule or Ohmic heating will occur. The power dissipated by joule heating on a system is described by Equation (42). When working with a system that has an electrical current present it is important to control the heat of the system, so materials do not melt, and fluids don't boil [26].

$$\mathrm{P} = \mathrm{I}^2 R = VR = \frac{V^2}{R} \tag{41}$$

This equation represents the power dissipated by the resistive fluid and will lead to the progressive heating of a system [26].

In a microfluidic system, Joule heating is concentrated around areas of high current. Causes of regional heating of fluid from Joule heating include: regions around an electrode, in constriction in a microfluidic device that force current through small openings, and regions along in the shortest path from one electrode to the next [32].

2.6.2 Electrothermal Flow

The electrothermal flow (ETF) is an electrohydrodynamic phenomenon that causes electrothermal forces to act on the bulk fluid in the presence of conductivity or permittivity gradients in an electrolyte solution due to temperature gradients [32]. Temperature gradients causing flow imparting a drag force on particles that can be on the order of or larger than the DEP force [32]. This phenomenon exists in both the DC and AC regimes. At frequencies close to zero, electrothermal flow velocity can be large and

at higher frequencies the electrothermal flow will be a smaller contributor to fluid velocity [32]. The highest velocities will coincide with the same regions described in Joule heating.

2.7 Biofluid Applications

The possibilities for the application of DC DEP are extensive and when used in biofluids, could turn out to be a strong tool for filtration for diagnostics. When using DEP on biofluids it all comes down to fine tuning the parameters of the device to optimize the device for the desired environment.

2.7.1 Blood

A major area of interest in DEP filtration is for particle filtration in blood. Using microfluidics allows for low volumes and applying iDEP can separate specific particles like cancer cells, red blood cells, leukocytes, or proteins. By using iDEP on blood, cancer cells could be captured, concentrated, and tested to make a diagnosis [2]. Something like this could be an add on to already existing dialysis technology where blood could be tested while undergoing dialysis or done on low volume blood testing since the volume requirements are on the scale of microliters.

2.7.2 Saliva

Another readily available biofluid to test is saliva, which in recent studies has shown that saliva can contain DNA of cancerous cells that could indicate for pancreatic, breast, and periodontal cancers. Application of iDEP could allow for cell or DNA separation from macroparticles and allow for easy access to possibly cancerous DNA or

test for other diseases. Even though cancer analysis for saliva using DC iDEP has yet to be performed on the range of cancer types observed in this study, it leaves open the possibility for new realms of early cancer detection [27].

CHAPTER 3 COMSOL TESTING AND DEVICE DEVELOPMENT

When this thesis began, a legacy wafer was inherited so the focuses was on: determining if the given device will operate as intended, what improvements could be made to the device, and if the device does not perform its desired task, what changes could allow future devices to function correctly. Additionally, it should be noted that even though this is an inherited project, there is little to no; information, 3D models, COMSOL models, or documentation on what was performed previously to determine the viability of the legacy device design. The lack of background information proved extremely difficult in all aspects of the project as information had to be resynthesized to explain the design choices. Therefore, a comprehensive analysis of the device will be conducted through COMSOL simulations and experimental testing.

3.1 Legacy Device

The first technique used to create the legacy device was reactive ion etching (RIE). Fabrication of the legacy device was done at University of California Santa Barbara since their microfabrication lab manufacturing capabilities allow for RIE of the small features ($\sim 1.2 \mu m$) designed into the legacy device.

The legacy device is designed to be an iDEP device where particles flow into the device and into the main chamber where the insulative post array resides. Once particles enter the main chamber, they will either be repelled or unaffected by the DEP force. Particles acted upon by DEP will be levitated above the post array and carried by pressure driven cross flow to the outlet on the other side of the main chamber. Unaffected particles will descend through the insulating post array under dominant EKs, then carried

by pressure driven flow to the lower outlet channel. By having both affected and unaffected particles, the legacy device can separate two type of particles at a time.

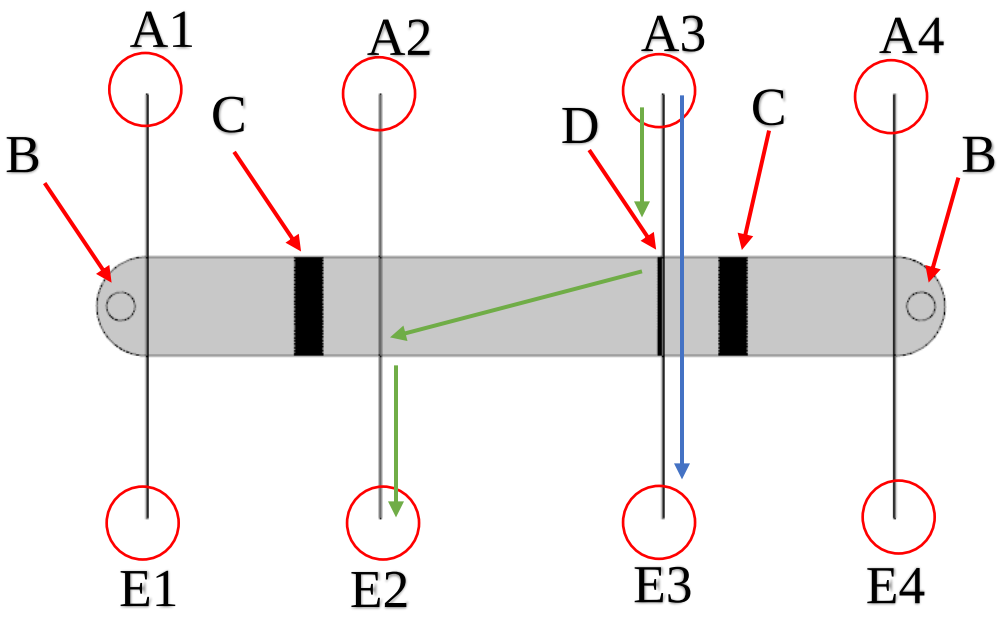

Figure 10: Shows the legacy device and various important regions, (A) fluid inflows (B) electrode ports, (C) bubble weir filters, (D) insulating post filter, and (E) fluid outflow. The blue arrow indicates path of levitated particles and green arrow indicates path of particles passing through the filter.

The device has five major components as seen in Figure 10: four fluid inflows (A1-4), two electrode ports (B), two bubble filters (C), one particulate filter (D) composed of insulating posts, and four fluid outflows (E1-4). The channels of the device stand 15 microns tall. Particles flow into the device via A3 fluid inflow and are intended to exit through either outflow E2 or E3. Inflow A2 is designed to equalize the inflow of

fluid to the central region of the device and deliver into the device. E3 is the outflow port that the particles that are levitated will exit through and E2 will have the unaffected particles. Inflows A1 and A4 deliver fluid to the electrode ports with the intent of cycling fluid in the electrode chambers to reduce temperature and remove bubbles formed by electrolysis. Bubble filters are composed of weirs approximately 1.2μm in width with 2 μm wide channels between them. These filters are included to prevent bubbles from entering the main chamber of the device. In the event of bubble entrance to the main chamber, the electric fields will become distorted, fluid flow will become disordered, and cause an unwanted pressure driven flow in the device. Finally, the insulating post filter is where iDEP filtration occurs. Particles will either be levitated above the posts and exit at E3 or will pass through to exit at E2 (Figure 10). The insulating post region is the "filter" in this thesis.

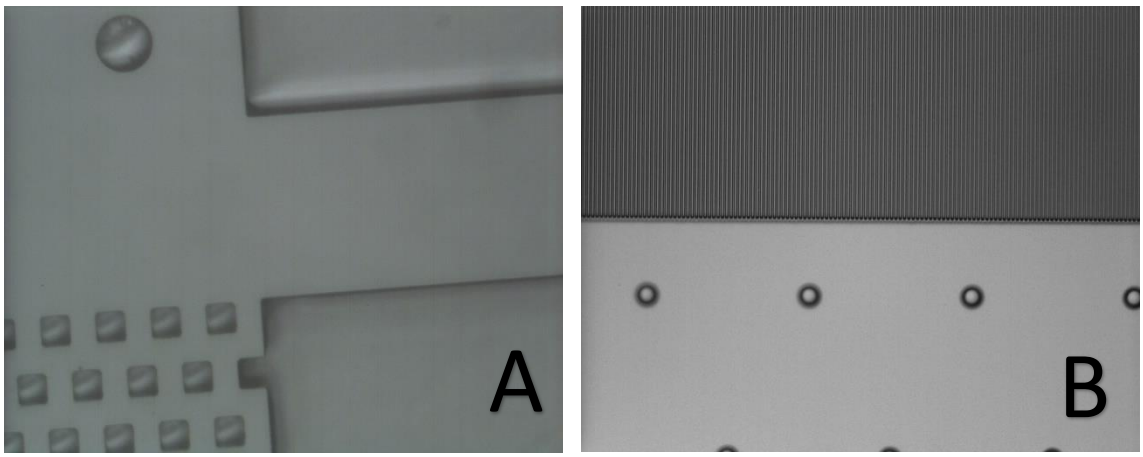

Figure 11: Zoomed in images of the legacy device focusing on (A) the array of insulating posts in the filter with an exit channel going off to the right and (B) the bottom of the bubble weirs filter.

3.2 Simulation Simplification

In order to properly test the viability of this device and its ability to use DC to perform iDEP and avoid filter fouling, the first step was to construct a recreation of the device in COMSOL and test how the device as a whole operated. However due to the lack of source files, exact dimensions of the components of the device had to be measured. Imaging the wafer was done with the microscope in the Cal Poly Microfabrication lab and dimensions of components were measured based on a known length, using ImageJ. Measurements of the device resulted in the dimensions shown in Table 01.

Table 01: Dimensions of components of the legacy device.

Component	Length	Width	Distance between elements
Insulating Posts	12.5μm	12.5μm	7.5μm
Bubble Filter Weirs	1mm	1.2 μm	2 μm
Inlet/Outlet Channels	1cm	55 μm	NA
Main Chamber	3cm	2mm	NA

Due to the overall complexity of the device, simplifications to the simulation were necessary to reduce computation times and improve the information regarding individual elements of the model and how they each contribute to the overall device operation. These smaller simulations were created in order to find the optimal operating conditions and determine if certain components could be excluded entirely or have as assumptions in the simulation. These simplification simulations focused simulations focused on the bubble filter weirs and the insulating post array.

The first simulation that was conducted to simplify the full simulation was to test the bubble filter weirs. The focus here was to look at the EO flow across the weirs and to determine if the weirs imparted hydrodynamic resistance on the fluid that would travel

through them. The parameters set for this simulation are shown in Table 02 and an image of part of the geometry tested is seen in Figure 11.

Table 02: Parameters of weir EO testing.

Parameter	Value
Voltage potential	40, 80, 120, 160, 200, 240, 280, 320, 360, 400 V
Length of chamber	1.2 μm
Width of chamber	320 μm
Weir length	12.5 μm
Weir width	1.2 μm
Distance between weirs	2.0 mm
Relative permittivity of water	78.5
Conductivity of water	1 $\mu S/m$
Zeta potential	-0.01 V

When observing an isolated case where only iDEP acts on particles, the particles in the simulation will migrate away from regions of high ∇E^2 to regions of low ∇E^2 (Figure 12). This test assumes that the zeta potential is 0 in order to isolate the effects of the DEP force. The two acting forces in this system are the DEP force and drag force on moving particles in the system to show that the drag force only affects the speed of particle movement.

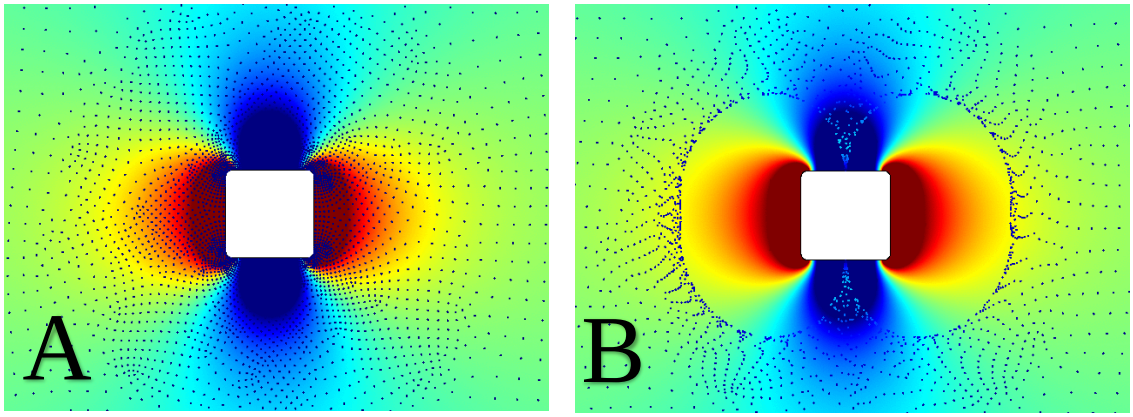

Figure 12: Shows particles with negative DEP properties at (A) the starting position of particles around an insulating post and (B) particles at t>0 around an insulating post.

3.3 Device Verification and Optimization

3.3.1 iDEP Verification and Optimization

To allow the device to operate as intended, particles must be able to be filtered. The desired outcome is to separate our desired particles from other particles in a medium and this can either be achieved by allowing desired particles to pass through the filter and keep undesired particles above the post filter or allow undesired to pass through the filter and keep desired particles above the post filter. To optimize the device there needs to be a knowledge of the required voltage potential across the device to produce a DEP force large enough to filter particles. To test this, a simulation on a focused region of the posts was used and is shown in Figure 13. This geometry was chosen to only look at how particles acted around the insulating post array.

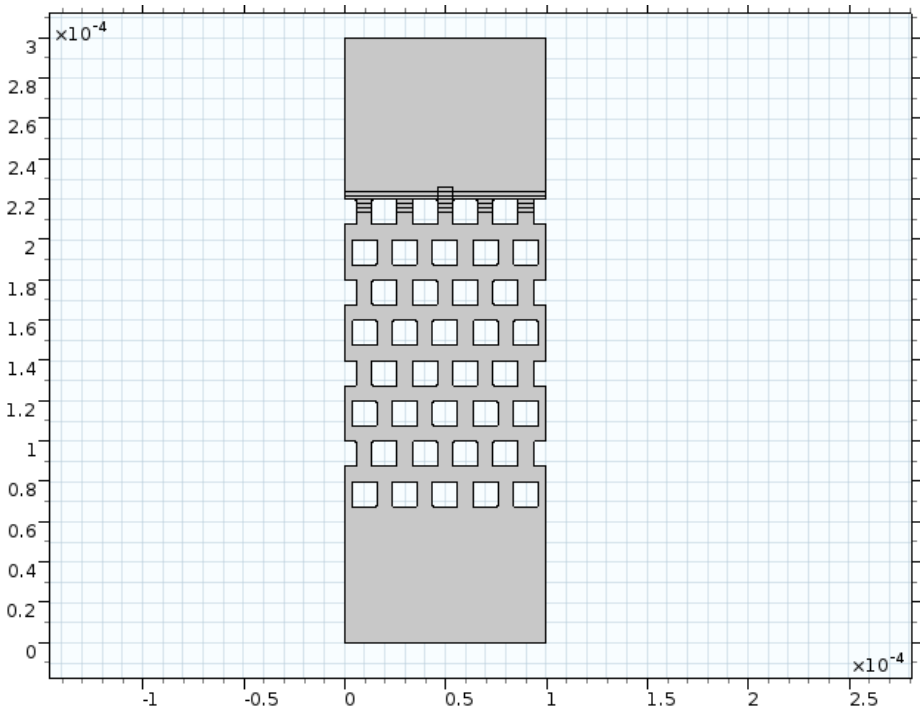

Figure 13: Shows the geometry used in particle separation test for optimization and used to isolate iDEP force acting on particles as they encountered the top row of posts.

The test was designed to have a particle with different electrical properties. Particles were released from the chamber above the posts and acted on by DEP force and drag force induced by EO flow. Parameters for the simulation are detailed in Table 03. The voltage potentials were chosen to reflect the same electric fields produced in the optimization tests. The geometry was meshed using free triangular, semiconductor with a refinement of fine.

Table 03: Parameters of post and particle testing.

Parameter	Value
Voltage potential	10, 20, 30, 40, 50, 60, 70, 80, 90, 100 V
Length of chamber	300 μm
Width of chamber	100 μm
Post side length	12.5 μm
Distance between posts	7.5 μm
Relative permittivity of water	78.5
Conductivity of fluid	1 $\mu S/m$
Conductivity of particle	100 S/m
Zeta potential	-0.01 V

Due to the physical constrains of achieving a CM factor of -0.5, it was necessary to simulate particles with CM of -0.10, -0.20, -0.25, -0.30, -0.40, and -0.50, with all other properties remaining the same to simulate more real world conditions where the conductivity of the surrounding fluid is larger than that of the particles or the conductivities are similar in magnitude.

When simulating DEP, COMSOL assumes the system is operating with AC and therefore changing the conductivity does not affect the simulation. The COMSOL Particle Tracing User's Guide for version 5.4 states that stationary fields are defined by Equation (33). To account for this, the permittivity of the fluid was defined first since it is a contributing factor of the DEP force then the permittivity of the particle to achieve a particular CM factor was calculated using Equation (34). Changing the permittivity of the particle only affects the CM factor so this modification should not affect the overall accuracy of the simulations. To account for this, a parameter called FCM_mod was created in COMSOL. The permittivity of the fluid is entered into both the fluid and particle permittivity values in the DEP module. Particle permittivity of the fluid is then

multiplied by the value of FCM_mod desired. Values for FCM_mod are shown in Table 04.

Table 04: Shows values for FCM_mod to correct COMSOL simulations.

FCM_mod	CM Factor
1	0
0.72	-0.10
0.5	-0.20
0.4	-0.25
0.305	-0.30
0.14	-0.40
1e-6	-0.50

Additionally, since COMSOL only looks at the AC regime, the DEP force equation used in COMSOL includes a root mean square of the electric field gradient which results in Equation (40). This Since these simulations are operating in the DC regime, the gradient of the electric field for DC must be included manually for plots and in the DEP module the permittivity of the particle and fluid were multiplied by 2 to account for this. This was confirmed through a quick simulation where the frequency of the electric field was set to be 0 Hz and 50 GHz using a parametric sweep. The particles in the simulation did not change trajectories, velocities, or locations at the end of the simulated time frame and therefore must be included by altering parameters.

Once the trapping conditions of the posts were determined, the crossflow required to create a foul-less filter was determined. This was accomplished by taking the simulation used for particle trapping conditions and modifying it to have an inlet channel across the top of the posts with a width of $75\mu m$ and the overall geometry can be seen in Figure 14.

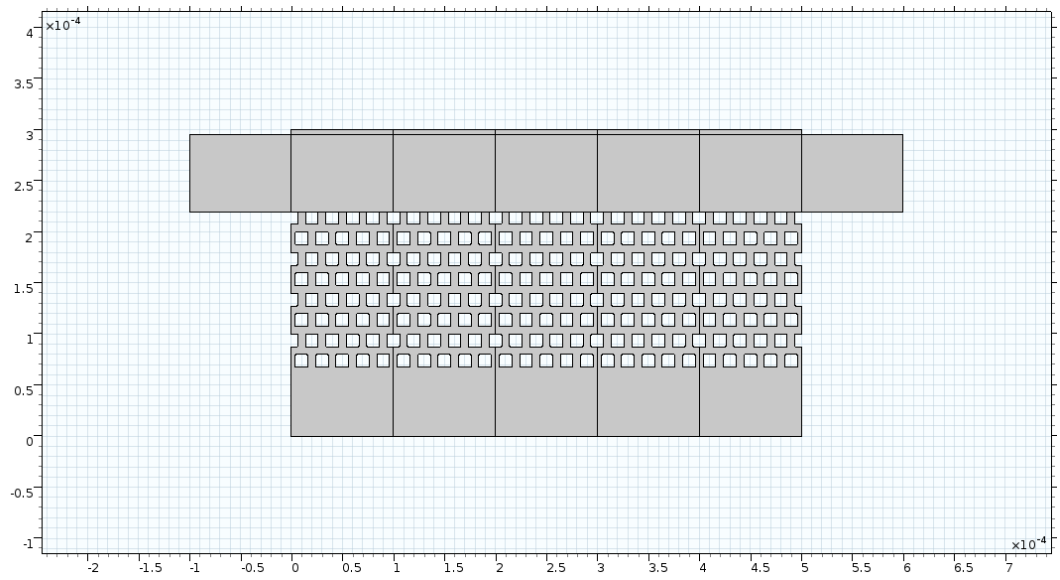

Figure 14: Geometry used for simulating cross flow with particles of varying properties and in varying aqueous solution conditions.

The inlet for fluid and particles was defined as the channel inlet on the left side and outflow was defined as the right side of the channel. The top and bottom of the geometry were defined as open boundaries to allow EO flow to occur without recurrent flow. The rest of the boundaries were defined as walls. Using the trapping simulation an estimate of the inlet velocity required to levitate particles could be made. For the voltage potential the ground was defined at the top of the geometry and the high potential was defined at the bottom of the geometry. For voltage potentials of 10 to 100V, inlet velocity range was tested between 1 mm/s and 10 mm/s.

Table 05: Parameters for cross flow simulations.

Parameter	Value	Units
Inlet/outlet velocity	1, 2, 3, 4, 5, 6,7, 8, 9, 10	mm/s
Voltage potential	10, 20, 30, 40, 50, 60, 70, 80, 90, 100	V
Net zeta potential	-0.005	V
Fluid Permittivity	78.5	
CM Factor	-0.10, -0.20, -0.25, -0.30, -0.40, -0.50	
Particle radius	2.5E-6	m

3.3.2 Fluid Dynamics Verification and Optimization

Once the conditions to perform iDEP and iDEP levitation were determined, the next main component that needs verification is the fluid dynamics of the device and where particles that pass through the insulating post array will end up. This is extremely important to the foul-less component that is in question. Even if the posts are optimized and properly repel or allow particle passage, if the fluid dynamics don't properly remove particles from the system and they get stuck somewhere in the device, the device does not meet the operation requirements.

To determine how the fluid dynamics of the system perform, a full model of the device was constructed in 2D and simplified as needed from the conclusions of other optimization tests. The posts were excluded from tests that looked at how particles with an CM factor of 0, under the assumption that since they would only be acted on by Stoke's drag and therefore follow the path of the fluid. The device would operate properly if the fluid flow would take the particles from the top fluid flow inlet to the bottom fluid flow outlet. For particles with a CM factor not equal to 0, the simulation included the insulating posts, but did not consider dielectric force on the particles. Instead the simulation looked at if the fluid flow in the x direction remained positive from the top fluid flow inlet all the way to the top fluid flow outlet. The models used for this set of simulations can be seen in Figure 15.

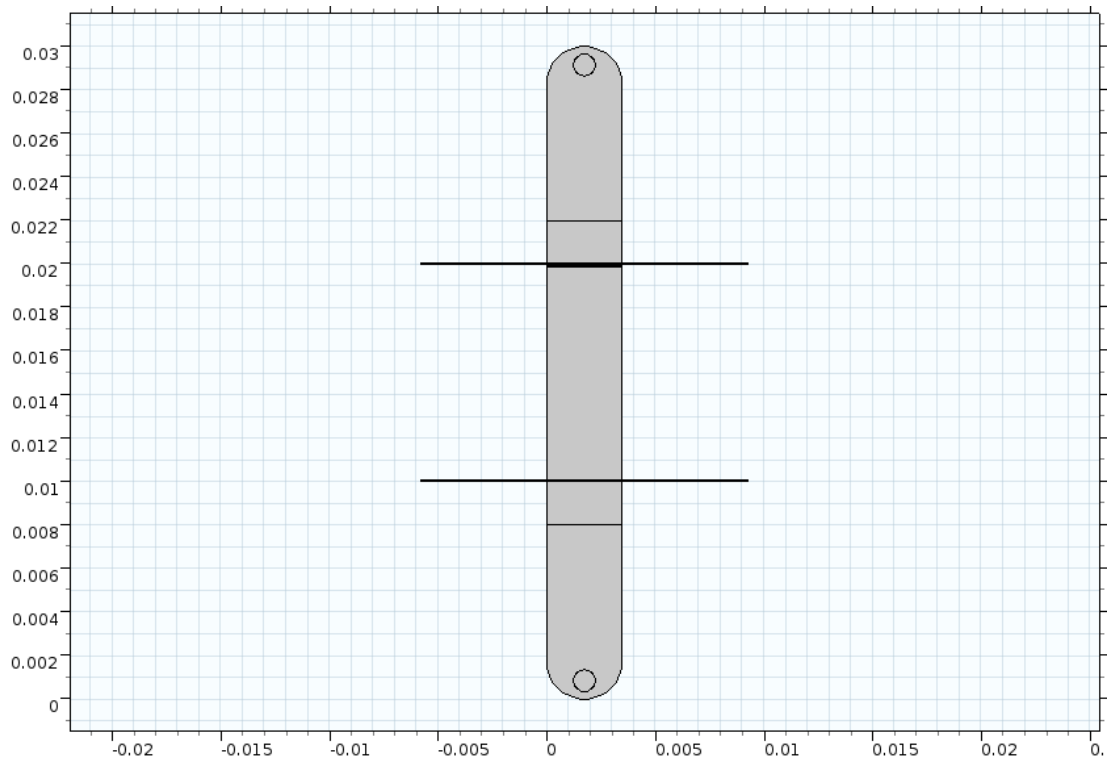

Figure 15: Image of the geometry of the fluid dynamics verification and optimization simulations for CM factor equal to 0.

Device was meshed using free triangular, semiconductor at a refinement of finer. Images were taken for each of the simulation parameter combinations with streamline of fluid velocity. Depending on how the streamlines acted, an inference of where particles would likely go was made.

3.4 Legacy Device Lab Testing

The legacy device needed to be tested to ensure the viability of the simulations performed within this thesis and to determine if the device operates as it is intended to. In the current wafer there are different devices in total. Two of the devices are the complete constructs of the legacy device and the other six are slight variations of one another, based on the iDEP device detailed by Moncada-Hernandez [8], but modified to include

the post arrays included in the full builds. PDMS casted devices were made for all devices for testing as they all include a post array and one of the main goals is to determine the functionality of the insulating array of posts and their ability to perfume insulative DEP separations.

3.4.1 Device Construction

All devices tested were created in the Cal Poly Microfabrication lab over several rounds of casting devices with some devices were PDMS plasma bounded to glass and some were PDMS plasma bonded to PDMS. In the end it was found to be easier to build devices by binding PDMS to glass for observation means under SVM due to the variable thickness from fabrication of a PDMS substrate. This extra layer of PDMS often resulted in the channels being too far from the objective to observe on the SVM. PDMS casting process is detailed in Appendix C.

3.4.2 Experimental Setup

Testing of the devices was needed to determine their functionality and relatedness to the simulations run. The conditions determined to be used in the iDEP verification step were approximately room temperature water, NaCl was used as the symmetrical salt used in solution, and yeast was chosen as the particle.

Table 06: Geometric and electrical properties of four-layer yeast model [28]

Region	Thickness/ Radius (μm)	Relative Permittivity	Conductivity (S/m)
Cytoplasm	-/2.5	53	1
Membrane	0.008/2.508	5	10e-7
Inner Wall	0.2/2.708	60	0.012
Outer Wall	0.05/2.758	6.2	0.021
Suspending Medium	-	78.5*	0.001*

*Indicates altered parameter from source.

To prep devices for testing they needed to be primed with the solution needed for DEP testing. The equivalent conductivity of yeast was calculated using Equation (37) and the values are shown in Table 07. The max effective conductivity of yeast seen in literature was found to be 2.52E-3S/m [28]. In order to reach a CM factor as close to -0.5 as possible, a concentration of 0.03M NaCl was determined to be appropriate to achieve the max negative CM factor when compared to conductivity values for yeast [8] [28]. At this concentration of NaCl in solution, the conductivity of the fluid is 3.78E-1S/m.

Table 07: Conductivities and CM factors of different NaCl concentrations.

FCM	Conductivity Multiplier	Conductivity of Medium (S/m)	Conc NaCl (mol/m^3)	Conc NaCl (mmol/L)	Mass NaCl (g/L)
-0.5	150	3.78E-01	29.9	29.9	1.75
-0.4	7.00E+00	1.76E-02	1.39	1.39	0.0815
-0.3	3.1	7.81E-03	0.62	0.618	0.0361
-0.25	2.5	6.30E-03	0.50	0.498	0.0291
-0.2	2.00E+00	5.04E-03	0.40	0.398	0.0233
-0.1	1.4	3.53E-03	0.28	0.279	0.0163

Prior to running experiments on the devices, simulations for the operating conditions were run to determine the CM factor, net zeta potential, and electric field strength required. Depending on conditions, the required voltage potential was determined from the data output by those simulations.

DI water was used to have the lowest possible starting fluid conductivity and 400mL was obtained and placed into a flask. The desired amount of NaCl was measured out on a scale and mixed with the water. Devices were placed into a Petri dish sufficiently large to allow two devices to sit flat on the bottom. NaCl solution was poured into the Petri dish until the devices were completely submerged in fluid. Any remaining fluid was placed on a hot plate set to 35°C and allowed to heat. If more solution was needed it was mixed in a 100mL flask and placed in the hot plate. The Petri dish with

devices was then placed into the glass vacuum chamber. The vacuum chamber was turned on and devices were left to prime for 1 hour with agitation every few minutes to get bubbles off the devices. Devices were then removed from the vacuum and visually inspected for bubbles within the channels.

The yeast solution was prepared in a 50mL flask with 20mL of DI water. Packets of dry active yeast were used in all experiments. A small amount of yeast pellets was poured into the 10mL of water and stirred manually on the hot plate until no pellets were visible. Solution was allowed to sit for 1 hour to allow the yeast to activate in the DI water.

Viewing of the devices was done with a Lab Smith SVM4300, using a color or black and white camera, with a 10X magnification objective. Prior to testing the SVM was turned on and the area of interest was found and focused in frame. Solution from the heated flask of NaCl solution was poured into the Petri dish until all but the top surface of the device was covered in solution. Depending on the test being performed, electrodes from the HVS448 3000 (HVS) were attached to electrode ports. In the HVS software, desired electrical voltages were chosen for the test. The HVS has a voltage output range of -1500V to 1500V or 0V to 3000V and the current allowed is 6250μA.

Using a 3mL syringe, about 0.1mL of yeast solution was taken and then 1mL of NaCl solution was taken up into the syringe. Syringe was shaken to mix the yeast solution and NaCl solution prior to testing. To prime the device with yeast solution, the mixed yeast and NaCl solution was placed into a pipette tip and then placed into the desired port. Solution was then allowed to gravity feed into the device. The pipette tip was removed once yeast had successfully entered the device.

A Petri dish was used as the viewing platform for the devices in case of fluid spills or overflows. The metal stage plate on the SVM was removed and the Petri dish was placed over the camera to allow for viewing. Primed devices were placed in the Petri dish and electrodes were placed in their respective ports. The camera was adjusted to be directly under the insulating post array and focused. Testing conditions for the device were chosen and the HVM would be activated and videos would be taken.

CHAPTER 4 LEGACY DEVICE SIMULATION AND TESTING RESULTS AND CONCLUSIONS

This section looks at the results of the bubble filter weir EO flow simulation.

4.1 Simulation Simplification results

In the bubble filter weir EO flow test, fluid velocity due to EO flow was simulated to determine if the weirs caused any kind of hydrodynamic resistance to the fluid flowing through them. Fluid flow was simulated, and the average velocity of the fluid was taken across the outflow line along the bottom of the chamber as seen in Figure 16 and then compared to theoretical values for EO flow at these voltages and zeta potential. The results of this test can be seen in Table 08.

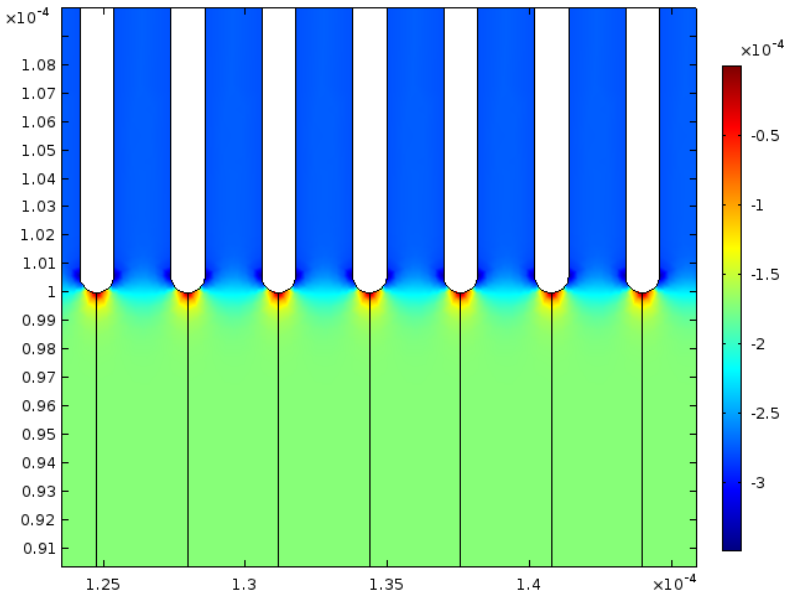

Figure 16: Shows the geometry used for the bubble weir testing. This is a zoomed in representative image of the velocity surface plot just below the weirs, given by COMSOL in meters per second.

Table 08: Shows results of the bubble filter weir simulation and compares them to theoretical values. Shows no difference between outflow fluid velocity and theoretical values.

Voltage Potential (V)	COMSOL Average Outflow Velocity (m/s)	Electric Field Strength (V/m)	Theoretical Electroosmotic Velocity (m/s)	Percent Difference from Open Channel (%)
40	-0.00172	3.33E+05	-1.74E-03	1.10
80	-0.00154	3.00E+05	-1.56E-03	1.10
120	-0.00137	2.67E+05	-1.39E-03	1.10
160	-0.0012	2.33E+05	-1.21E-03	1.10
200	-0.00103	2.00E+05	-1.04E-03	1.10
240	-8.58E-04	1.67E+05	-8.68E-04	1.10
280	-6.87E-04	1.33E+05	-6.94E-04	1.10
320	-5.15E-04	1.00E+05	-5.21E-04	1.10
360	-3.43E-04	6.67E+04	-3.47E-04	1.10
400	-1.72E-04	3.33E+04	-1.74E-04	1.10

From the results in Table 08, it is determined that the outflow velocity of fluid is approximately the same to that of the theoretical EO flow velocity. This therefore shows that the bubble filter weirs can be ignored in a full simulation of the DEP device. When accounting for this in the full device simulation, the weirs will either be represented as an open boundary or will be fully excluded, but include an internal wall to prevent particle movement since most particles are too large to travel through the weirs and will therefore get stuck along the weirs.

4.2 Validation and Optimization Simulation Results

4.2.1 iDEP Validation and Optimization

In the post and particle simulation particle were released at time 0 (t=0) and observed over a 0.1 second period of time. Particles with CM factors of 0, -0.10, -0.20, -0.25, -0.30, -0.40, and -0.50 were released in the upper part of the chamber and allowed to move under the influence of DEP force and drag due to EO flow. The metric for successful filtration was determined by if red particles descended below the top layer of posts, indicating that the drag force overcame the DEP force. It should be noted that no particle-particle interactions were defined so particles can stack on top of each other.

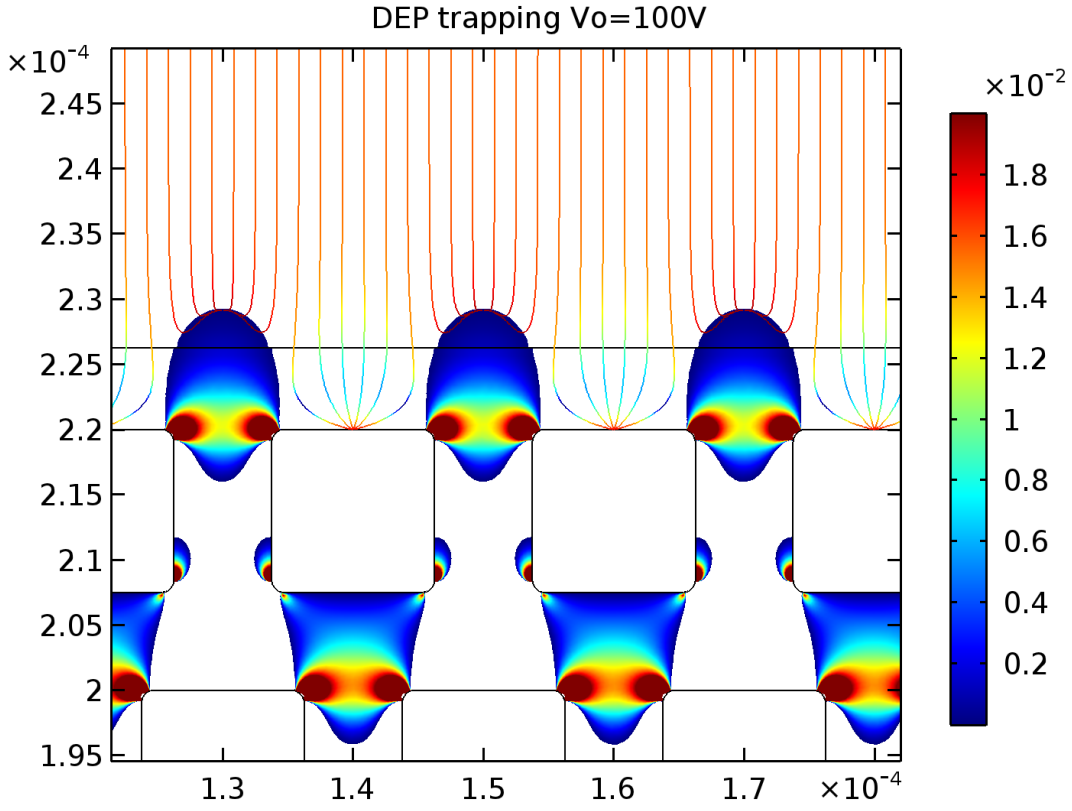

Figure 17: Example of COMSOL output of particle trajectories with CM factor of -0.5, permittivity of 78.5, net zeta potential of -0.005, and 100V potential (-333333 V/m).

As seen in Figure 17, the particle pathlines are impeded by DEP force and are held above the posts. The colored fields represent regions where the velocity of the particles is positive in the y-direction. The results of the remaining CM factors can be seen in Table 09, where the conditions were rated on a pass/ fail basis depending on if the DEP force kept particles out of the filter or not. By using the information in Table 09 the specific conditions for operation of the device in water can be determined for separation of particles in water.

Table 09: Conditions for operation of the DEP filter in the legacy device using water (Relative permittivity = 78.5 and $\zeta = -0.005V$).

Voltage	Electric Field Strength (V/m)	-0.50	-0.40	-0.30	-0.25	-0.20	-0.10	0.00
100	3.33E+05	Pass	Pass	Pass	Pass	Pass	Pass	Fail
90	3.00E+05	Pass	Pass	Pass	Pass	Pass	Pass	Fail
80	2.67E+05	Pass	Pass	Pass	Pass	Pass	Pass	Fail
70	2.33E+05	Pass	Pass	Pass	Pass	Pass	Pass	Fail
60	2.00E+05	Pass	Pass	Pass	Pass	Pass	Pass	Fail
50	1.67E+05	Pass	Pass	Pass	Pass	Pass	Fail	Fail
40	1.33E+05	Pass	Pass	Pass	Pass	Pass	Fail	Fail
30	1.00E+05	Pass	Pass	Pass	Pass	Pass	Fail	Fail
20	6.67E+04	Pass	Pass	Pass	Fail	Fail	Fail	Fail
10	3.33E+04	Fail	Fail	Fail	Fail	Fail	Fail	Fail

From observing Figure 18, the point at which the lowest DEP force occurs at the top of the posts is the midline between two posts and if the DEP force is not sufficient then this is where particle will enter the filter first. This can also be expressed by plotting the y-direction force along a line just above the posts as seen in Figure 18. This indicates that the net force on a particle should be calculated from the midline between posts to determine if the DEP force is enough to keep particles above the top of the posts.

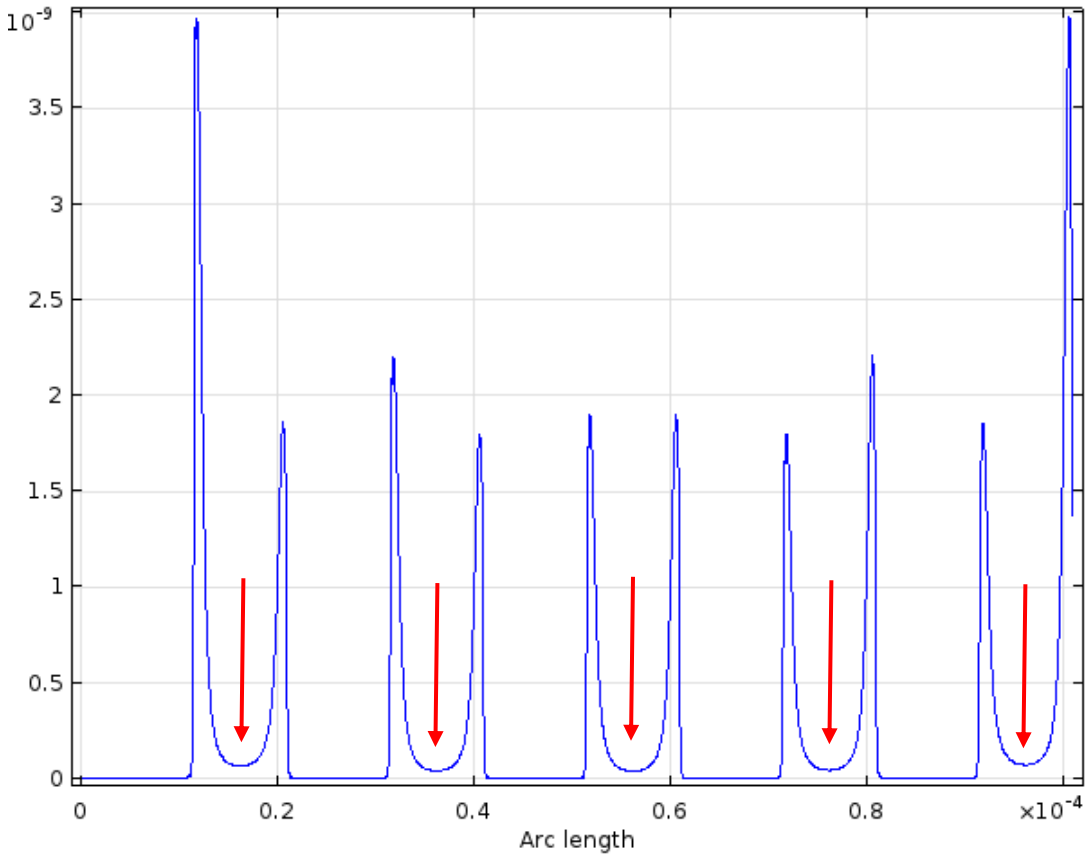

Figure 18: Shows the net force acting on particles in the y-direction along the top of the insulating post array. The minimum force between posts is shown to be at the midpoint between posts, characterized by the bottoms of the troughs indicated by the red arrows.

Then by taking a log-log plot of the CM factor along the midline between posts, the distance from the top of the posts that particles will stop at a given voltage potential can be found as seen in Figure 19. The conditions being observed can be adjusted to different conditions of the zeta potential, fluid permittivity, or changes in particle radius.

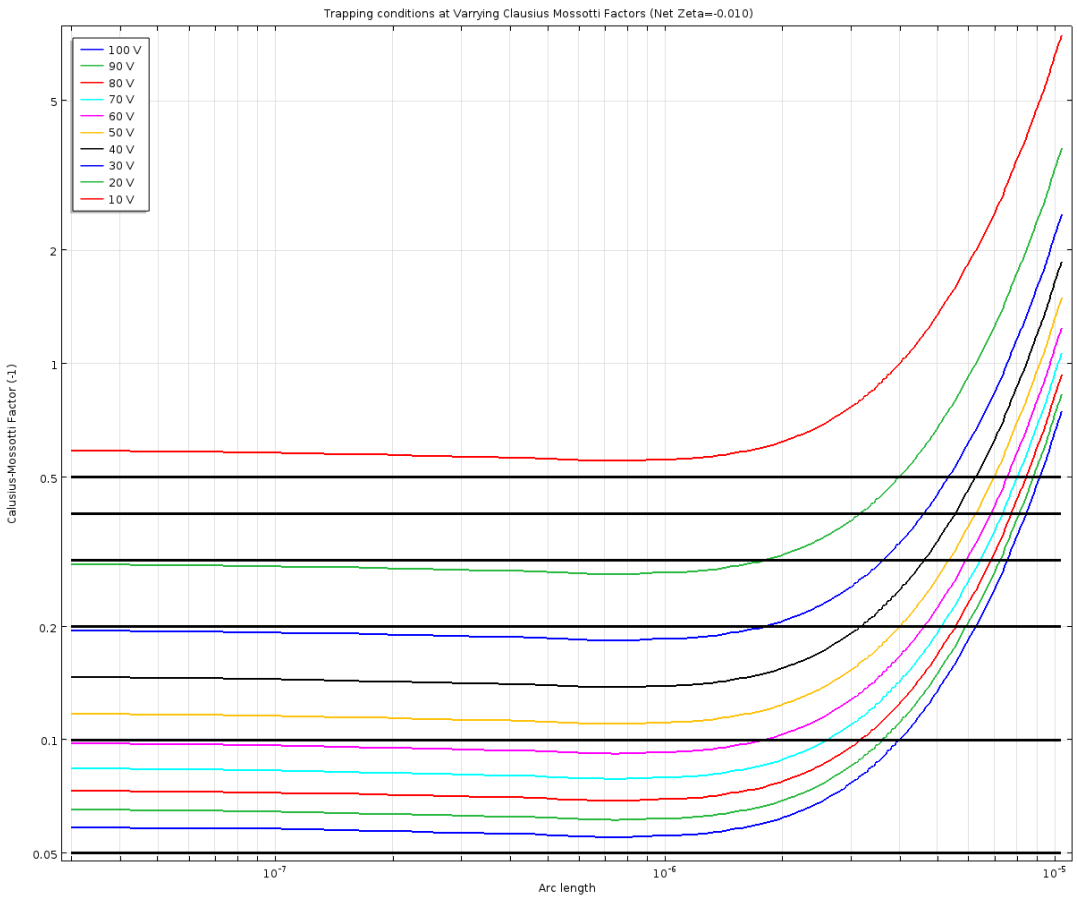

Figure 19: Shows a log-log plot of the CM factor at different voltage potentials at a net zeta potential of -0.010 V. Intersections of voltage potential lines and CM factor lines indicate the distance from the top of posts where particles will be trapped in the y-direction.

The zeta potential can be adjusted in the log-log plots to determine the Pass/Fail of particle trapping above posts. This allows Trapping conditions to be determined and additional data for this can be seen in Appendix B. Although this does show that the device can be used to trap particles above the posts, the purpose of this device is to prevent fouling and trapping particles still counts as filter fouling. The device includes channels that cross the main chamber of the device, designed to carry particles across the device. A cross flow was then applied to the simulation to determine the crossflow

velocity that particles affected by DEP will levitate across the top of the insulating posts to the outlet.

The results from the iDEP simulation tests showed a wide range of conditions where the iDEP filter will work. However, it should be noted that the designed length of the device is 3 cm in length from one electrode port to the next. This leads to a voltage potential of 1000V for a voltage potential of 10V across the filter to 10,000V for a voltage potential of 100V across the filter. This requirement requires significant lab equipment and infrastructure to achieve these voltages. For real world testing at these parameters, the device needs to be modified to reduce the distance between wires decreasing the voltage potential across the device. Additionally, in future iterations of the device, the decreased distance between electrodes should be designed into the device.

These tests do indicate that in the legacy device design will repel particles from the post filter by negative DEP. This also means, and is indicated by the simulations performed here, that particles will be attracted to the center of the top of posts due to the attractive negative DEP force thus creating a need for the high fluid velocities needed to produce particle levitation and design changes to the posts to reduce attractive DEP at the top of the posts. Results of this test indicate that particles can be levitated by increasing zeta potentials decreases the operable conditions.

4.2.2 Cross Flow Testing

Taking the information from the iDEP testing it was time to test for the conditions required to foul-lessly filter particles using a cross flow simulation. By setting up a parametric sweep of the conditions desired, the conditions for the cross flow to operate could be found. For conditions to pass this test, the particle pathlines needed to levitate

above the posts as they traveled across the top of the posts. An example of this can be seen in Figure 20.

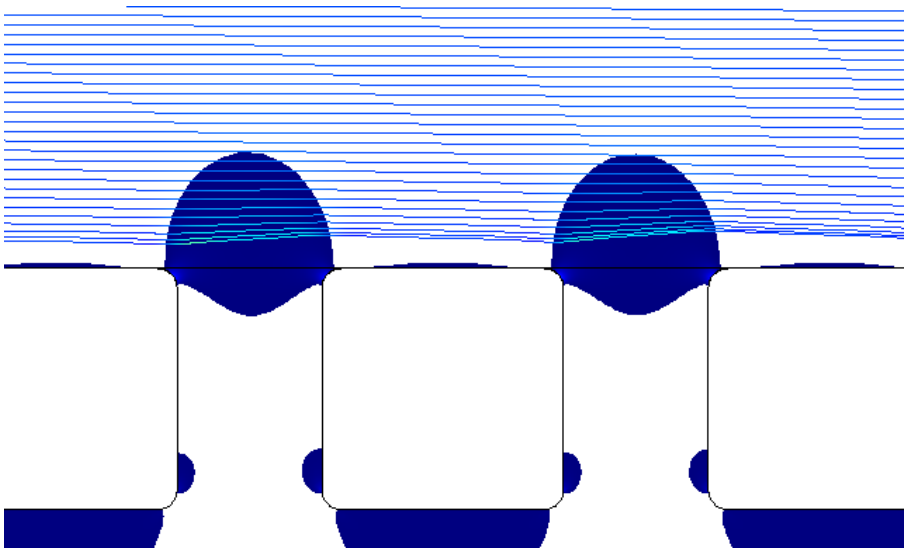

Figure 20: Condition for passing the crossflow testing where the particle pathlines (blue lines) levitate across the top of the insulating posts from left to right. The colored lines symbolize the pathlines of the particles in question as they are repelled by the DEP force from the filter.

If the pathlines indicate that the particle will be pulled to the posts or between them, it is considered to be a failure (Figure 21).

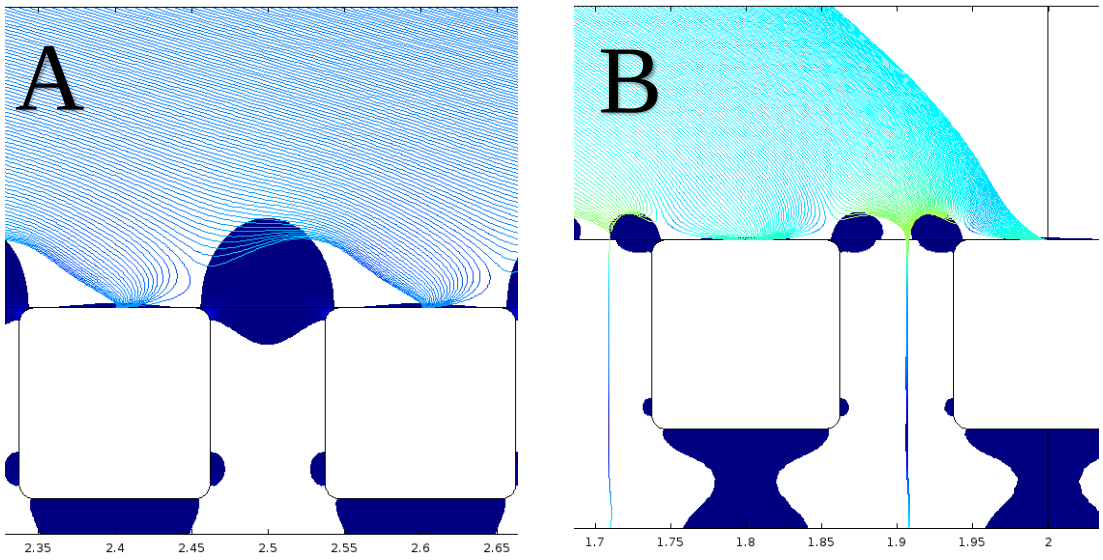

Figure 21: Conditions for failure to foul-lessly filter particles as set forth; (A) pathlines indicating particles will foul to posts and (B) pathlines indicating that particles will pass through filter.

Under the tested conditions and the pass criteria there were no instances where the particle pathlines were able to cross the entire channel without either fouling to a post or passing through the filter. The conditions that presented the best outcome was a voltage potential of 20V and a flowrate of 0.1m/s which results in ΔP in excess of 1600Pa which is too high to perform on an actual device. At these conditions the pathlines would skip across the top of the filter to approximately the mid-way point of the filter then foul to the post. So, for the pass criteria set forth no conditions passed this test.

A possible source of error in this simulation was the fact that pathlines were not restricted the size of the particle radius. If this were accounted for, the minimum distance that the pathlines could get to the posts would be the radius of the particles in question. This could play a role in preventing fouling along the top of the filter. Additionally, the fluid velocities observed to get the closest to performing this are far beyond the possible

conditions of operation. High flowrates like this would result in high pressures, transition to regions of turbulence and device failure.

4.2.3 Fluid Dynamics Validation and Optimization

To test the fluid dynamics, stationary simulations of creep flow coupled with electric currents were conducted. The range of values used for inflow velocity and voltage potential used in the simulations can be seen in Table 10.

Table 10: Parametric sweep parameters used for fluid dynamics testing.

Parameter	Values	Units
Inflow velocity	5e-4, 5e-3, 5e-2, 5e-1	m/s
Voltage Potential	46.67, 466.7, 4667, 46670	V

In order to reduce simulation times, particles were assumed to follow fluid pathlines in conditions where the CM factor was equal to zero and an example particle following fluid path lines can be seen in Figure 22. This indicates that the fluid-particle interaction module in COMSOL is not required for finding particle paths when the conductivity of the fluid is equal to that of the particle.

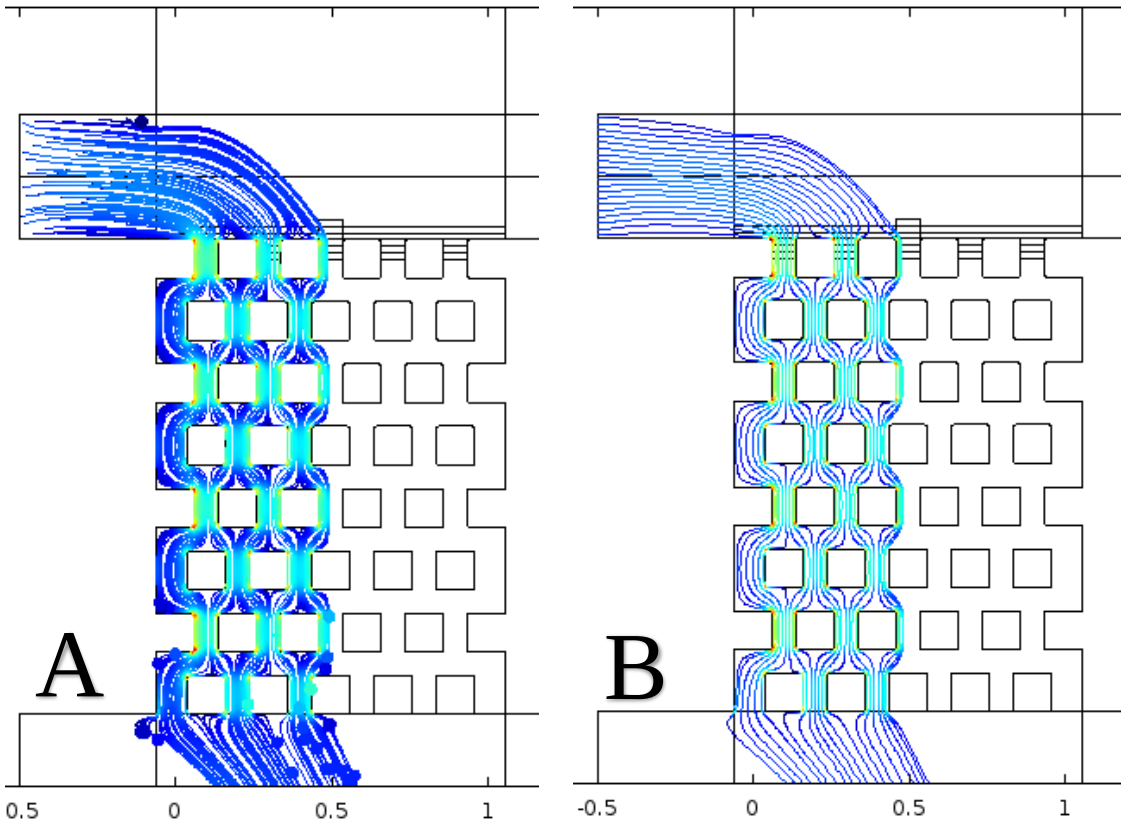

Figure 22: Shows (A) particles and their path lines and (B) fluid flow path lines. Shows that particle trajectories of particles with CM factor of 0 can be assumed to follow fluid flow path lines.

When taking this information and applying it to the legacy device, the same assumption that the particles will follow the fluid pathlines under a CM factor of 0. Conditions required for iDEP particle levitation was tested be in the range of 33,333.3 V/m to 333,333.3 V/m electric field which in this simulation translates to a 466.7 and 4667 V potential for a simplified chamber 14 mm in length. The voltage potential range with the inflow velocities for the legacy device can be seen in Figure 23 and Figure 24.

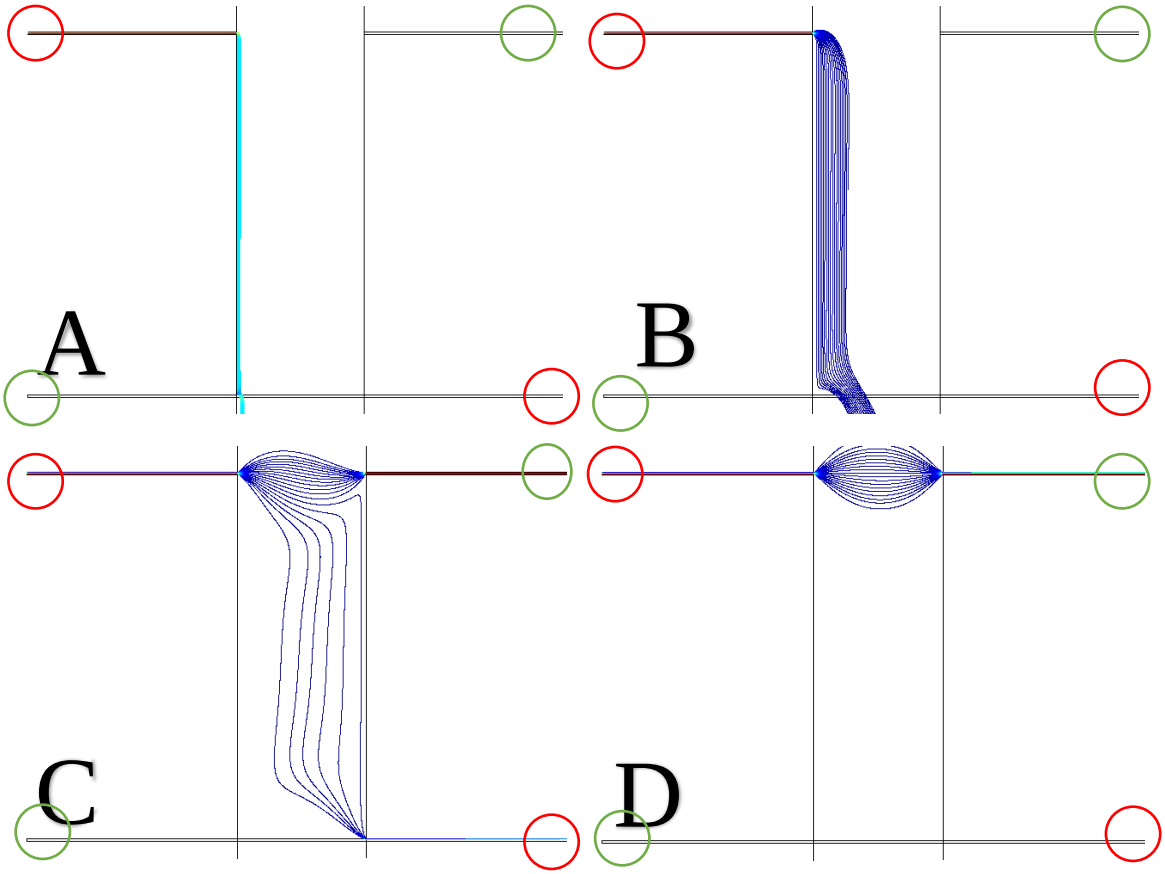

Figure 23: Results of fluid dynamics testing with the particle inlet and outlet marked with red circles and fluid only inlet and outlets marked by green circles. Each image shows changing inflow velocity and voltage potential of 10 V across the filter. Conditions for each simulation are (A) 466.7 V potential with 5e-4 m/s inflow, (B) 466.7 V potential with 5e-3 m/s inflow, (C) 466.7 V potential with 5e-2 m/s inflow, and (D) 466.7 V potential with 5e-1 m/s inflow.

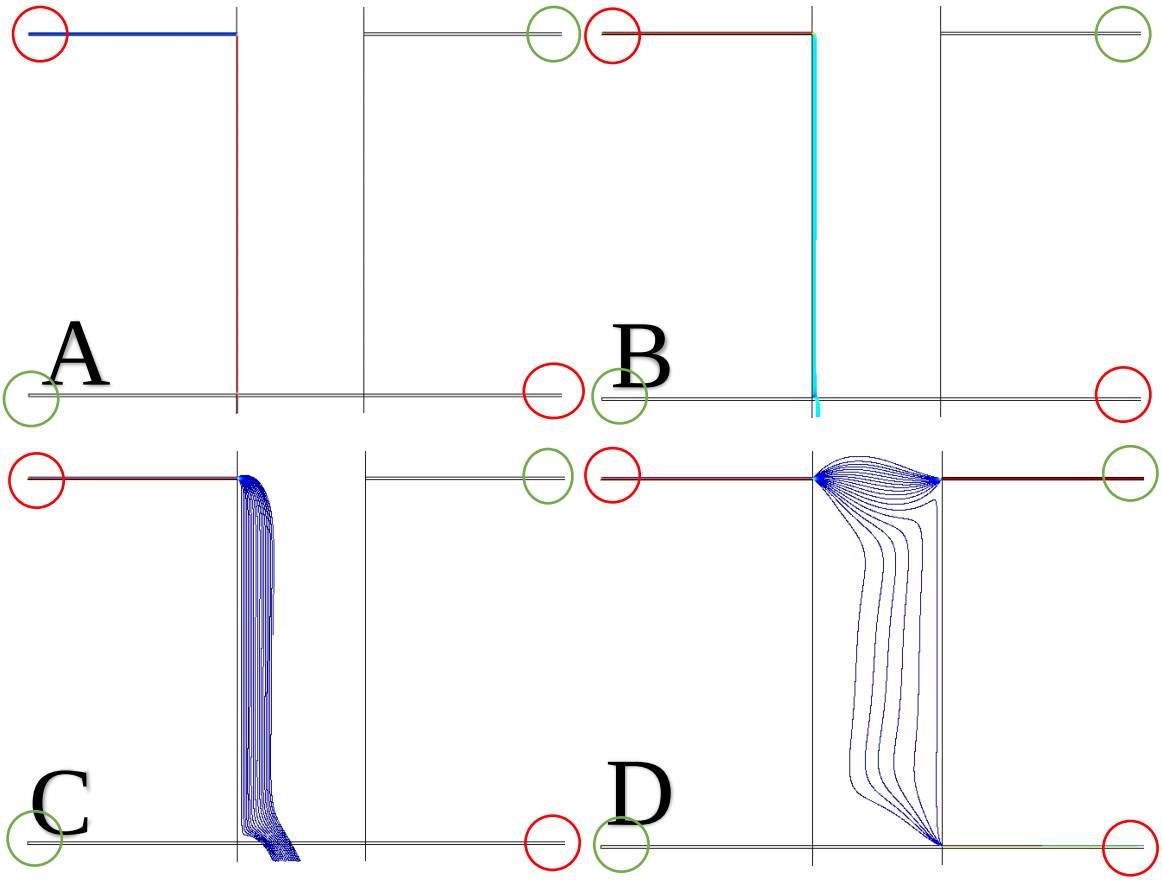

Figure 24: Results of fluid dynamics testing of changing inflow velocity and voltage potential of 100V across the filter. (A) 4667 V potential with 5e-4 m/s inflow, (B) 4667 V potential with 5e-3 m/s inflow, (C) 4667 V potential with 5e-2 m/s inflow and (D) 4667 V potential with 5e-1 m/s inflow.

The results of these simulations found the fluid streamlines entering the device from the top fluid inflow (top left) appear to enter the main chamber then run along the left wall of the center of the device. This result was to be expected since the fluid would enter from pressure driven flow then as the pressure driven flow in the horizontal direction decreases and EO flow in the vertical direction takes over as the main driver of fluid movement. This shows that particles with a CM factor of 0 will likely pass through the filter within the first few hundreds of microns across the filter. Figures 21 and 22 also

show that if inlet/outlet flowrates are not sufficient, particles will descend below the bottom outflow channel. If particles do this, they will foul along the bottom bubble filter weirs, disrupting EO flow of the device and failing to meet the foul-less criteria. Particle outflow on the bottom outflow is not seen until inflow/outflow velocities of 5e-2 m/s and 5e-1 m/s for voltage potentials of 466.7 V and 4667 V respectfully. For a device of this scale, it is likely not possible or practical to operate at these conditions.

From this it is shown that a lower contribution of EO flow improves the function of the device and decreases the inflow velocity needed to clear particles. By further dividing the voltage potential into smaller increments, the optimal voltage potential and inflow velocity were determined as seen in Figure 25.

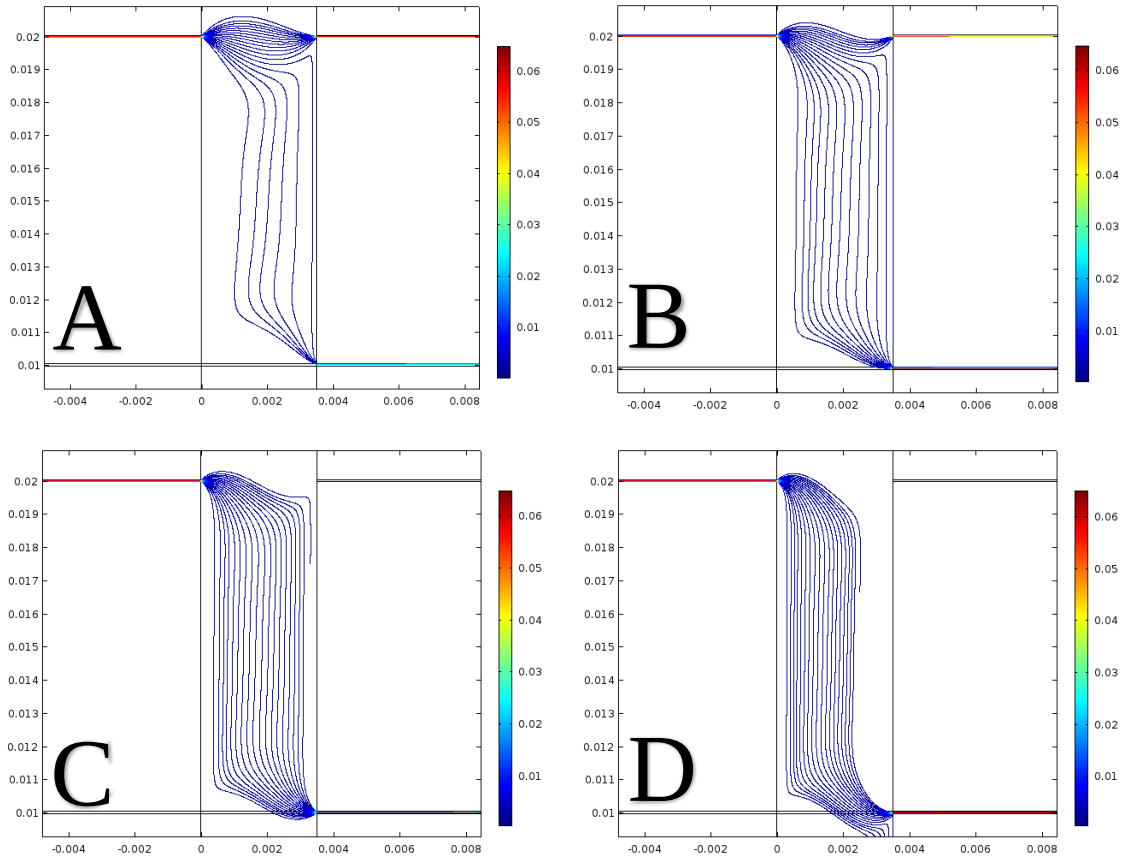

Figure 25: Results of fluid dynamics testing of changing voltage potential with inflow velocities of 5e-2 m/s and particles entering from the top left channel. (A) Voltage potential of 466.7 V, (B) voltage potential of 933.4 V, (C) voltage potential of 1400 V, and (D) voltage potential of 1867 V.

From the results shown in Figure 25 the optimal operating conditions the fluid dynamics of this device is a voltage potential of 1400 V, equating to an equivalent voltage potential of 30V across the filter or 3000 V from electrode port to electrode port, which is within the operation conditions determined by the DEP force optimization for large CM factors and is at the upper limit of the producible voltage of the HVS. However, an inlet velocity of 5 cm/s is extremely high for a microfluidic device of this scale. Pressures required to produce this inflow velocity causes large pressures and this

COMSOL simulation predicts pressures upwards of 700 Pa and attempts to run the device under these parameters could result in delamination and significant deformation of the device.

4.3 Legacy Device Experimental Results

When testing the for the legacy device, both the fully constructed device and the band-aid style devices were considered legacy devices when it came to observe EK and DEP at the posts since their post geometries were identical. Many rounds of devices were produced and tested.

4.3.1 Soft Lithography Observations

Several generations of devices were made and issues with PDMS resolution and bonding to their substrates were seen often. Most obvious issues were seen with the post array or the bubble weirs. On the fully constructed devices, weirs were commonly either not fully intact or had completely occluded the channel due to the short distance between them and short channel height. This prevented any kind of current through the devices and ultimately prevented flow. Another issue commonly seen throughout all versions of devices and over several generations of devices was the post array resolution or post arrays not fully intact. Devices with defects in the post array were often still used to try testing EK of particles.

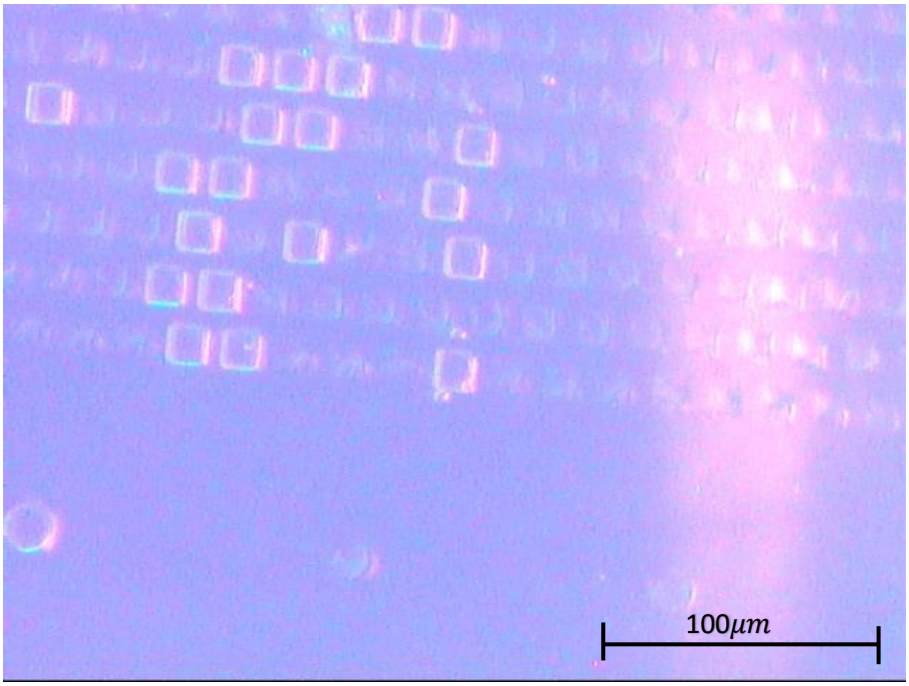

Figure 26: A common issue seen while fabricating devices with PDMS casting included posts in the post arrays not remaining intact. Seen on at least one device in particular so could have been an issue with a single device.

4.3.2 Electrokinetics Testing

In one of the band-aid style devices, a video of pure electrokinetics of the system was observed. Videos taken of the device while in operation were used to calculate the electrokinetics of the yeast particles. Calculation of particle velocity was done by processing the videos in ImageJ. This was done by using the multipoint tool to mark the locations of the particles at points on two frame intervals until the particle left the field of view. The program was calibrated to have the correct length scale by measuring the length of know components in the device. Points were placed on the same particle 2 frames apart. ImageJ measures the locations of particles in the device by their coordinates, so Excel was used to determine particle velocity. Velocities were found by finding the change in x and y locations of points and finding the hypotenuse of the

change in distance, divided by the time between points (0.0667 seconds). At a known electric field strength of 200V/cm, the mobility of the yeast particles was determined to be 2.420E-8 $\frac{m^2}{Vs}$ which is comparable to literature [8]. In successive tests to try to increase the data pool for electrokinetics, none were successfully able to have pure EK due to bubble formation causing pressure driven flow within the microfluidic device.

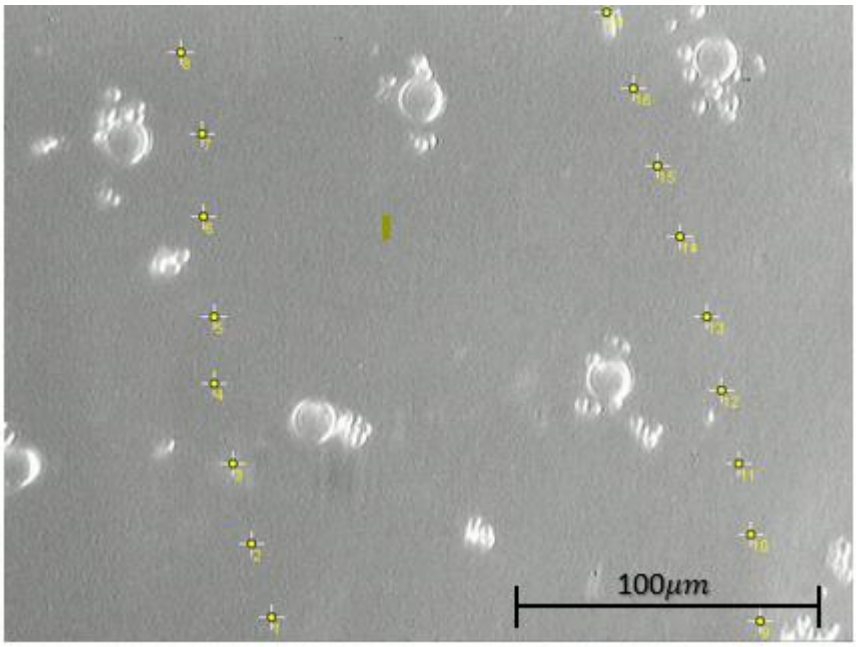

Figure 27: Multipoint marking in ImageJ to find particle velocities. Points taken are two frames apart in a video taken at 30 frames per second.

4.3.3 Bubble formation

While running tests on the legacy devices, the device would only operate for short periods of time and if voltage potentials were increased, the time of operation would decrease. This was due to observed electrolysis and what seemed to be boiling of the fluids within the device. Electrolytic byproducts and bubbles formed at the ground wire consistently over all devices. Over time the electrolytic byproducts would adhere to the surfaces of the channel, eventually blocking flow and the electrical connection. Bubble

wetting from the ground wire was not observed as often since fluid flow due to EO flow was towards the ground wire, but if the polarity of the wires were switched at any point, bubbles would immediately wet the channels and cut off flow. Additionally, if the current was allowed to run too long, bubbles around the ground wire would fill the port that it was in and cut off current supply.

At high voltages, bubbles would spontaneously form inside the channel and would continue to expand until power was turned off. Once power was switched off, bubbles would shrink and disappear, turning back into water. It was noted that some of these bubbles would recede back to supporting posts in the channel and tiny air pockets could be observed under the SVM. The bubble seen in Figure 28 is likely pinched between the glass slide and the supporting post. Bubble formation like this is likely due to boiling of the fluid within the channels due to the high currents and voltages required to perform DC iDEP.

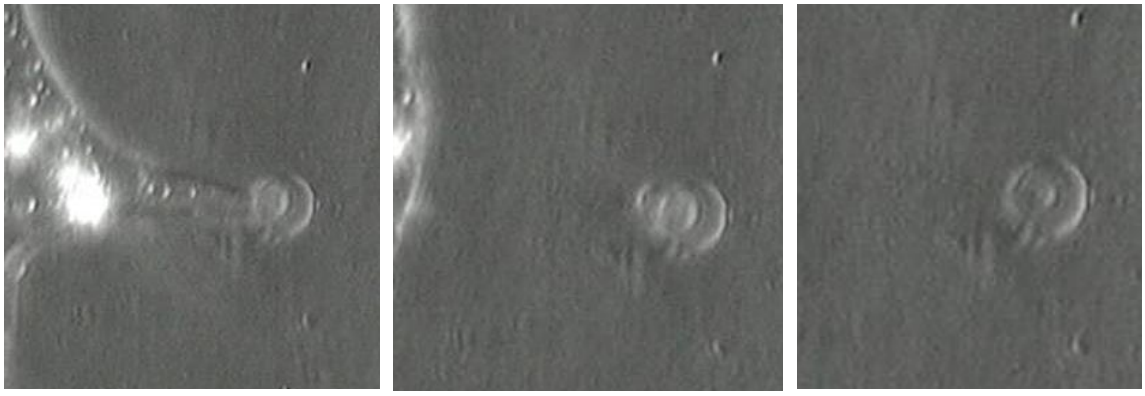

Figure 28: The recession of large bubbles in the channel after electric current is turned off and small bubbles forming around the supporting posts of the channel. (A) Shows the large bubble just before it detaches from a smaller bubble attached to the supporting post, (B) the bubble retracts to the supporting post, and (C) the bubble shrinks and embeds itself in or between the post and glass slide.

Spontaneous bubble formation in the device was observed everywhere, including the bubble weirs which are intended to prevent the entrance of bubbles into the system. Bubbles were found to rapidly form within and around the weirs, quickly expanding and fulling weirs, blocking current and fluid flow. Therefore, the bubble weirs are not useful since, if bubbles appear, they will block or wet the weirs. Bubble formation was likely from Joule heating leading to boiling of the water in the channels, since the conductivity of the system is high from the high electrolyte concentration in solution.

4.3.4 Filter fouling

The particles themselves were observed to be an issue in blocking the post array. One source of this issue was found to be a priming issue. If particles were pressure driven by syringe into the device (even at low concentrations), they would foul the post array. This led to a change in the procedure of using a pipette tip full of water and adding a small amount of yeast solution into the pipette tip to slowly get yeast into the device.

While running an electric field, particles became trapped in what seemed to be the attractive DEP zones on top and within the filter since the DEP force was not large enough to prevent particle entrance into the post array. Yeast particles were observed to flocculate together, forming large conglomerates of particles that would become stuck in the post array due to the dominating EK of the device. Figure 29 shows particles fouled and occluding the post array. Individual particle fouling within the filter was to be expected since the electric field produced was not sufficient to induce particle trapping above the post array and therefore were able to pass through the top row and the attractive DEP in combination with the EK pulled particles to the filter posts. This is reflected in COMSOL simulations with pathlines signifying the mobilities of particles.

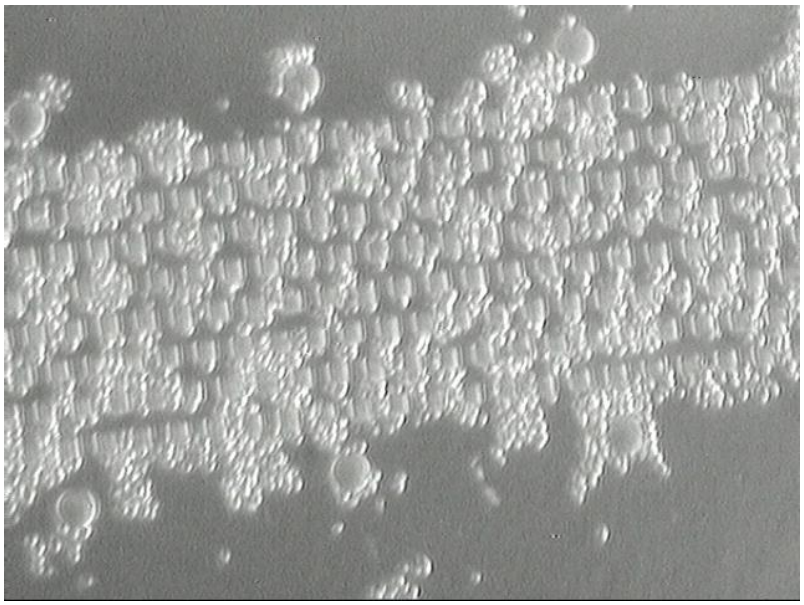

Figure 29: Fully occluded insulating post array with yeast particles.

4.3.5 Legacy Device Conclusions

The legacy device as it is, does have specific conditions under which it theoretically could operate as a continuous flow DC DEP filter. Assumptions required for operation are as follows:

1. The device is assumed to isothermal and Ohmic heating is a nonfactor.
2. Device has infinite fluid saturation that allowing the EO flow to pull and push fluid out of the device to avoid flow reversal.
3. Exact zeta potential of the surface and the particle are known.
4. Electrolysis does not occur.
5. The device is not in any way deformed under flow or pressure caused by pressure driven flow.
6. The walls of the system are perfectly insulating.

Due to these requirements to levitate particles, it is determined that the legacy device will not perform foul-less filtration under any experimental operating conditions. In order to avoid these issues in future iterations of this type of device, the size of the device and its components must be altered. Necessary changes that need to be made are:

1. Shortening of the distance between electrodes to reduce voltage potentials.
2. Elimination of the bubble weirs as they do not perform their intended function.
3. Increasing the size of the insulating posts.
4. Reduction the number of rows in the post array.
5. Do not stagger post rows.
6. Increased size of crossflow channels to allow for higher cross flow velocities.

CHAPTER 5 NEW DEVICE SIMULATIONS AND TESTING

5.1 Overview

From all the tests and simulations run up to this point it is evident that the prospect of a DC iDEP filter is not a simple feat to accomplish. By using a DC system, there becomes a need to carefully balance the four major players in the system; DEP force, EO flow, EP flow, and pressure driven flow. Each one has its own unique properties and by finding the range of parameters to operate DC iDEP is required.

When looking at the devices used as well, it is evident that using insulating features on the scale of tens of microns is not necessary to achieve the conditions required to induce particle levitation. This revelation in conjunction with recent improvements in 3D printing resolution gives the unique opportunity to rapid prototype new device designs prior to spending more time, energy and money microfabricating devices in the clean room.

Unfortunately, in the scope of this thesis it was found that the legacy device was found to not be adequate to perform the functions of a DC iDEP foul-less filter. Using COMSOL and 3D printed model testing, some new information about the next steps to produce a DC iDEP foul-less filter can be made. To accomplish this, new post designs were considered to further project the DEP force into the channel to levitate particles. Larger inlet/outlet channels were tested, and the pressure driven flow across them was simulated for the operating conditions.

5.2 iDEP Post Optimization

The first COMSOL simulation to be run was to determine optimal post geometry to project the DEP force into the channel to levitate particles. This was done using a

parametric sweep in a 2D COMSOL simulation and the basic geometry seen is shown in Figure 30. The posts in this geometry were altered in four different ways to increase the magnitude of the ∇E^2. The parameters of the posts that were changed were the overall dimensions of the posts, the radius of the filet on the top two corners, the chamfer on the bottom two corners, and the length of the posts. All simulations were run at 1000V/mm to ensure the electric field in all simulations were the same.

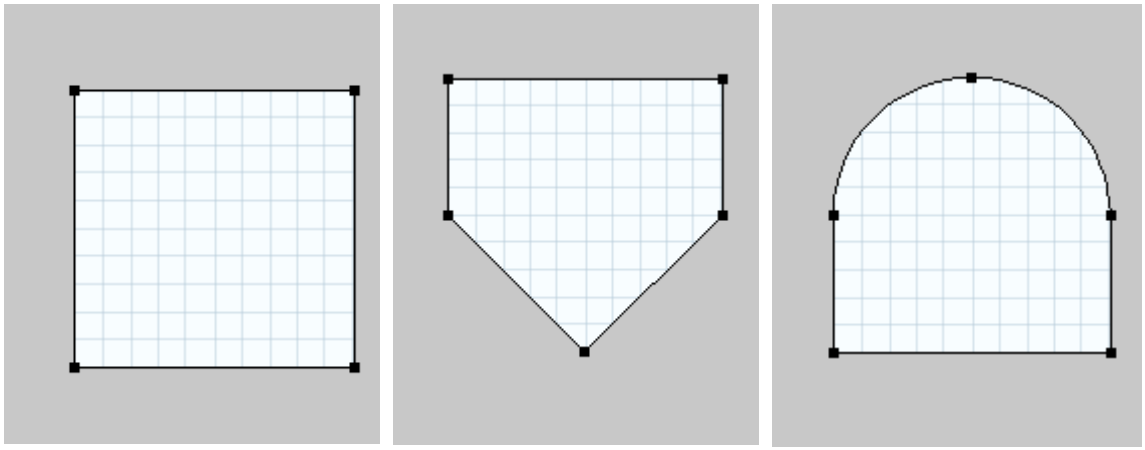

Figure 30: (A) Square geometry with dimensions 12.5E-6m x 12.5E-6m (B) changes to chamfer at bottom corners (6.25E-6m shown) (C) changes to filet at top corners (6.25E-6m shown).

A parametric sweep was run to test each combination of conditions detailed above and the plots below are taken from each of the parameters. The horizontal line plots are taken from a line 1 micron above the top of the posts for the chamfer, fillet, and post length simulations. For the overall change in post size for the entire chamber and posts the horizontal line plot was placed 2.5 microns from the tops of the posts. Vertical line plots are taken from the centerline between the centermost two posts.

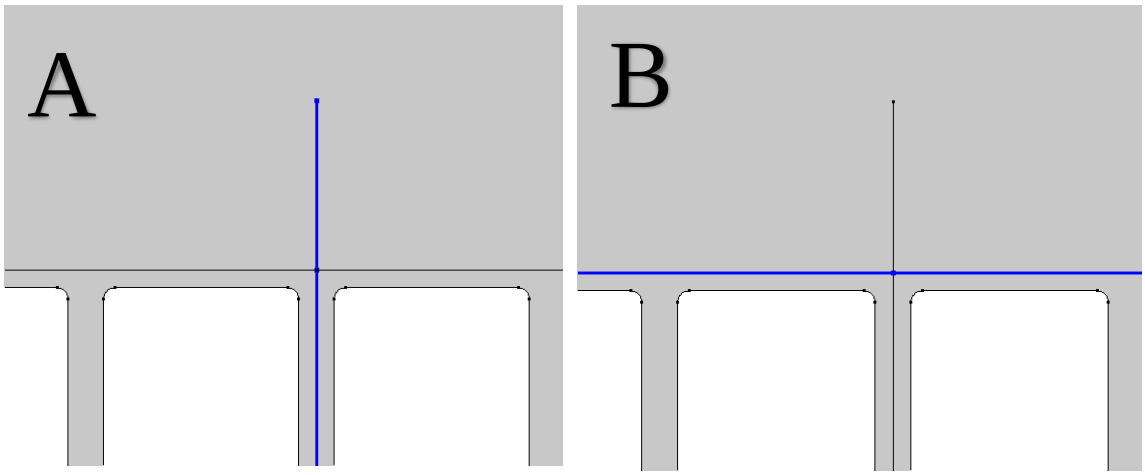

Figure 31: Shows the (A) vertical line used to take ∇E^2 values at the centerline between posts highlighted in blue and (B) the horizontal line 1 micron above the insulating post array used to collect ∇E^2 data highlighted in blue.

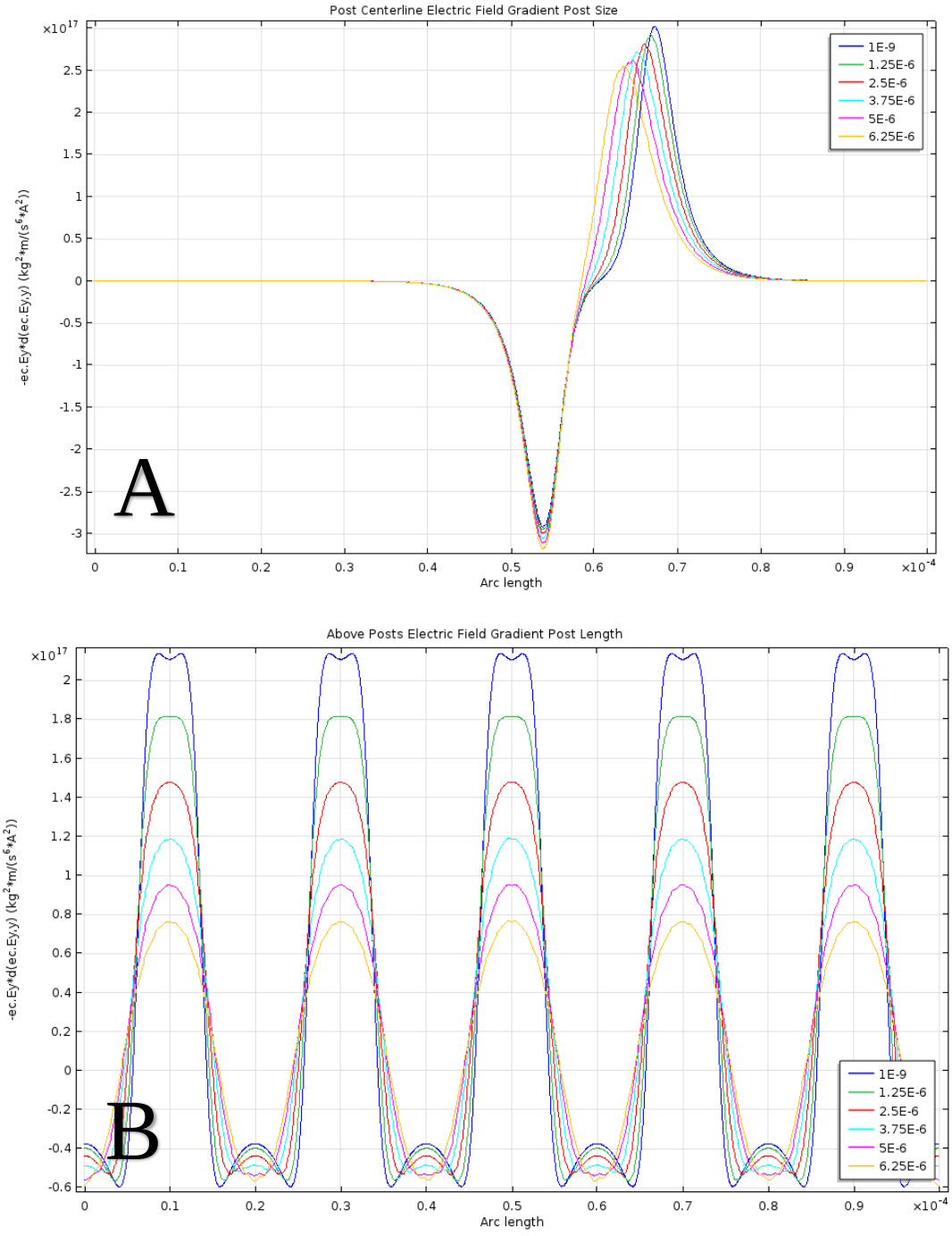

Figure 32: Line plots of ∇E^2 at (A) the centerline between posts and (B) 1 micron above the top of the post array with a changing top fillet radius.

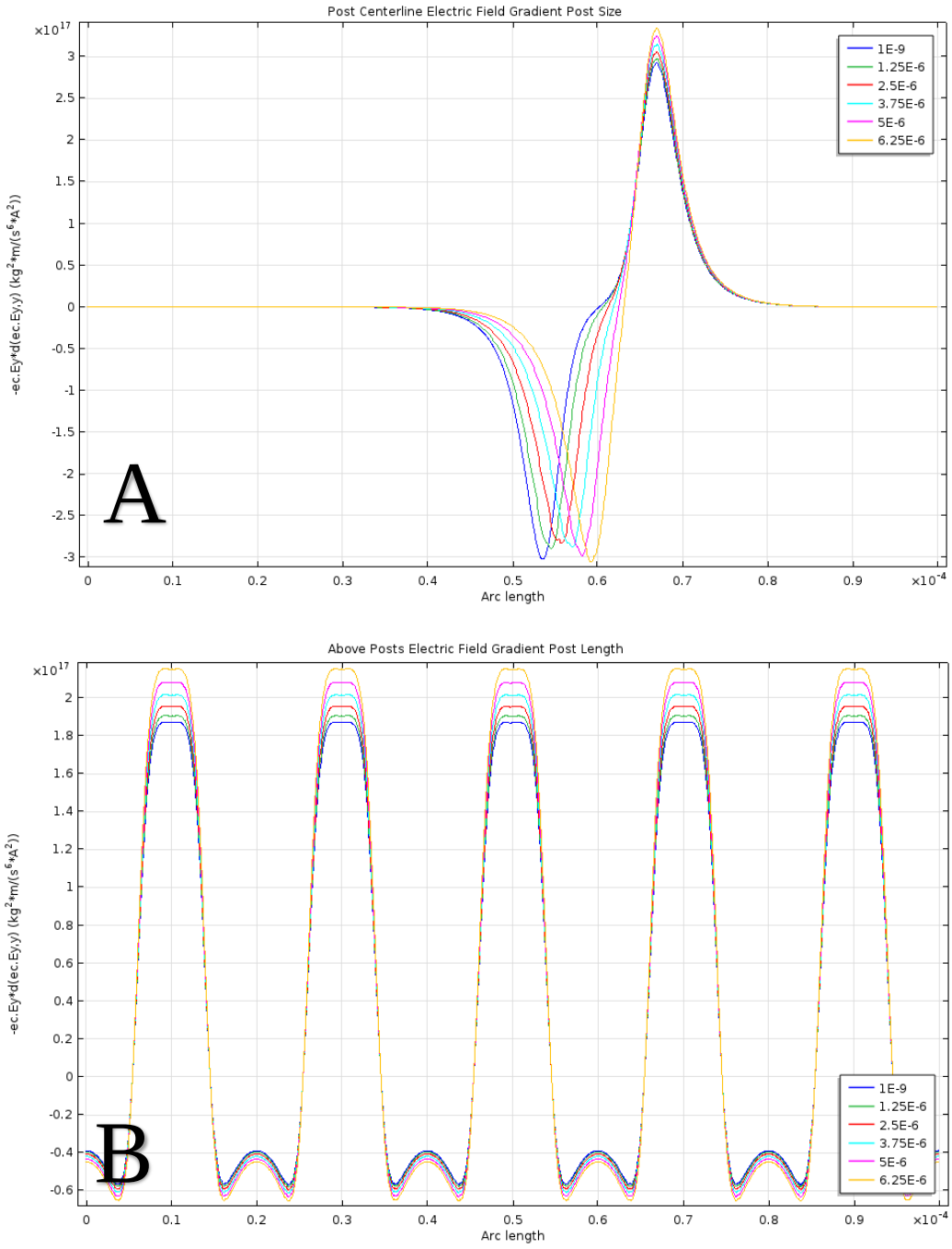

Figure 33: Line plots of ∇E^2 at (A) the centerline between posts and (B) 1 micron above the top of the post array with a changing chamfer distance from the bottom corners.

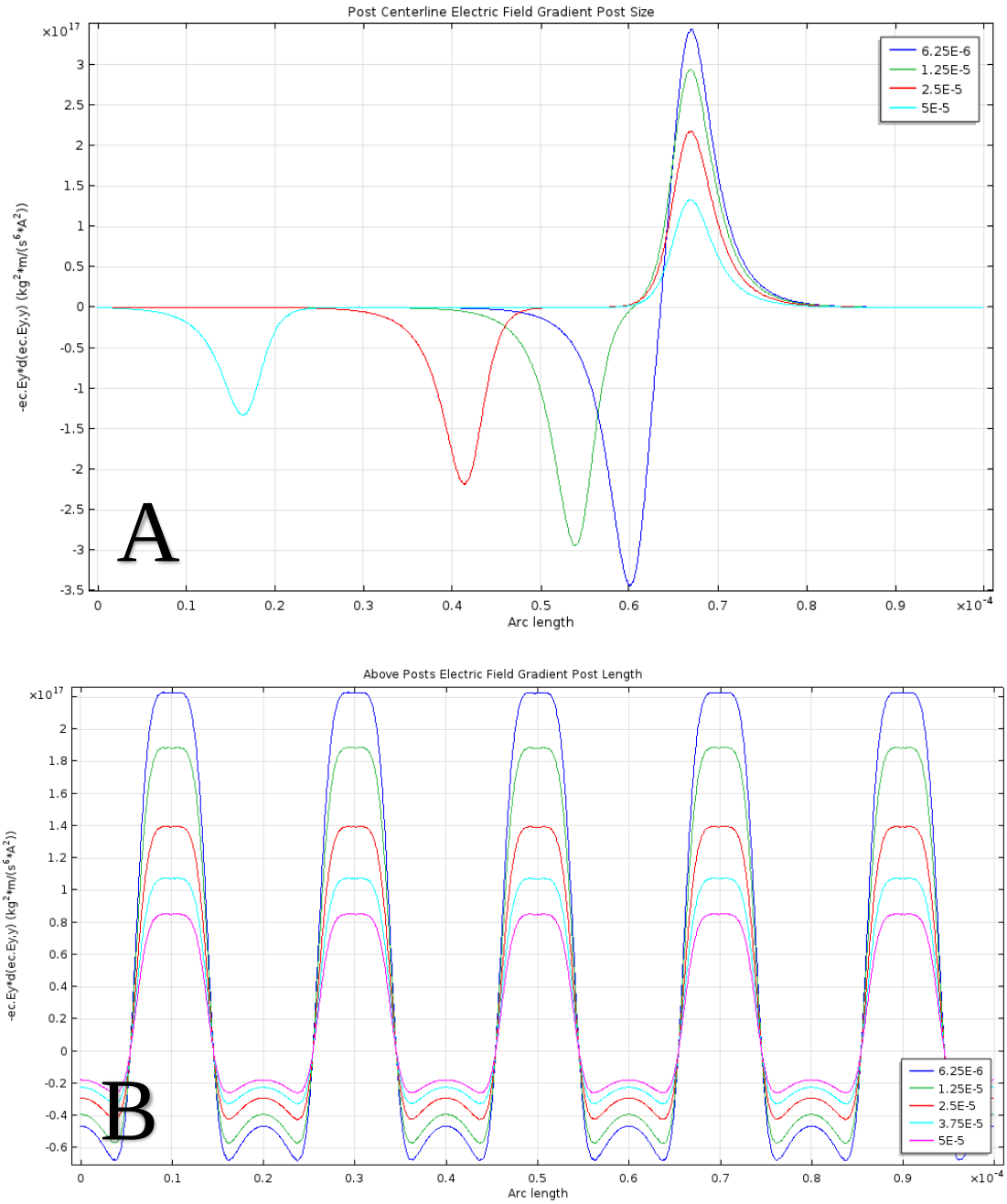

Figure 34: Line plots of ∇E^2 at (A) the centerline between posts and (B) 1 micron above the top of the post array with a changing post length.

From these figures it can be determined that decreasing the fillet radius at the top corners of the post, increasing the chamfer distance from the corner, and reducing the length of the posts all trend towards increasing the DEP force above the posts. Presumably, decreases in spacing between posts can also lead to increases in DEP force since increases and decreases in ∇E^2 are directly related to the width of the channels between posts. Differentials of each parameter can be seen in Table 11.

Table 11: Post geometry evaluation data with increasing feature size.

Parameter	Max ∇E^2 Differential (%)	∇E^2 2.5μm Above Posts Differential (%)
Chamfer	-16.4	-176.9
Fillet	14.2	14.9
Length	-61.3	-61.8

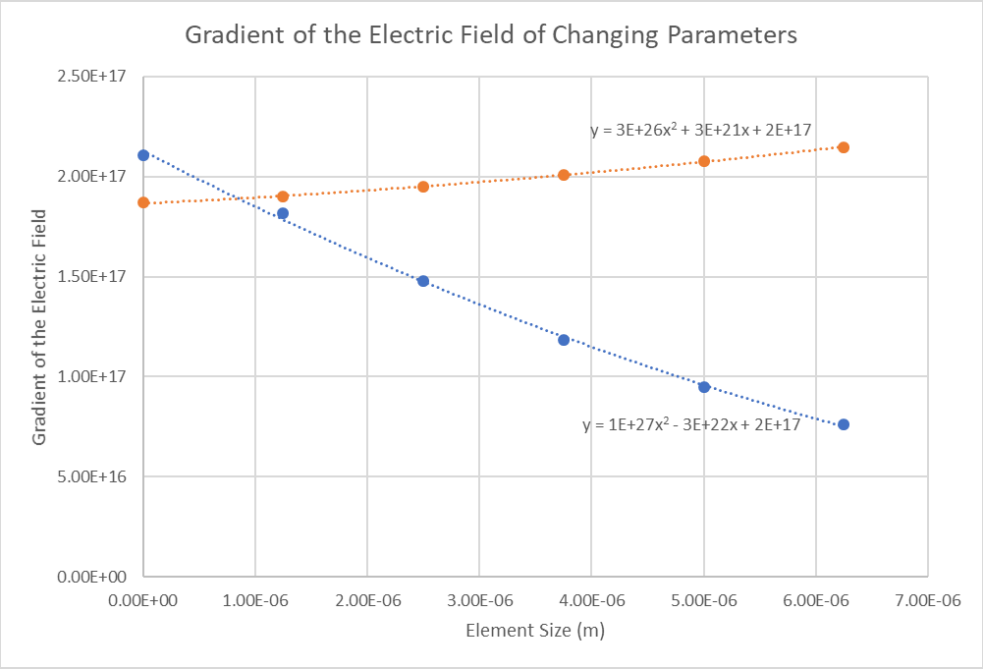

Figure 35: Scatter Plot of the changes in ∇E^2 at for changing fillet radius (Blue) and changing chamfer distance (Orange). Increased fillet radius trends toward decreased ∇E^2 and increased chamfer distance trends towards increased ∇E^2.

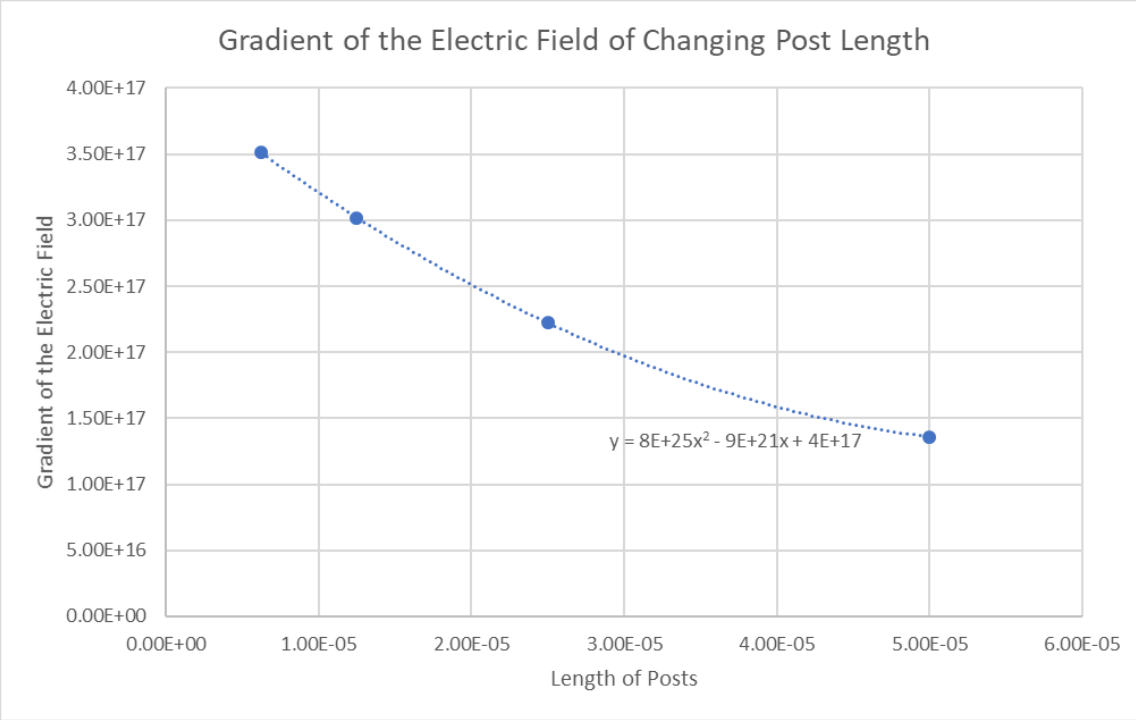

Figure 36: Scatter Plot of the changes in ∇E^2 at for changing post length. Post length trends towards decreased ∇E^2 with post length increases.

Considering the issues seen in the legacy device like particle trapping in the post array and flocculation of particles, it is my belief that larger spaces between posts is required to try to reduce these effects on the overall function of the device. In the legacy device the spacing between posts is 7.5μm, only 2.5μm larger than the diameter of yeast particles seen in the testing so in order to avoid fouling, the distance between posts must be sufficiently larger to accommodate the passage of multiple particles simultaneously. To counter the increased gap distance between posts, the size of the post must be increased. Blanca's DC iDEP device uses a 25:3 ratio of overall chamber cross sectional area to cross sectional area between posts to achieve particle trapping. Blanca also used a

linear post array style in favor of staggered rows and pointed posts on the ends of the array to avoid attractive DEP fouling of the device.

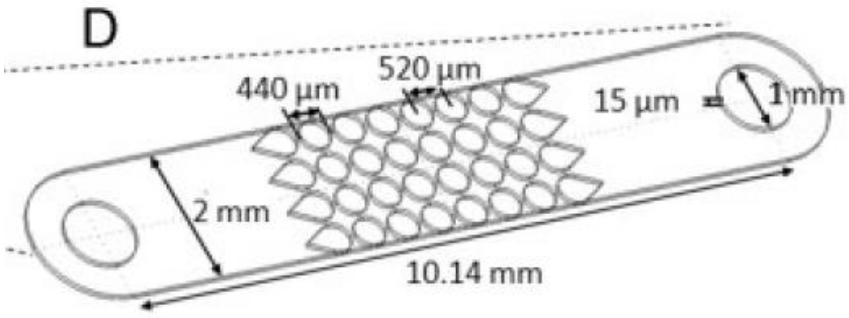

Figure 37: Device used by Blanca to perform iDEP particle trapping [8].

Taking this information from Blanca, it would be better to go with larger insulating posts without a staggered row pattern. Larger insulating posts allow for easier fabrication possesses, but also requires a larger ratio of chamber cross sectional area to cross sectional area between posts.

5.3 3D Printed Device Design and Testing

Another form of rapid prototyping is 3D printing, and since the Cal Poly Biomedical Engineering department has a FormLab 2 3D printer there was a desire to try to create microfluidic devices using the printer. The 3D printed design was built in Fusion 360 and designed as a boat so all PDMS could be poured directly over the features in the design. Four different device designs were built into the design including: an open channel design to test EK, a narrowing channel design with a 40μm gap, a "home plate" design device, and a "Blanca" recreation device (Figure 38). Once printed the features of the devices were observed under a light microscope to see the quality of the features (Figure 38).

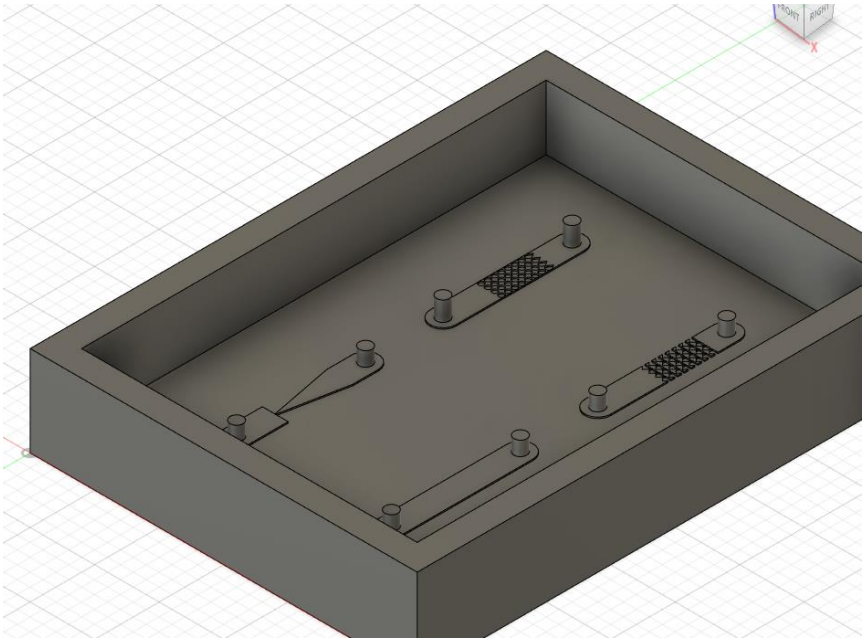

Figure 38: Fusion 360 model used for 3D printed device to try to test iDEP and EK.

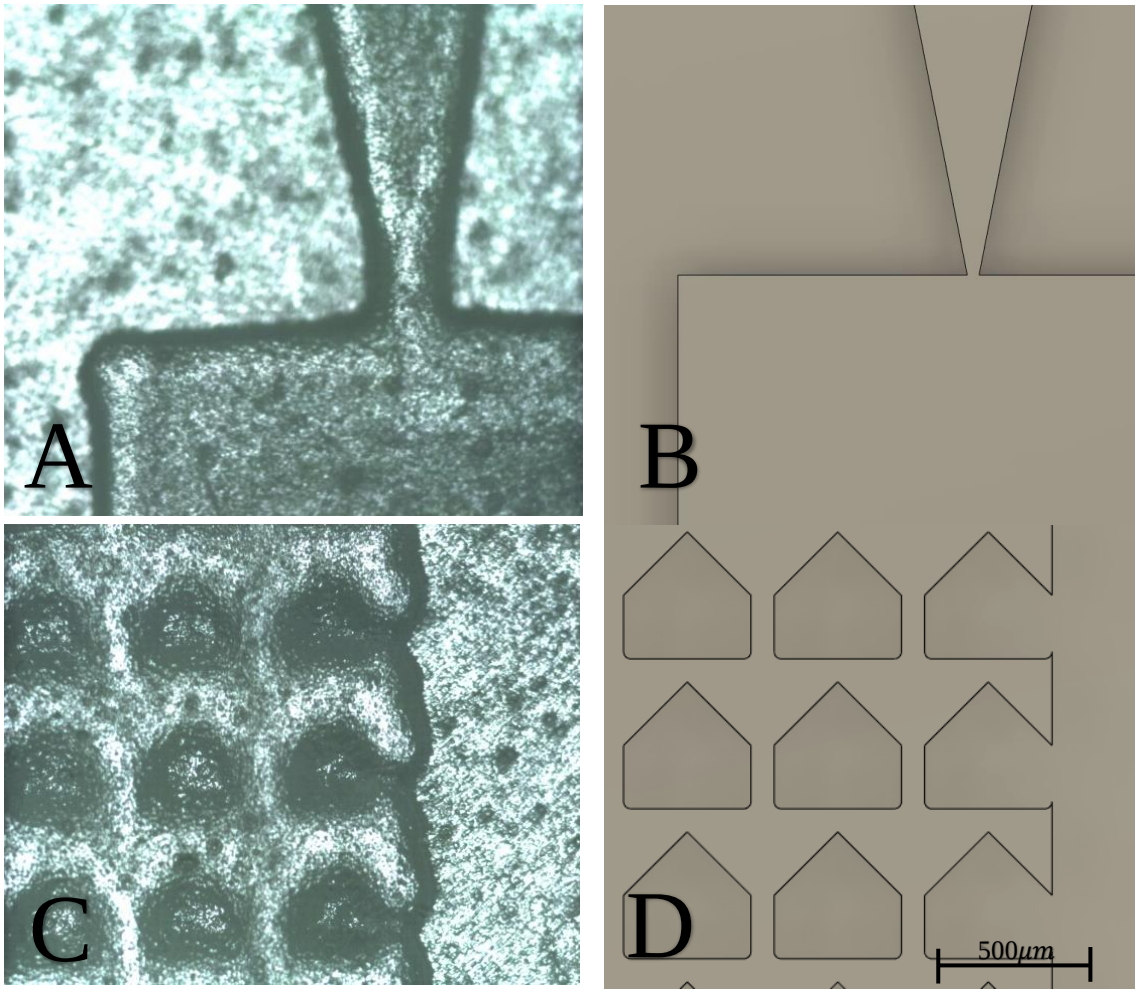

Figure 39: Comparision of the neck in the necking device of the (A) 3D printed device and (B) the 3D model design. Comparison of the "Home Base" posts of the (C) 3D printed device and (D) the 3D model design.

Comparison of the features as they were intended showed that the 3D printed device did not have good resolution. This was to be expected since the FormLab 2 is rated to make features as small as 25μm in the height (z direction) of the device. In the plane observed (x-y plane) the 3D printer was not able to achieve that level of resolution and seemed to achieve a resolution in the x-y plane of 200μm.

Devices created from the 3D printed mold and tested were the open channel and the necking channel to observe the electrokinetics and to observe dielectrophoresis. Both were tested using the testing parameters set forth for the previous test; resulting in bubble formation in the open channel and necking channel and overall failure.

5.4 New Device Design and Wafer Fabrication

By taking the information gained from the iDEP post optimization and what was found from the legacy device testing, several new device designs were able to be designed. On the new wafer, 8 designs were created. Of these 8 designs there were: four narrowing channels, one circular post device [Blanca], a triangular post device, a "home plate" post device, and an open channel. The mask used to create these devices is shown in Figure 40.

Devices 1, 5, 6, and 7 are the narrowing channel devices and were designed for two reasons; see if features this small could be reproduced in the Cal Poly lab and to create the optimal conditions to induce iDEP. The gap distances of these devices are $80\mu m$ for device 5, $40\mu m$ for devices 1 and 5, and $20\mu m$ for device 7. Device 2 is the "home plate" post design. Device 3 is a recreation of the device used by Blanca without the pointed ends on posts at the top and bottom of the array. Device 4 is the triangular post design. Finally, device 8 is the open channel for observation of electrokinetics.

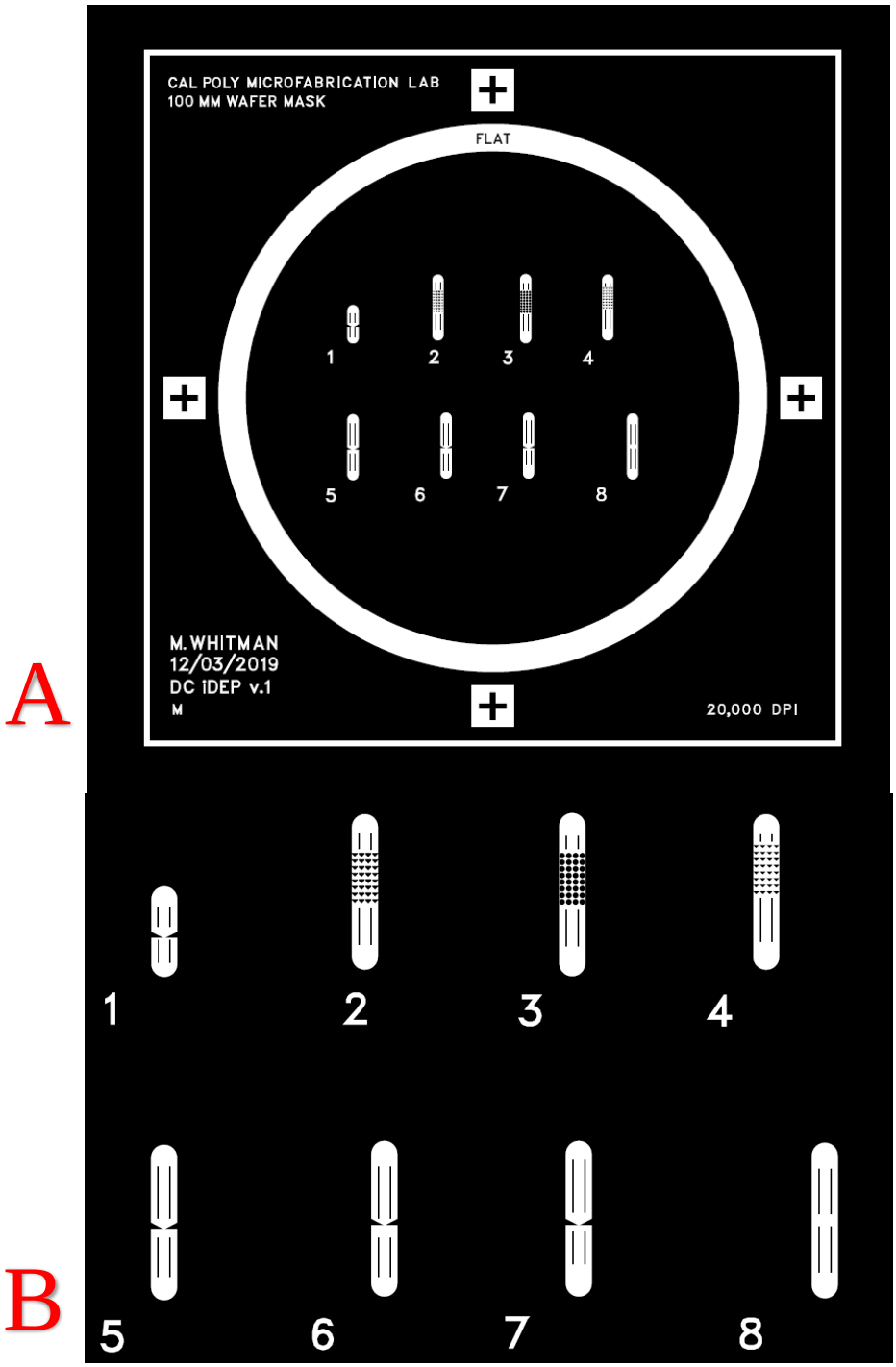

Figure 40: Shows images of the (A) mask used in photolithography and (B) zoomed in view of the devices created.

Fabrication of the new designs was done in the Cal Poly microfabrication lab using photolithography. Two Si wafers were put through the fabrication process from start to finish. Prior to fabrication, 2007 SU-8 was placed out in the lab 24 hours ahead of time to allow heating to room temperature. Once in the lab a heating plate was turned on and set to 95°C, the heating lamp on the GAMM mask aligner was checked to make sure it was on, and Piranha was heated to 70°C. Wafer cleaning was then performed in the following order:

- Immerse wafers in 70°C Piranha for 10min.
- DI water quench wafers.
- Immerse wafers in buffer oxide etchant (BOE) for 30 seconds.
- DI water quench wafers.
- Spin rinse and dry in Spin Rinse Drier (SRD).
- Dehydration bake at 150°C.
- Allow wafer to sit on cooling plate.

The next step in the fabrication process was to spin coat the SU-8 onto the wafers. The spin coater was then covered in aluminum foil without having the spinning chuck come in contact with the foil. The wafer was then taken from the cooling plate, placed into the centering tool, and applied a vacuum to hold the wafer in place on the chuck. SU-8 was poured into the center of the wafer and the lid to the spin coater. Using the SU-8 data sheet, the steps to create the desired $10\mu m$ film of 2007 SU-8 in the spin coater were programmed as:

- Step 1: 20sec, 400rpm, ACL=1
- Step 2: 35sec, 1500rpm, ACL=6

- Step 3: 5sec, 300rpm, ACL=5

Wafers were then removed from the spin coater and placed on the 95°C hot plate for a 3-minute soft bake.

Wafers were then ready for exposure and the required exposure energy for a $10\mu m$ thick film was approximately $125mJ/cm^2$. The GAMM mask aligner is capable of producing $15mW/cm^2$ so the exposure time used was 10sec. The layers for the exposure were stacked in the following order from bottom to top:

- 5x5 blank glass
- Wafer with photoresist facing up and major flat facing the rear of the aligner.
- Transparency mask with the printed side facing down.
- 5x5 blank glass

Wafer then underwent exposure and then was removed from the stack for a 4min post exposure bake (PEB) on the 95°C hot plate. After PEB wafers were placed onto a cooling plate.

The wafers were then loaded into a Teflon cassette and immersed in developer for 3 min. After development wafer was taken to the spin coating hood and sprayed down with Acetone then IPA and dried with N2 gas. The second wafer still had a white coating to it, so it was placed back into the developer for an additional two minutes and repeated the wash step. Once dry wafers were placed onto the 150°C hot plate for a hard bake and moved to the cooling plate after 5 min.

After wafers cooled back to room temperature, they were brought to the optical microscope to observe features. Wafer was determined to have the feature sizes desired for testing since wafer one went through an extra spin coat step that caused the SU-8 film

to become too thin. Some defects were observed in the devices on the wafer, but not that would affect the overall function of the device were seen so the fabrication was determined to be a success.

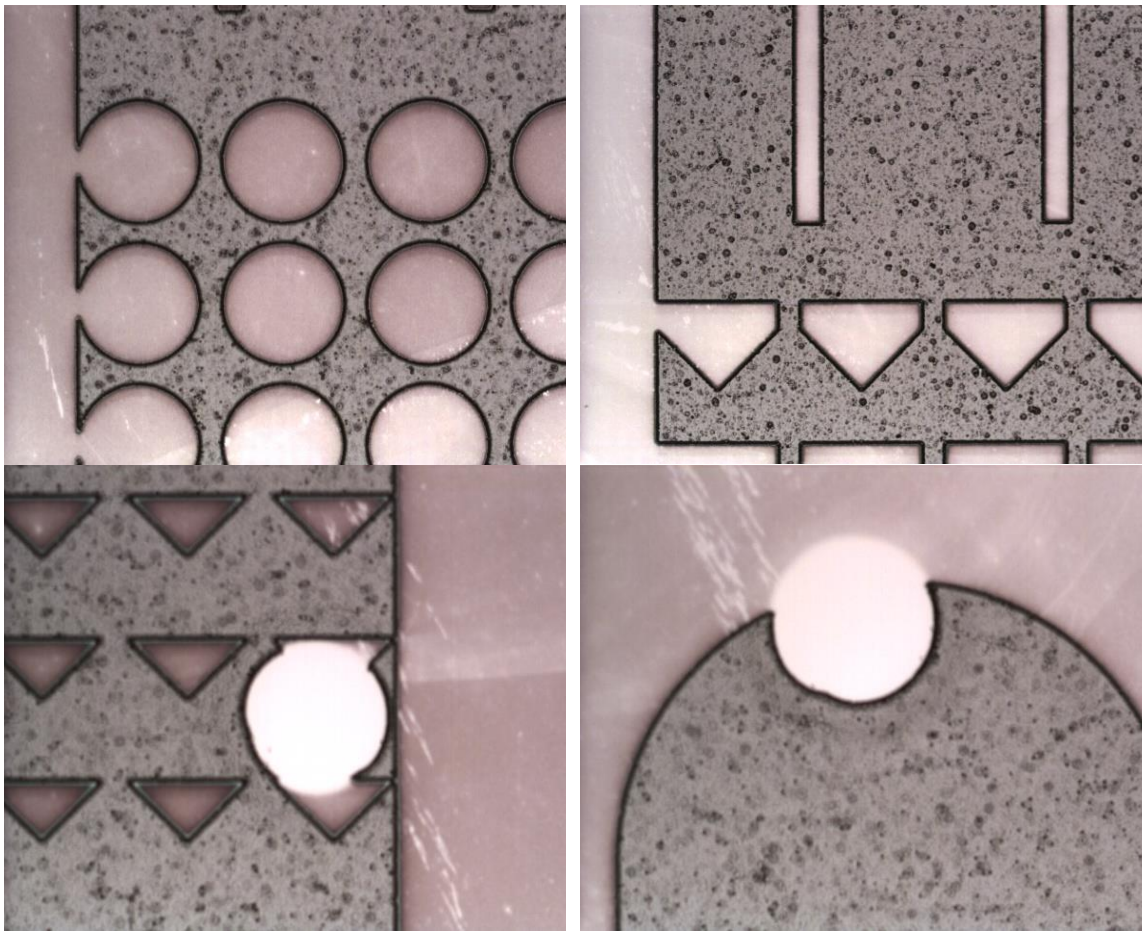

Figure 41: Images of the new devices made from soft lithography. (A) The blanca recreation device and (B) the “Home Plate” device. Some devices contained defects from the fabrication process, but the defects shown in (C) and (D) did not impair the overall function of the devices.

5.5 New Device Testing

For testing the new devices, the same testing procedure as the legacy device was followed with the adjustments of reducing the concentration of NaCl in water to create a

FCM of -0.4 (0.033g of NaCl per 0.4L of water) instead of -0.5 (0.7g of NaCl per 0.4L of water). This was done to reduce the current running through the device to reduce the effects of joule heating on the system.

Devices were submerged in the NaCl solution and vacuum pumped down for one hour to prime properly with agitation to remove bubbles (hit that bell jar). After priming the device was removed from the bath and taped down into a Petri dish. Using a syringe, solution was pooled around each port to the device and a pipette tip was filled with solution and allowed to drip while inserting into each port. The inlet side (high potential) was chosen and a few drops of the yeast mixed with NaCl solution were dripped into the top of the pipette tip via syringe. Using another syringe solution was removed from the outlet (low potential) pipette tip and the device was allowed to get yeast into the entrance of the device via pressure driven flow. Once yeast could be observed at the entrance port using the SVM camera, solution was placed back into the outlet port to equalize the pressures. Electrode wires were dangled into their respective pipette tips and at this point testing was ready to commence.

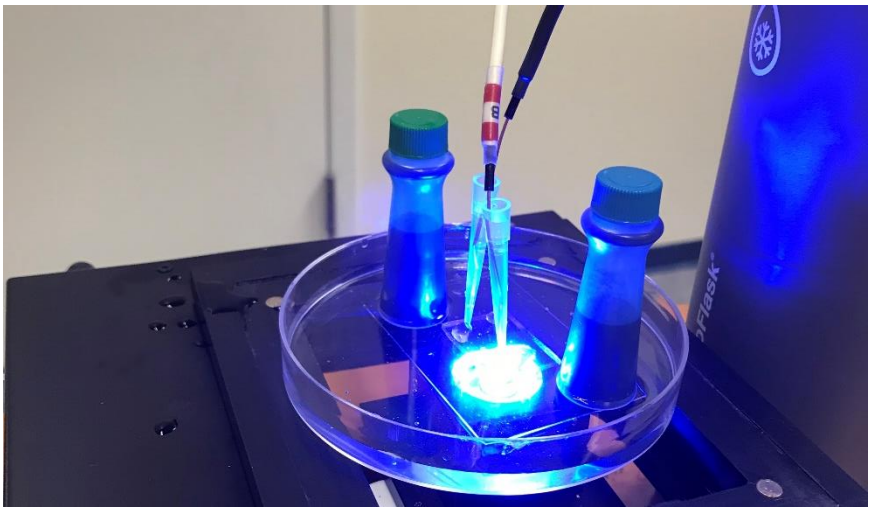

Figure 42: Final testing setup with pipette tips raising electrodes off the device.

5.6 New Device Results

For all the new devices tested, the electrode orientation in videos and images was oriented to have the low potential at the top and the high potential at the bottom. Since electrodes were dangled into the pipette tips the distance between electrode tips needed to be estimated to be the length of the device plus about 1cm.

5.6.1 Testing Round 1

In the first round of PDMS device creation device 7 ($20\mu m$ necking channel) became damaged and was not able to be used in in the first round of testing. Additionally, the two other 1cm long necking channel devices were tested with the electrodes placed directly into the device and this caused bubble formation and electrolytic products to occlude the device. The order of device testing for the final testing setup was open channel device for EK, the "shorty" device, the "home plate" device, the "Blanca" recreation device, and the triangle post device.

5.6.1.1 Open Channel EK

To test the electrokinetics of the new device, ImageJ was used to track the particles as they moved through the frame. Particles were tracked one frame apart from each other at both 400V and 200V potentials to determine the electrokinetic mobility of yeast. Using COMSOL, the testing setup was recreated in 3D and the electric file strength in the device was confirmed to be 400V/cm and 200V/cm for 400V and 200V potentials respectively. Results for each of the EK tests can be seen in Table 12. The EK testing showed that the data found is comparable to literature [8]

Table 12: Results of EK testing in Open Channel device.

400V potential (400V/cm)	Value	Units
Average Velocity	36.36	microns/frame
	0.001091	m/s
Average EK mobility	2.727E-08	$m^2/(Vs)$
200 V Potential (200V/cm)		
Average Velocity	22.74	microns/frame
	0.0006823	m/s
Average EK mobility	3.412E-08	$m^2/(Vs)$
Combined Estimate		
Average EK Mobility	3.069E-08	$m^2/(Vs)$
Blanca Yeast EK Mobility [8]	2.931E-08	$m^2/(Vs)$

By taking the found EK mobility the net zeta potential of the system could be determined and was found to be -39.3mV.

5.6.1.2 "Shorty" Device Testing

Taking the information gained from the open channel testing the "shorty" device was chosen to test next. The setup for this device was done similar to the open channel except only a voltage potential of 200V was used which equates to an electric field strength of 400V/cm.

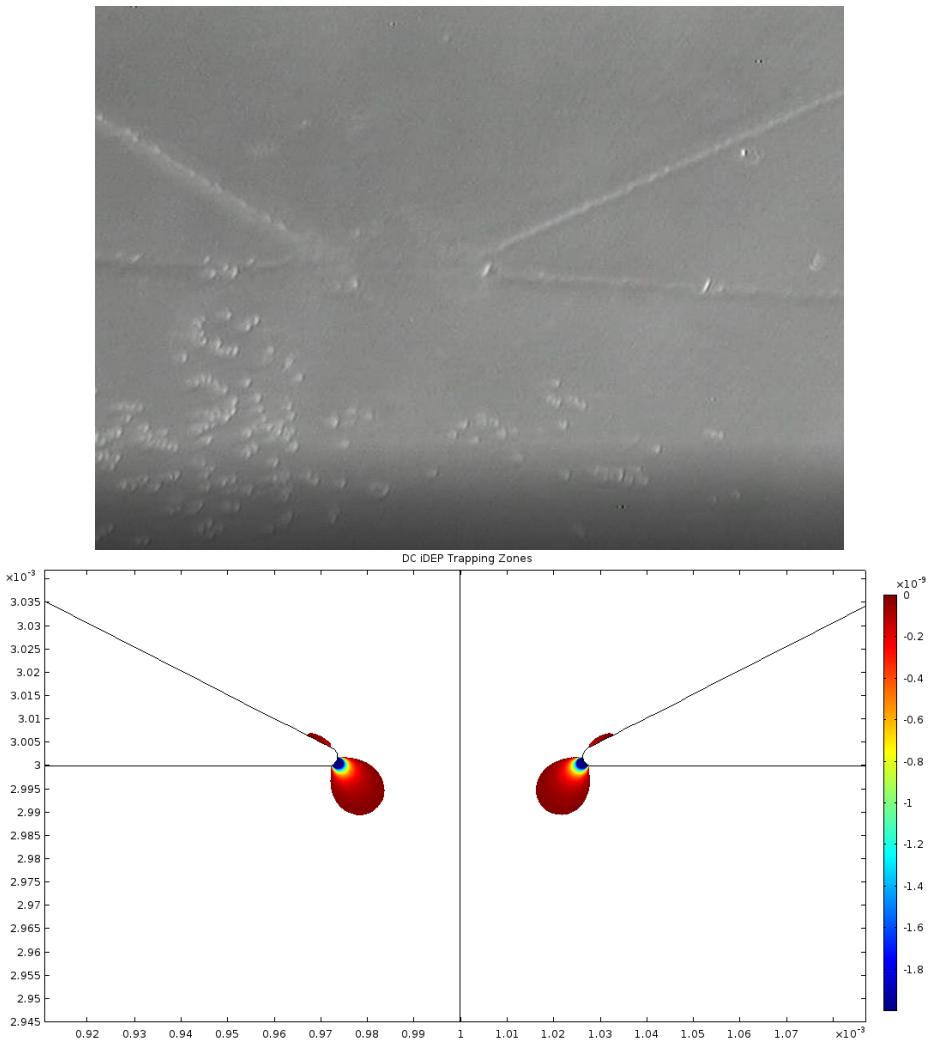

Figure 43: Images of iDEP of the "shorty" device (A) in the lab at 400V/cm and (B) force balance in COMSOL at 400V/cm.

It is evident that doing the force balance in COMSOL with certain assumptions is not enough to accurately show the correct particle trapping zones for DC iDEP. To get the COMSOL simulation to accurately represent the regions that experience iDEP trapping the DEP force must be multiplied by a factor of 4, seen in Figure 44.

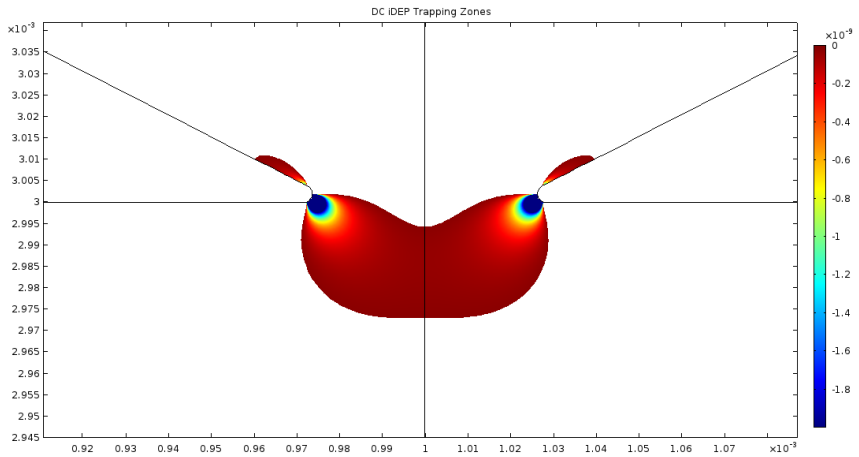

Figure 44: Image of iDEP of the "shorty" device simulation with factor of 4 multiplier. The multiplication factor was added to more accurately represent experimental results.

5.6.1.3 "Home Plate" Device Testing

The "Home Plate" device was tested with the same setup and tested at both 400V/cm and 800V/cm. Upon turning on the electric current particles were observed to undergo DC iDEP around the posts (Figure 45A). However, when looking at the central and right-side channel, not particles were seen to get to those openings. Additionally, when looking around the device it was observed that yeast particles had become trapped in a along the left side of the device in the open part of the channel leading up to the posts (Figure 45B). Most of the open portion of the channel on the high potential side of the device was void of any yeast particles, leading to believe that either the device had become occluded during preparation for the experiment, during plasma bonding to the glass slide, or the SU-8 film in that region had become too thin during the production process. Even though iDEP was observed during this test, it is necessary to redo the test with a new device to retrieve better data.

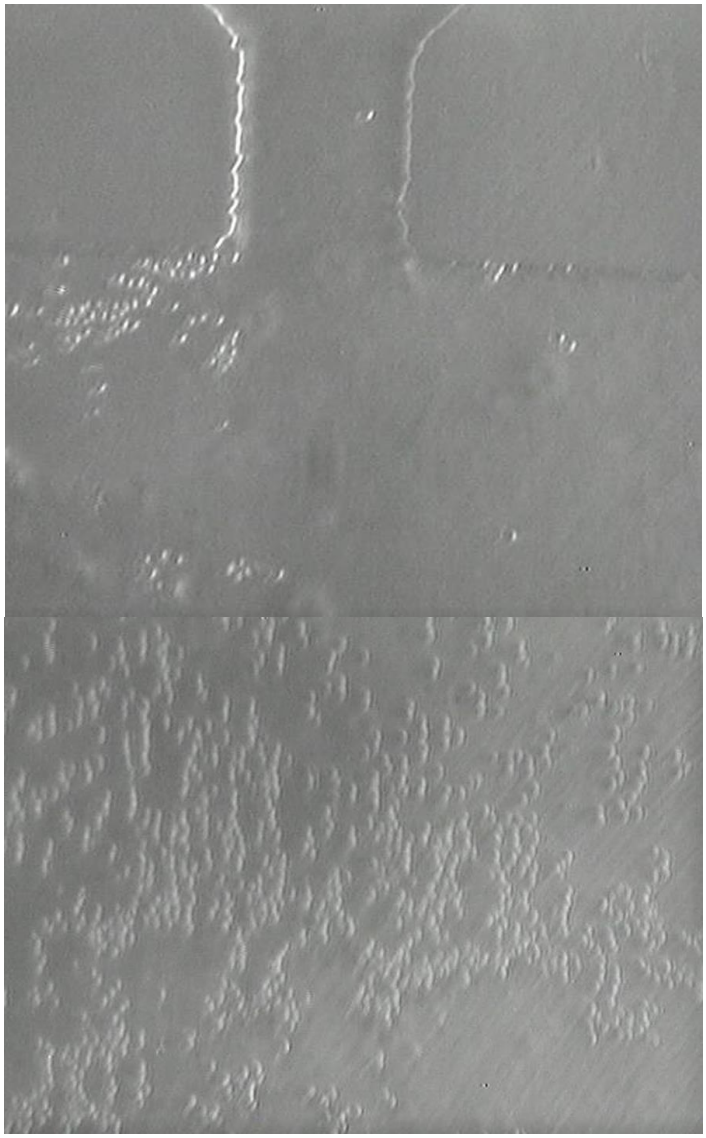

Figure 45: Images of the “Home Plate” device (A) iDEP trapping at the posts and (B) channel occulsion away from the insulating posts.

5.6.1.4 Blanca Recreation Device Testing

The device recreated from [7] was tested to confirm that the testing procedure done in this thesis is indeed sufficient to produce iDEP in a microfluidics device and as a baseline to compare against. This device was tested at electric field strengths of 400V/cm

and 800V/cm. At both electric field strengths iDEP was observed consistently across all post channels in the device (Figure 46).

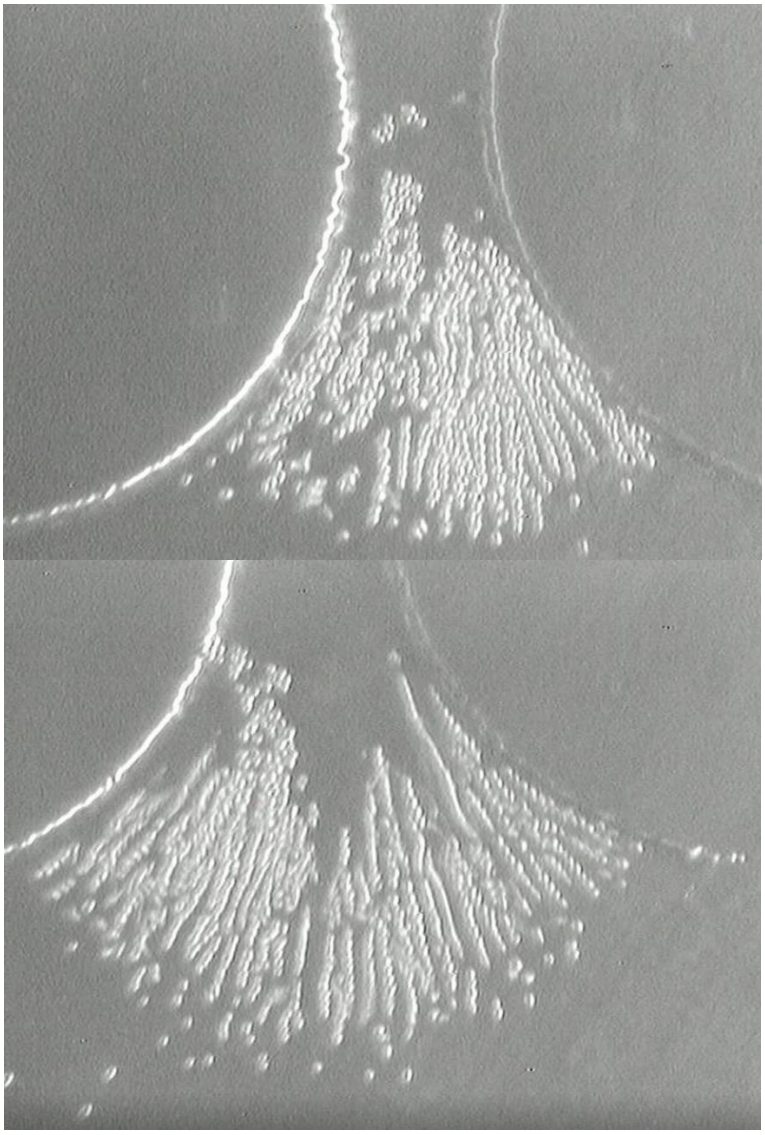

Figure 46: Images of the Blanca device (A) iDEP trapping at the posts with electric field stength of 400V/cm and (B) iDEP trapping at the posts with electric field stength of 800V/cm.

When comparing these results to COMSOL simulation, the required multiplier for to recreate these results was 4 (Figure 47).

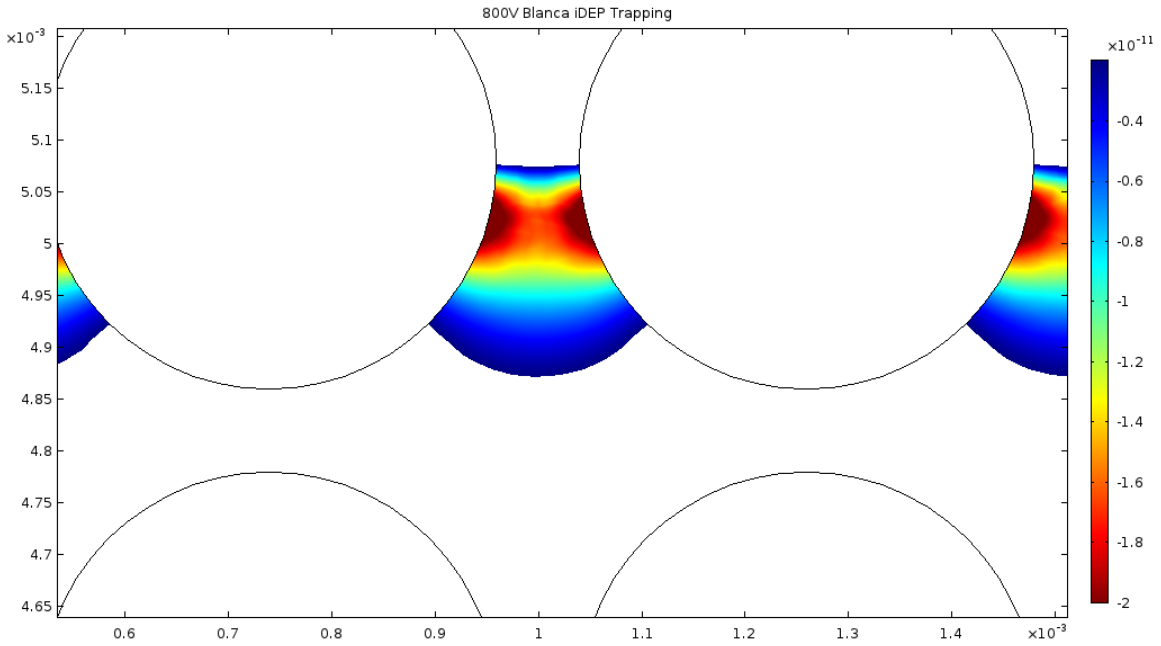

Figure 47: Image of the Blanca recreation device, showing the iDEP trapping between posts with electric field stength of 800V/cm. Similar trapping area compared to what was seen in the lab. *(Includes changing viscosity)

5.6.1.5 Triangular Post Device Testing

When testing began for the triangle post device it became evident that much of the device was occluded, like the “Home Plate” device. DEP was observed in the left most post channel (Figure 49), but something happened during the first few second of the test that altered the conditions in the device since flow began flowing in the opposite direction that it should have been, resulting in a failure of this test. This failure necessitated another device to be made and had similar sources of failure like the “Home Plate” device.

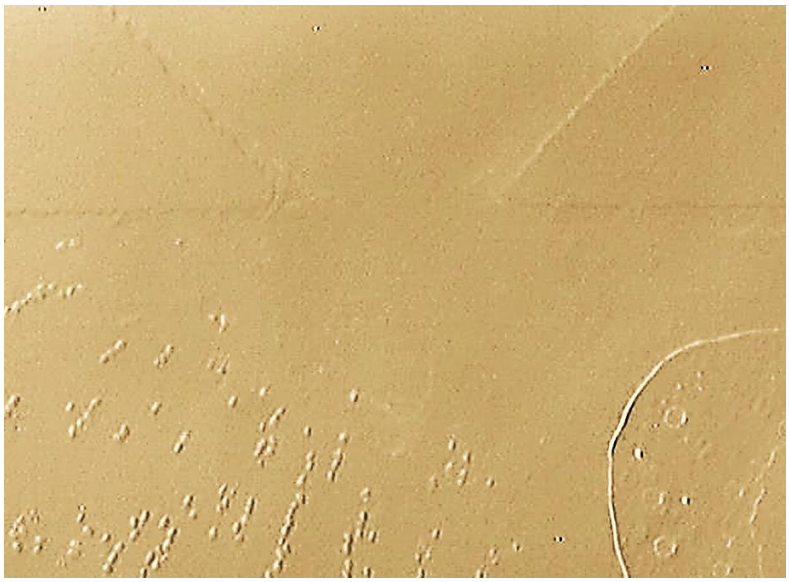

Figure 48: Triangle post device DEP observed within the first few seconds of testing before flow direction switched. Image was edited to better show the posts.

5.6.2 Testing Round 2

A second round of testing was performed on the “Home Plate” and triangular post devices since in the first round of testing both had been occluded during the device fabrication process. On the second try both devices were fully patent and testing for both was successful. The same testing conditions were used as the first round of testing to compare to the other devices.

5.6.2.1 “Home Plate” Device Testing

In the second round of testing for the “Home Plate” device, iDEP was able to be created successfully. DEP was observed at both 400V and 800V potentials or 400V/cm and 800V/cm respectively.

It should be noted that on the first attempt at performing the experiment at 800V, the flow direction switched. Particles began flowing in the opposite direction (ground to high voltage) they were supposed to. When the voltage polarity was switched, then the

particles would switch directions again. This was interesting since it shows that the particles were still under the influence of the electric field, so EP had taken over and EO flow had likely been blocked or impeded. To remedy this and remove some of the bound yeast particles the device was flushed with 2mL of NaCl solution using a syringe. This did result in some blockage of channels due to large debris, but DEP was still observable in unblocked channels.

Once an electric field of 400V/cm was applied, it appeared that particles were able to pass through the bottom of the post array once the system reached steady state. Once the device was flushed and tested with 800V/cm, particles were held below the post array. However, in both cases, it was noted that particles began passing the posts or would hover the closest to the posts at the midpoint between them, as was noted in the post testing simulations.

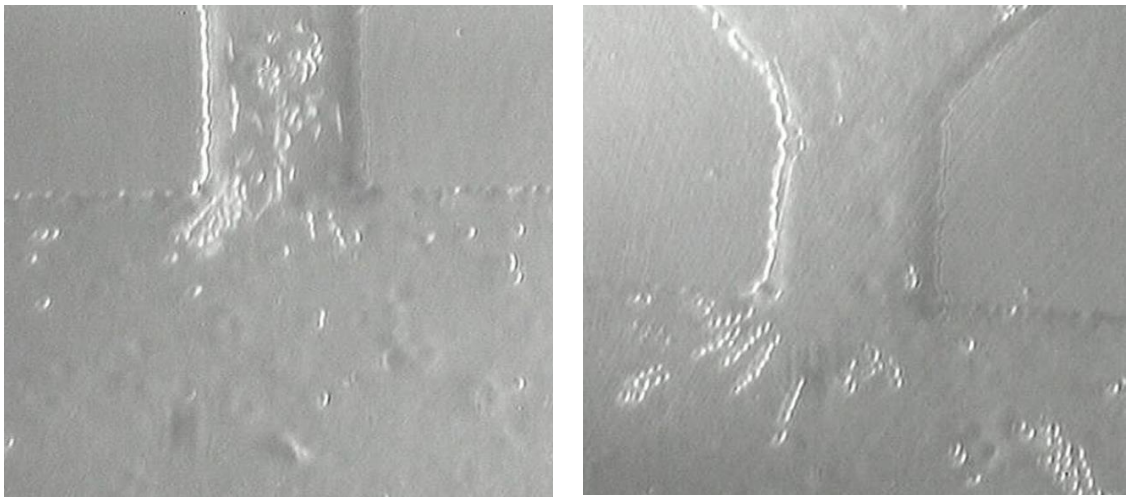

Figure 49: Images showing the “Home Plate” device at (A) 400V/cm with particles passing through the filter and (B) 800V/cm with particles being held below the filter.

When comparing this to what is seen in COMSOL simulations there seems to be a relatively good comparison to experimental values. To better represent the results seen in

experiments, the corners of the posts were rounded with a chamfer, which better represents the geometry for the device itself.

5.6.2.2 Triangular Post Device Testing

For the triangular post design iDEP was observed in both the 400V/cm and 800V/cm electric fields. The flow in this test briefly switched directions but was remedied after removal and resetting the pipette tips. The 400V/cm test showed good DEP trapping below the posts, but some yeast particles did manage to make it through the filter.

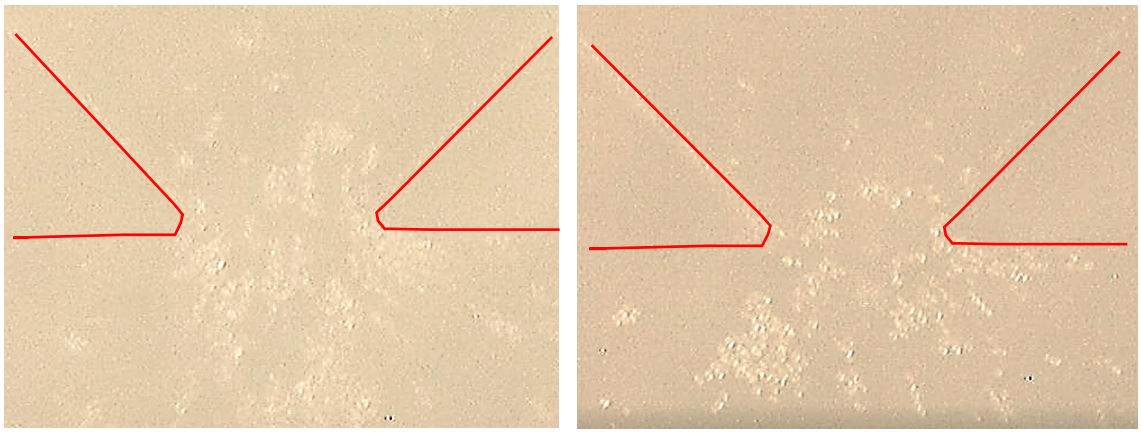

Figure 50: Images showing the triangular post device at (A) 400V/cm with particles both being held below the filter and passing through and (B) 800V/cm with particles being held below the filter and some passing the filter. Red lines indicate the outline of the posts.

When comparing these results to COMSOL simulations there were some similarities to be found and was found to be a decent representation of what is happening. To get COMSOL to produce better results the points on the corners of the tringle had to be rounded with a chamfer which represents the resulting device geometry better.

5.7 New Device Discussion

Overall the results of the first round of devices and testing resulted in devices that did produce iDEP and gave comparable data to that of literature [8].

The open channel device allowed for the determination of the EKs of the yeast particles and the net zeta potential between the yeast surface and PDMS surface. Additionally, this was the first instance in this set of tests that showed that combining raising the electrodes off of the device in pipette tips and reducing the conductivity of the medium to reflect a CM factor of -0.4 did not produce bubbles and reduced electrochemical byproducts. After longer tests electrolysis debris still occurred, but in reduced amounts.

The "shorty" device confirmed particle trapping at electric field strengths as low as 400V/cm. It was also found in this test at there is a disparity between what happens in experimental tests vs. COMSOL tests. In order to more closely simulate iDEP in the computer some of the assumptions made need to be changed. Since bubble formation was observed, this means that the fluid is heating up and boiling with the higher conductivities. With the reduction of fluid conductivity, the medium was not observed to boil, but the fluid is likely still experiencing Joule heating. If fluid temperature increases, there will be reductions in fluid viscosity [29]]. By taking the dynamic viscosity values found from [30] and graphing them in Excel, a second order polynomial equation for the viscosity in relation to temperature was found to be:

$$\eta = 2x10^{-7} * T^2 - 3x10^{-5} * T + 0.0016 \quad (43)$$

Viscosity is in terms of $Pa * s$ and T is the temperature in Celsius. This was included in COMSOL simulations by replacing the dynamic viscosity term in the written force

balance on surface plots. Simulations with this included were done at steady state under the assumption that new fluid introduced to the system would flush the heated fluid with room temperature fluid.

With the addition of the Joule heating module to the simulation this was able to reduce the multiplication factor required to replicate the experimental results. With the addition of a changing dynamic viscosity, the model is no longer able to be mapped using the mobility term since both the EK and DEP mobilities have an inverse dynamic viscosity term that would cancel out. To include the changing dynamic viscosity the forces on the particles need to be used since the viscosity affects the drag force on the particle, but not the DEP force; allowing for a decreased multiplication factor of 2 to produce the equivalent trapping regions.

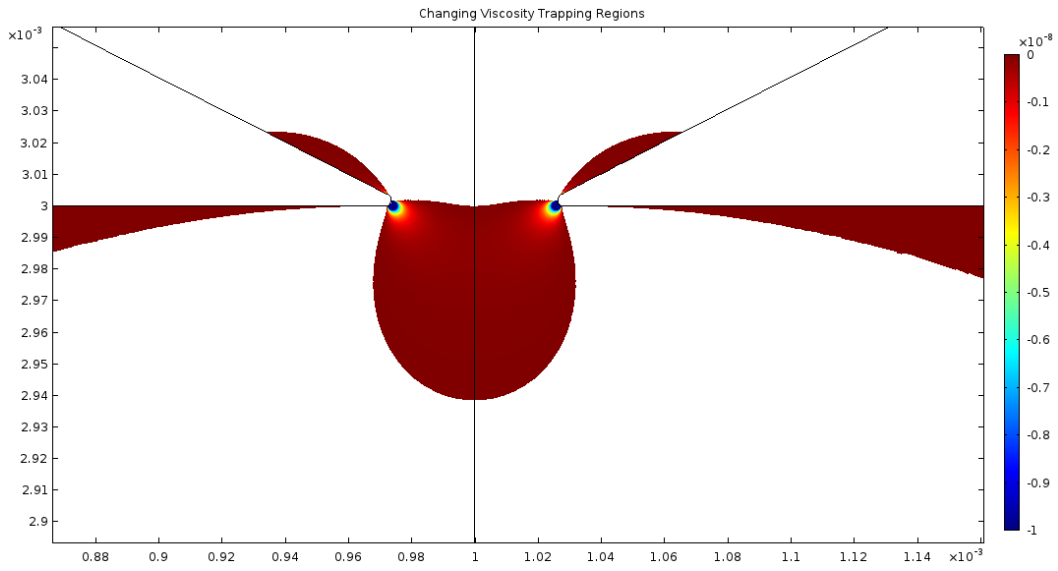

Figure 51: COMSOL simulation of the “shorty” device with the changing viscosity term included. More closely resembles what was seen in the lab than a constant dynamic viscosity term.

When the changing viscosity is added to the triangular and “Home Plate” post designs they both show close resemblance to where particles will have a force in the negative y-direction act on them (Figures 50A and 50B). Another issue seen in COMSOL was that the mesh affects the areas that will show up in the surface plots. Some of the simulations had to have their mesh size reduced in order to properly show the regions of force in the negative y-direction (Figure 53A and 50B).

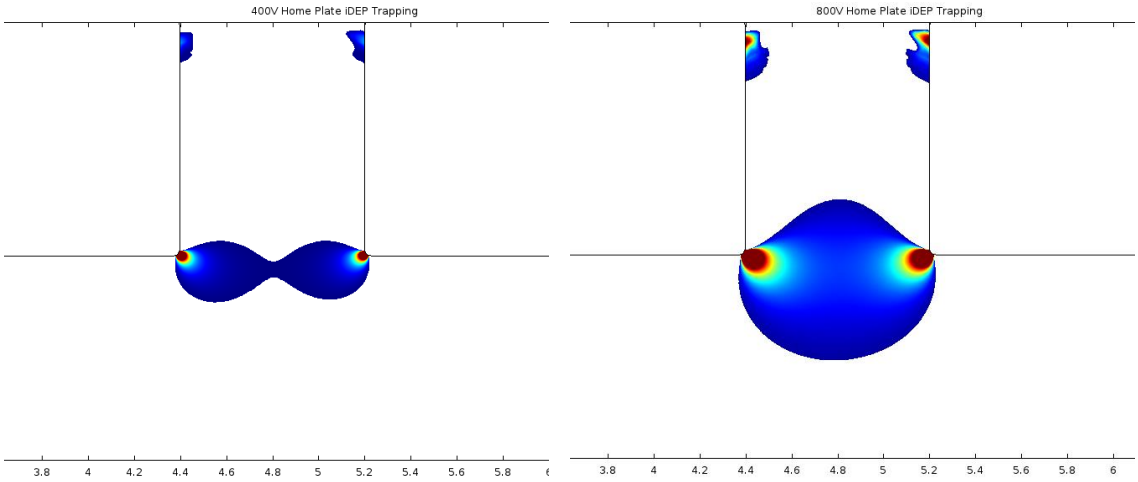

Figure 52: Images showing COMSOL simulation results of the “Home Plate” device force on particles in the negative y-direction at (A) 400V/cm with strong negative forces at the corners of the post and decreased force at the midpoint between postes and (B) 800V/cm increased force below the posts.

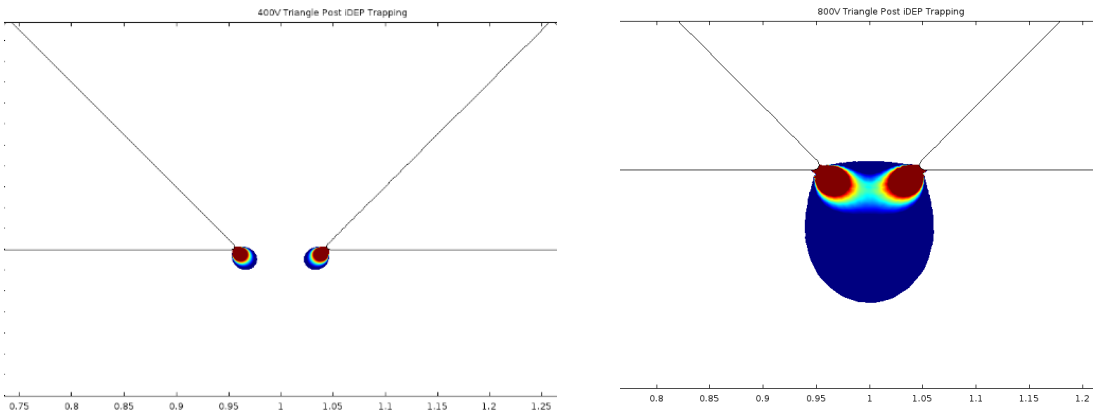

Figure 53: Images showing the COMSOL triangular post device simulations at (A) 400V/cm showing particles can pass through the posts and (B) 800V/cm showing that particles will be trapped below the post array.

CHAPTER 6 DISCUSSION

6.1 Legacy Device Discussion

Throughout the course of the simulation and testing process there were a lot of takeaways from each set of simulations and tests. Starting off on the legacy device, a lot was taken from the numerous tests done on the legacy device. A major takeaway was that there can be a disparity between what is simulated using COMSOL and what will be seen in the lab.

When conducting initial simulations, there was no consideration for Joule heating; thus, the effects of temperature on viscosity or the changing chemical and electrical conditions at the interfaces. Electrolysis also was not considered and how bubble and debris formation would affect device operation. Rapid formation of bubbles from high conductivity contributed to improper function of the device and the realization that Joule heating must be considered.

When observing the legacy device as a whole; it quickly became apparent that certain aspects of the legacy device were not needed. The bubble weirs did nothing to prevent the entrance of bubbles into the main chamber of the device and often found themselves filled with bubbles. Therefore, elimination of the bubble weirs and the top and bottom crossflow channels is an easy design change that can be made in future iterations. Secondly, the device itself is long (3cm from electrode port to electrode port) forcing higher voltage potentials and increased current and Joule heating. The device could be significantly shortened as was demonstrated in the “shorty” device, lowering voltages, improving safety, and allows for easier operation.

The post array itself needed to be adjusted as well. The staggered post array design does show to have an effect on increasing the DEP force along the top of the filter; however, any benefit of increasing DEP force is eliminated when particles that pass the first row rapidly foul the succeeding rows of posts. Another way to reduce the possibility of fouling is to reduce the number of rows in the filtration array since if particles are going to pass the top row, they will either pass through the whole filter or will just foul onto a post in the array. This led to the desire to test out different post designs to try to increase the DEP force and reduce the chances of fouling, which led to the "Home Plate" and triangle post designs since there projected the DEP force the most.

Many of the early simulations showed that the legacy device would work at least as an iDEP trapping device at some higher voltages, but experimentally that was not the case. Since it was not able to perform its basic function as an iDEP filter this immediately brought up red flags when thinking if the device was designed properly. Even during the brief time in tests before bubbles formed, at no point were particles observed to be affected by iDEP, even at a high CM factor (-0.5). Since iDEP did not occur, the insulating post array would rapidly foul with yeast particles or allow yeast particles to readily pass through the array.

The final observation that was made for the legacy device is that the fluid dynamics of the system are not designed to perform the desired operation. From the simulations and seen in testing; if particles are going to pass the filter they will do so in the first few columns of posts and flowrates needed to escort the particles to their desired exits are not reasonable for microfluidic devices since they are on the order of centimeters per second or decimeters per second.

6.2 New Devices Discussion

This insight was taken and applied to designing the new devices and significant improvements were observed. Overall operation of devices significantly improved due to new designs and altered operating conditions. DEP was observed in all the devices where DEP was supposed to occur, EK values from literature were able to be replicated, no bubble formation was observed at the reduce fluid conductivity, there was a reduction in electrolysis debris, and inclusion of changing temperature and viscosity parameters lead to more accurate simulation results.

Comparing the natures of each type of post design showed that the “Home Plate” and triangle post designs are a step in the right direction for producing a foul-less filter. Also, with the addition of the necking channel, the DEP force could be maximized to a single point. All were able to produce a large enough DEP forces at 800V/cm to keep the majority of the yeast particles outside the post array. Some particles were able to pass, however it is unclear if this was due to failure of the filter, those particular yeast cells were dead (meaning their electrical properties were the same as the surrounding fluid and therefore do not experience DEP), or if their properties were different than other yeast cells. This is an improvement over what was seen in the Blanca recreation device and by Blanca and Moncada-Hernandez [7][8], where particles mostly became trapped within the post array. Particle passage also could be affected by the sheer number of particles that get trapped in the post array, increasing the EK forces on the larger mass of cells, pushing some through. Additionally, it was noted that trapped particles in the Blanca recreation device demonstrated a counterclockwise rotation in the trapping region. This

rotational motion could be due to ETF imparting localized pressure driven flow at the constrictions in the device, pushing particles in and out of the post array.

Some issues that the new device designs had were that there were still some debris observed after extended testing and the fact that none of the devices achieved being foul-less. Even prior to activating the electric field, yeast cells would adhere to the surface of both the glass and the PDMS already fouling prior to operation. Particularly for PDMS, this is likely due to the tendency of bioparticles to adsorb to PDMS surfaces [31]. Particles also flocculated together creating large clumps which in the shorter channel size compared to the legacy device, proved to be a continued issue. As a whole, this proved to be a step in the right direction and has helped to lay the groundwork for continuation of this project.

CHAPTER 7 CONCLUSIONS AND FUTURE DIRECTIONS

7.1 Conclusions

In conclusion, this thesis has set the framework for continued research into a DC iDEP foul-less filter. Particle levitation outside a post array was successfully demonstrated, proper testing conditions were observed, and a framework for proper simulation testing has been shown. The primary conclusions found in this thesis were:

1. Reductions in the length of the device are beneficial for reducing operating voltages so future devices should be designed with a focus on minimizing electrode to electrode length as demonstrated by the “shorty” device. If designed properly, the device could be even smaller.
2. CM factor should be adjusted appropriately to avoid excessive conductivities while also providing necessary properties to perform iDEP. This thesis aimed for a fluid conductivity that produced a CM factor of -0.4 instead of a -0.5 CM factor since the -0.5, although producing stronger DEP force in theory, also was the root cause of the bubble formation and electrolysis debris issues seen throughout legacy device testing. A CM factor of -0.4 was sufficient to perform the desired function and further decreases in conductivity could improve long term function if the insulation posts/design is sufficient.
3. Improved post shapes were simulated to project DEP force above the post array and confirmed in testing that the triangular and “Home Plate” designs projected the DEP field outside the post array to prevent yeast cell entrance.

4. Post array is recommended to not be staggered to prevent fouling. The staggered design in the legacy device easily fouled while the new designs and literature [6][7][8] all show the aligned post design not fouling on posts.
5. Electrodes should be “off device”. This was accomplished by dangling electrode wires in water filled pipette tips (Figure 42). This helps reduce electrolysis debris and helped prevent electrolysis bubbles from wetting the device. Does not have a significant effect on the voltage requirements. Even if the electrodes are lifted off device, the length of the device determines the electric filed strength. For example: if the device is 1cm long and a voltage potential of 400V is applied, even if the path through the fluid from electrode to electrode is 3cm, due to the cross-sectional area of the device the electric field will be about 400V/cm.
6. The scale of features does not need to be on the order of tens of microns and can be done effectively with features on the scale of hundreds of microns. This was demonstrated in the new devices and is shown in literature to be successful [7][8]. The more important factor is the ratio of cross-sectional area between posts to total cross-sectional area. The necking “shorty” device is a great example of 20micron width at the necking point compared to the 2mm channel width (1:100) which produced a strong iDEP trapping region (Figure 43).
7. Temperature and viscosity cannot be assumed to be constant. Bubble formation was likely due to Joule heating to the point where the water in the channel boiled. Even with the reduced conductivity, the water will still heat up and as temperature goes up, dynamic viscosity will decrease. Usage of the joule heating module in COMSOL with the heat transfer in fluids (instead of the default heat transfer in

solid) can help predict temperatures and Equation ## in mathematical models will help with prediction of conditions.

8. EKs are significant dictators of fluid flow and particle motion. When using DC this is the main opponent to DEP. For every type of particle being tested, the EKs should be well know and tested for prior to DEP testing. Understanding the net zeta potential will help with testing in COMSOL.

7.2 Future Directions

For those that consider continuing this project it is recommended to closely consider the conclusions of this thesis. Primary steps going forward should include but are not limited to further optimization of post geometry to project the DEP force, looking into if temperature affects the zeta potential, look into using combination AC and DC fields for increased control over EKs and reduce required DC field strengths, and look at ways to possibly coat channels or change substrates to reduce the zeta potential and particle adhesion [31]. In future device designs, inclusion of fluid cross flow channels to see if it could work with the designs made in this thesis or with other new post designs and inclusion of a second particle type to properly demonstrate iDEP separations. Finally, another design change would be to have a way to introduce cells one at a time into the system to help reduce flocculation and clogging.

BIBLIOGRAPHY

[1] Agyei, Dominic, and Michael K. Danquah. "Industrial-Scale Manufacturing of Pharmaceutical-Grade Bioactive Peptides." *Biotechnology Advances*, vol. 29, no. 3, 14 Jan. 2011, pp. 272–277., doi:10.1016/j.biotechadv.2011.01.001.

[2] Gascoyne, P.r.c., et al. "Dielectrophoretic Separation of Cancer Cells from Blood." *IAS 95. Conference Record of the 1995 IEEE Industry Applications Conference Thirtieth IAS Annual Meeting*, vol. 33, no. 3, 1997, pp. 670–678. *Nih.gov*, doi:10.1109/ias.1995.530461.

[3] Järup, Lars. "Hazards of Heavy Metal Contamination." *British Medical Bulletin*, vol. 68, no. 1, Jan. 2003, pp. 167–182., doi:10.1093/bmb/ldg032.

[4] Duruibe, J, et al. "Heavy Metal Pollution and Human Biotoxic Effects." *Heavy Metal Pollution and Human Biotoxic Effects*, 20 Apr. 2007.

[5] Batton, John, et al. "Trapping Heavy Metals by Using Calcium Hydroxyapatite and Dielectrophoresis." *Journal of Hazardous Materials*, vol. 139, no. 3, 18 Apr. 2007, pp. 461–466., doi:10.1016/j.jhazmat.2006.02.057.

[6] Cummings, E.b. "Streaming Dielectrophoresis for Continuous-Flow Microfluidic Devices." *IEEE Engineering in Medicine and Biology Magazine*, vol. 22, no. 6, 2003, pp. 75–84., doi:10.1109/memb.2003.1266050.

[7] Lapizco-Encinas, Blanca H., et al. "Insulator-Based Dielectrophoresis for the Selective Concentration and Separation of Live Bacteria in Water." *Electrophoresis*, vol. 25, no. 1011, 2004, pp. 1695–1704., doi:10.1002/elps.200405899.

[8] Moncada-Hernandez, Hector, et al. "Insulator-Based Dielectrophoresis of Microorganisms: Theoretical and Experimental Results." *Electrophoresis*, vol. 32, no. 18, 2011, pp. 2502–2511., doi:10.1002/elps.201100168.

[9] Gebel, Erika. "Making Insulin." *Diabetes Forecast*, The Healthy Living Magazine, July 2013, www.diabetesforecast.org/2013/jul/making-insulin.html.

[10] Chen, Jianrong, et al. "Membrane Fouling in a Membrane Bioreactor: High Filtration Resistance of Gel Layer and Its Underlying Mechanism." *Water Research*, vol. 102, 2016, pp. 82–89., doi:10.1016/j.watres.2016.06.028.

[11] Bruus, Henrik. *Theoretical Microfluidics*. 3rd ed., Oxford University Press, 2008.

[12] Pritchard, Phillip J. *Fox and McDonalds Introduction to Fluid Mechanics, 9th Edition*. Wiley, 2014.

[13] Probstein, R. F. *Physiochemical Hydrodynamics*. 2nd ed., John Wiley & Son, Inc, 2003.

[14] Butt Hans-Jürgen, et al. *Physics and Chemistry of Interfaces*. 3rd ed., Wiley-VCH-Verl., 2013.

[15] "Stanford University." *Electrokinetic Bioanalytical Systems*, microfluidics.stanford.edu/Projects/Archive/bioanal.htm.

[16] Kumar, Bharat, and Scott R Crittenden. "Stern Potential and Debye Length Measurements in Dilute Ionic Solutions with Electrostatic Force Microscopy." *Nanotechnology*, vol. 24, no. 43, 2013, p. 435701., doi:10.1088/0957-4484/24/43/435701.

[17] Kirby, Brian J., and Ernest F. Hasselbrink. "Zeta Potential of Microfluidic Substrates: 1. Theory, Experimental Techniques, and Effects on Separations." *Electrophoresis*, vol. 25, no. 2, 2004, pp. 187–202., doi:10.1002/elps.200305754.

[18] Kirby, Brian J., and Ernest F. Hasselbrink. “Zeta Potential of Microfluidic Substrates: 2. Data for Polymers.” *Electrophoresis*, vol. 25, no. 2, 2004, pp. 203–213., doi:10.1002/elps.200305755.

[19] Israelachvily, Jacob N. *Intermolecular and Surface Forces*. 2nd ed., Academic Press, 1991.

[20] Guan, Qian, et al. “Electrophoretic Separations in Poly (Dimethylsiloxane) Microchips Using a Mixture of Ionic and Zwitterionic Surfactants.” *Electrophoresis*, vol. 33, no. 2, Jan. 2012, pp. 379–387., doi:10.1002/elps.201100259.

[21] Qian, Cheng, et al. “Dielectrophoresis for Bioparticle Manipulation.” *International Journal of Molecular Sciences*, vol. 15, no. 10, Oct. 2014, pp. 18281–18309., doi:10.3390/ijms151018281.

[22] Jones, T.b. “Basic Theory of Dielectrophoresis and Electrorotation.” *IEEE Engineering in Medicine and Biology Magazine*, vol. 22, no. 6, 2003, pp. 33–42., doi:10.1109/memb.2003.1304999.

[23] Huang, Chao, et al. “Characterization of a Hybrid Dielectrophoresis and Immunocapture Microfluidic System for Cancer Cell Capture.” *Electrophoresis*, vol. 34, no. 20-21, Nov. 2013, doi:10.1002/elps.201370191.

[24] Campbell, Stephen A., and Stephen A. Campbell. *Fabrication Engineering at the Micro and Nanoscale*. Oxford University Press, 2008.

[25] “Photoresist.” *Wikipedia*, Wikimedia Foundation, 13 Jan. 2020, en.wikipedia.org/wiki/Photoresist.

[26] Rizzoni, Giorgio. *Fundamentals of Electrical Engineering*. 1st ed., McGraw-Hill Higher Education, 2009.

[27] Sugimoto, Masahiro, et al. “Capillary Electrophoresis Mass Spectrometry-Based Saliva Metabolomics Identified Oral, Breast and Pancreatic Cancer-Specific Profiles.” *Metabolomics*, vol. 6, no. 1, Oct. 2009, pp. 78–95., doi:10.1007/s11306-009-0178-y.

[28] Franco, Jose Luis Sebastian, et al. “Dielectric Characterization Of The Yeast Cell Budding Cycle.” *Progress In Electromagnetics Research*, vol. 134, 2013, pp. 1–22., doi:10.2528/pier12100406.

[29] Suganthi, K.s., and K.s. Rajan. “Temperature Induced Changes in ZnO–Water Nanofluid: Zeta Potential, Size Distribution and Viscosity Profiles.” *International Journal of Heat and Mass Transfer*, vol. 55, no. 25-26, 18 Sept. 2012, pp. 7969–7980., doi:10.1016/j.ijheatmasstransfer.2012.08.032.

[30] Vaxasoft. “Dynamic Viscosity of Liquid Water from 0 °C to 100 °C.” *Dynamic Viscosity of Liquid Water from 0 °C to 100 °C*, Vaxasoft, www.vaxasoftware.com/doc_eduen/qui/viscoh2o.pdf.

[31] Ren, K., et al. “Whole-Teflon Microfluidic Chips.” *Proceedings of the National Academy of Sciences*, vol. 108, no. 20, Feb. 2011, pp. 8162–8166., doi:10.1073/pnas.1100356108.

[32] Hong, F.j., et al. “A Parametric Study of AC Electrothermal Flow in Microchannels with Asymmetrical Interdigitated Electrodes.” *International Communications in Heat and Mass Transfer*, vol. 38, no. 3, Mar. 2011, pp. 275–279., doi:10.1016/j.icheatmasstransfer.2010.11.004.

APPENDICIES

Appendix A

	charge of ion	diffusion coefficient of ion i	molar limiting conductivity of ion i	equivalent limiting conductivity of ion i	
Cation	**|z|**	**$D_i \cdot 10^{-9}$ [$m^2 s^{-1}$]**	**Λmi[S cm^2 mol^{-1}]**	**Λeq [S cm^2 mol^{-1}]**	**Ref**
Ag+	1	1.648	61.9	61.9	[V]
Al+3	3	0.559	188.9	63	[P]
Ba+2	2	0.848	127.4	63.7	[P]
Be+2	2	0.599	90	45	[V]
Ca+2	2	0.793	119.1	59.6	[P]
CaHCO3+	1	0.506	19	19	[P]
Cd+2	2	0.717	107.7	53.8	[P]
Co+2	2	0.732	110	55	[V]
Cr+3	3	0.595	201.1	67	[V]
Cu+2	2	0.733	110.1	55	[P]
Fe+2	2	0.719	108	54	[P]
Fe+3	3	0.604	204.1	68	[V]
H+	1	9.31	349.6	349.6	[P]
Hg+2	2	0.913	137.2	68.6	[V]
K+	1	1.96	73.6	73.6	[P]
Li+	1	1.03	38.7	38.7	[P]
Mg+2	2	0.705	105.1	53	[P]
MgHCO3+	1	0.478	18	18	[P]
Mn+2	2	0.688	103.4	51.7	[P]
Na+	1	1.33	50	50	[P]
NH4+	1	1.98	74.4	74.4	[P]
Pb+2	2	0.945	142	71	[P]
Sr+2	2	0.794	119.3	59.6	[P]
UO2+2	2	0.426	64	32	[V]
Zn+2	2	0.715	107.4	53.7	[P]
Inorganic Anions					
Anion	**|z|**	**$D_i \cdot 10^{-9}$ [$m^2 s^{-1}$]**	**Λmi[S cm^2 mol^{-1}]**	**Λeq [S cm^2 mol^{-1}]**	**Ref**
Br-	1	2.01	75.5	75.5	[P]
Cl-	1	2.03	76.2	76.2	[P]
CO3-2	2	0.955	143.5	71.7	[P]
CN-	1	2.077	78	78	[V]
CNO-	1	1.72	64.6	64.6	[V]
CrO4-2	2	1.132	170	85	[V]
F-	1	1.46	54.8	54.8	[P]
H2AsO4-	1	0.905	34	34	[V]
H2PO4-	1	0.846	31.8	31.8	[P]
HCO3-	1	1.18	44.3	44.3	[P]
HPO4-2	2	0.69	103.6	51.8	[P]
HS-	1	1.73	65	65	[P]
HSO4-	1	1.33	50	50	[P]
I-	1	2.045	76.8	76.8	[P]
KSO4-	1	0.746	28	28	[P]
MnO4-	1	1.632	61.3	61.3	[V]
MoO4-2	2	1.984	298	149	[V]
NaCO3-	1	0.585	22	22	[P]
NaSO4-	1	0.618	23.2	23.2	[P]
NO2-	1	1.91	71.7	71.7	[P]
NO3-	1	1.9	71.4	71.4	[P]
OH-	1	5.27	197.9	197.9	[P]
PO4-3	3	0.612	206.8	68.9	[P]
S-2	2	0.731	109.8	54.9	[P]
SeO4-2	2	1.008	151.4	76.7	[V]
SO4-2	2	1.07	160.7	80.4	[P]
Organic Anions					
Organic anion	**|z|**	**$D_i \cdot 10^{-9}$ [$m^2 s^{-1}$]**	**Λmi[S cm^2 mol^{-1}]**	**Λeq [S cm^2 mol^{-1}]**	
Acetate-	1	1.089	40.9	40.9	
Benzoate-	1	0.863	32.4	32.4	
Butyrate-	1	0.868	32.6	32.6	
Citrate-3	3	0.623	210.6	70.2	
Dihydrogencitrate-	1	0.799	30	30	
Formate-	1	1.454	54.6	54.6	
Hydrogenoxalate-	1	1.07	40.2	40.2	
Isovalerate-	1	0.871	32.7	32.7	
Lactate-	1	1.033	38.8	38.8	
Malate-2	2	0.783	117.6	58.8	
Maleate-2	2	0.824	123.8	61.9	
Oxalate-2	2	0.987	148.3	74.1	
Phenylacetate-	1	0.815	30.6	30.6	
o-Phtalate-2	2	0.696	104.6	52.3	
m-Phtalate-2	2	0.728	109.4	54.7	
Pivalate-	1	0.849	31.9	31.9	
Salicylate-	1	0.959	36	36	
Suberate-2	2	0.479	72	36	
Succinate-2	2	0.783	117.6	58.8	
Tartarate-2	2	0.794	119.3	59.6	

[P] PHREEQC (Version 3)–A Computer Program for Speciation, Batch-Reaction, One-Dimensional Transport, and Inverse Geochemical Calculations; [The diffus

[V] Petr Vanýsek: Ionic conductivity and diffusion at infinite dilution, Handbook of Chemistry and Physics, CRC Press, 1992/93 edition. Boca Raton, 1992. pp. (

Appendix B

Table 13: Conditions for operation of the DEP filter in the legacy device using water (Relative permittivity = 78.5 and $\zeta = -0.005V$).

Voltage	Electric Field Strength (V/m)	-0.50	-0.40	-0.30	-0.25	-0.20	-0.10	0.00
100	3.33E+05	Pass	Pass	Pass	Pass	Pass	Pass	Fail
90	3.00E+05	Pass	Pass	Pass	Pass	Pass	Pass	Fail
80	2.67E+05	Pass	Pass	Pass	Pass	Pass	Pass	Fail
70	2.33E+05	Pass	Pass	Pass	Pass	Pass	Pass	Fail
60	2.00E+05	Pass	Pass	Pass	Pass	Pass	Pass	Fail
50	1.67E+05	Pass	Pass	Pass	Pass	Pass	Fail	Fail
40	1.33E+05	Pass	Pass	Pass	Pass	Pass	Fail	Fail
30	1.00E+05	Pass	Pass	Pass	Pass	Pass	Fail	Fail
20	6.67E+04	Pass	Pass	Pass	Fail	Fail	Fail	Fail
10	3.33E+04	Fail	Fail	Fail	Fail	Fail	Fail	Fail

Table 14: Conditions for operation of the DEP filter in the legacy device using water (Relative permittivity = 78.5 and $\zeta = -0.010V$).

Voltage	Electric Field Strength (V/m)	-0.50	-0.40	-0.30	-0.25	-0.20	-0.10	0.00
100	3.33E+05	Pass	Pass	Pass	Pass	Pass	Fail	Fail
90	3.00E+05	Pass	Pass	Pass	Pass	Pass	Fail	Fail
80	2.67E+05	Pass	Pass	Pass	Pass	Pass	Fail	Fail
70	2.33E+05	Pass	Pass	Pass	Pass	Pass	Fail	Fail
60	2.00E+05	Pass	Pass	Pass	Pass	Pass	Fail	Fail
50	1.67E+05	Pass	Pass	Pass	Pass	Pass	Fail	Fail
40	1.33E+05	Pass	Pass	Pass	Pass	Fail	Fail	Fail
30	1.00E+05	Pass	Pass	Fail	Fail	Fail	Fail	Fail
20	6.67E+04	Fail	Fail	Fail	Fail	Fail	Fail	Fail
10	3.33E+04	Fail	Fail	Fail	Fail	Fail	Fail	Fail

Table 15: Conditions for operation of the DEP filter in the legacy device using water (Relative permittivity = 78.5 and $\zeta = -0.015V$).

Voltage	Electric Field Strength (V/m)	-0.50	-0.40	-0.30	-0.25	-0.20	-0.10	0.00
100	3.33E+05	Pass	Pass	Pass	Pass	Pass	Fail	Fail
90	3.00E+05	Pass	Pass	Pass	Pass	Pass	Fail	Fail
80	2.67E+05	Pass	Pass	Pass	Pass	Fail	Fail	Fail
70	2.33E+05	Pass	Pass	Pass	Fail	Fail	Fail	Fail
60	2.00E+05	Pass	Pass	Pass	Fail	Fail	Fail	Fail
50	1.67E+05	Pass	Pass	Fail	Fail	Fail	Fail	Fail
40	1.33E+05	Pass	Fail	Fail	Fail	Fail	Fail	Fail
30	1.00E+05	Fail	Fail	Fail	Fail	Fail	Fail	Fail
20	6.67E+04	Fail	Fail	Fail	Fail	Fail	Fail	Fail
10	3.33E+04	Fail	Fail	Fail	Fail	Fail	Fail	Fail

Table 16: Conditions for operation of the DEP filter in the legacy device using water (Relative permittivity = 78.5 and $\zeta = -0.020V$).

Voltage	Electric Field Strength (V/m)	-0.50	-0.40	-0.30	-0.25	-0.20	-0.10	0.00
100	3.33E+05	Pass	Pass	Pass	Fail	Fail	Fail	Fail
90	3.00E+05	Pass	Pass	Pass	Fail	Fail	Fail	Fail
80	2.67E+05	Pass	Pass	Pass	Fail	Fail	Fail	Fail
70	2.33E+05	Pass	Pass	Fail	Fail	Fail	Fail	Fail
60	2.00E+05	Pass	Pass	Fail	Fail	Fail	Fail	Fail
50	1.67E+05	Pass	Fail	Fail	Fail	Fail	Fail	Fail
40	1.33E+05	Fail	Fail	Fail	Fail	Fail	Fail	Fail
30	1.00E+05	Fail	Fail	Fail	Fail	Fail	Fail	Fail
20	6.67E+04	Fail	Fail	Fail	Fail	Fail	Fail	Fail
10	3.33E+04	Fail	Fail	Fail	Fail	Fail	Fail	Fail

Table 17: Conditions for operation of the DEP filter in the legacy device using water (Relative permittivity = 78.5 and $\zeta = -0.025V$).

Voltage	Electric Field Strength (V/m)	-0.50	-0.40	-0.30	-0.25	-0.20	-0.10	0.00
100	3.33E+05	Pass	Pass	Pass	Fail	Fail	Fail	Fail
90	3.00E+05	Pass	Pass	Fail	Fail	Fail	Fail	Fail
80	2.67E+05	Pass	Pass	Fail	Fail	Fail	Fail	Fail
70	2.33E+05	Pass	Fail	Fail	Fail	Fail	Fail	Fail
60	2.00E+05	Pass	Fail	Fail	Fail	Fail	Fail	Fail
50	1.67E+05	Fail	Fail	Fail	Fail	Fail	Fail	Fail
40	1.33E+05	Fail	Fail	Fail	Fail	Fail	Fail	Fail
30	1.00E+05	Fail	Fail	Fail	Fail	Fail	Fail	Fail
20	6.67E+04	Fail	Fail	Fail	Fail	Fail	Fail	Fail
10	3.33E+04	Fail	Fail	Fail	Fail	Fail	Fail	Fail

Table 18: Conditions for operation of the DEP filter in the legacy device using water (Relative permittivity = 78.5 and $\zeta = -0.030V$).

Voltage	Electric Field Strength (V/m)	-0.50	-0.40	-0.30	-0.25	-0.20	-0.10	0.00
100	3.33E+05	Pass	Pass	Fail	Fail	Fail	Fail	Fail
90	3.00E+05	Pass	Pass	Fail	Fail	Fail	Fail	Fail
80	2.67E+05	Pass	Fail	Fail	Fail	Fail	Fail	Fail
70	2.33E+05	Pass	Fail	Fail	Fail	Fail	Fail	Fail
60	2.00E+05	Fail	Fail	Fail	Fail	Fail	Fail	Fail
50	1.67E+05	Fail	Fail	Fail	Fail	Fail	Fail	Fail
40	1.33E+05	Fail	Fail	Fail	Fail	Fail	Fail	Fail
30	1.00E+05	Fail	Fail	Fail	Fail	Fail	Fail	Fail
20	6.67E+04	Fail	Fail	Fail	Fail	Fail	Fail	Fail
10	3.33E+04	Fail	Fail	Fail	Fail	Fail	Fail	Fail

APPENDIX C

Wafers were obtained and first cleaned prior to casing to remove as many particulates from the surface as possible to ensure the highest quality devices for testing. Wafer was taken and placed into a Teflon boat and placed into Piranha for 15 minutes to clean. Upon finishing the Piranha wash, the wafer was slowly dipped in the BOH rinse bath 4 times. Wafer was then washed with water in the sink to remove any remaining particulates from the wafer then dried in Spin Rinse Drier (SRD). Wafer was removed from the drier and placed into a large Petri dish and was ready for PDMS pouring.

Sylgard PDMS and hardener were used in the creating of all PDMS devices. PDMS and hardener were mixed at a 10:1 ratio in a cup for 5 minutes. For PDMS devices bound to glass 40g PDMS was mixed with 4 g of hardener and for PDMS devices bound to PDMS substrate 60g of PDSM and 6g of hardener were used. The mixed PDMS was then placed in the vacuum chamber to degas. Once all visible bubbles were gone from the fluid the cup was removed and poured into the Petri dish with the wafer. To create a PDMS substrate material for the PDMS on PDMS device a second Petri dish was used to pour the remaining PDMS into a thin substrate layer. PDSM was left to cure for in the oven at 70°C for 4 hours.

After curing was complete, devices were cut from the Petri dish and prepared for plasma bonding. Prior to plasma bonding, the vacuum chamber attached to the plasma bonder was isolated for the plasma bonding chamber and pumped down to reduce time to bond devices. Large glass slides were used as the base for the devices. Glass slides were washed with acetone and water, then dried. Devices were turned to have the microscopic features facing upwards and the access holes were cut using a sharpened 10-gauge

syringe tip and residual PDMS “plugs” were removed from the syringe tip with plyers. Scotch tape was placed over the feature side of the PDMS and carefully peeled away to remove any particulates that may have landed on the surface while cutting. Scotch tape was also used on glass slides.

A glass slide and PDMS device were both placed onto the glass “boat” with the side to be bonded facing up. The boat was placed into the plasma bonder and the door was closed and the gas valve was turned to the closed position. The valve connecting the vacuum chamber to the plasma bonding chamber was opened. Pressure was allowed to drop to 3psi, then was ready for plasma bonding. The settings used to bond devices was high setting for the plasma bonder for 15 seconds. Vacuum chamber was then isolated from the plasma bonding chamber again and the gas valve on the plasma bonder was opened again and allowed to pressurize. The boat was removed from the chamber and the PDMS device was grabbed and placed down onto the glass slide with the plasma exposed sides of glass and PDMS coming together. Device was carefully pressed onto the glass slide to removed air bubbles. PDMS on glass devices were done at this point. For PDMS on PDMS devices, the above steps were repeated to then bind PDMS to the PDMS substrate on a glass slide. Completed devices were put into the curing oven for another 4 hours, at which time they are ready to be used for testing.

APPENDIX D

The ∇E^2 is the gradient of the electric field intensity and in DC can be expressed as:

$$\nabla E^2 = \nabla(\underline{E} \cdot \underline{E})$$

$$\underline{\nabla}(\underline{E} \cdot \underline{E}) = \underline{e_i} \frac{\partial}{\partial x_i}(E_j \cdot E_j) = \underline{e_i}(E_j \frac{\partial E_j}{\partial x_i} + E_j \frac{\partial E_j}{\partial x_i})$$

$$= \underline{e_i}(2E_j \frac{\partial}{\partial x_i} E_j)$$

In AC, ∇E^2 uses the root mean square of the alternating electric field and will result in:

$$= \underline{e_i}(E_j \frac{\partial}{\partial x_i} E_j)$$

Therefore, when working in the DC regime, the DEP force is expressed as:

$$F_{i_{DEP}} \underline{e_i} = 4\pi a^3 \varepsilon_m Re[f_{cm}] \underline{e_i}(E_j \frac{\partial E_j}{\partial x_i})$$